AD-A152 073 DETERMINATION OF FAILURE CHARACTERISTICS OF MATERIALS AND STRUCTURES(U) GEORGE WASHINGTON UNIV WASHINGTON DC SCHOOL OF ENGINEERING AN.. H LIEBOWITZ 14 DEC 84 1/2

UNCLASSIFIED N00014-84-K-0027 F/G 20/11 NL

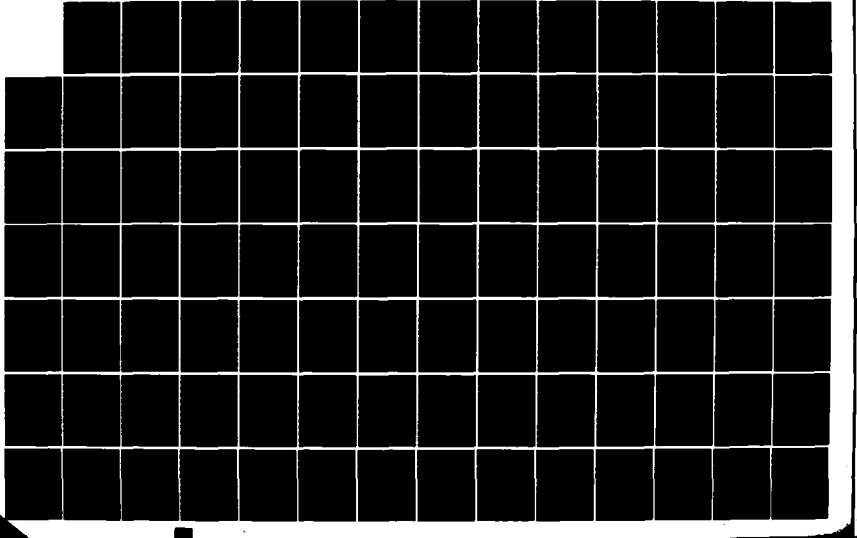

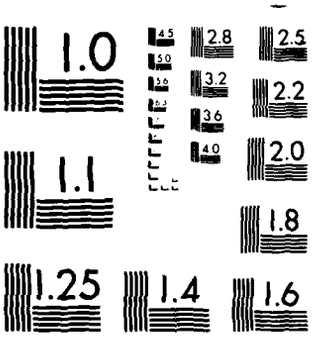

(6)

ANNUAL SUMMARY REPORT

ONR Contract #N00014-84-K-0027

DETERMINATION OF FAILURE CHARACTERISTICS

OF MATERIALS AND STRUCTURES

Principal Investigator: Dr. Harold Liebowitz

December 14, 1984

School of Engineering and Applied Science

The George Washington University

Washington, D.C. 20052

Work under ONR Contract N#00014-84-K-0027 has progressed significantly during the past contract year (11/1/83-10/31/84). The major emphasizes of the research were in the areas of three-dimensional plasticity characteristics in fracture specimens, mesh adaptive slow crack growth modeling, experimental plastic zone measurement and comparison with finite element results and the characterization of fatigue crack growth in surface cracked specimens. This work resulted in five completed publications and presentations (listed in Appendix A) and three publications pending completion.

The research in the area of crack front plasticity characteristics in three-dimensional fracture specimens demonstrated that hardening modeling (i.e., kinematic, isotropic, etc.) has a significant effect on the predicted local deformation in the neighborhood of the crack front even under monotonic loading. This result was demonstrated for various thickness specimens and for two-dimensional specimens under biaxial loading. This result suggests that the assumption of local-global load proportionality under monotonic loading with no crack growth is incorrect. Further investigations are underway to investigate the relation between the applied loading and the local deformation response. Subsequently the effect of specimen thickness has been studied and, for center-cracked panels (with through cracks), the results demonstrate that plastic

zones produced are not of plane-stress type even for very thin specimens. The mid-plane zones in these specimens are nearly plane strain type (as would be expected), however, surface zones show distinctly mixed characteristics. The results of these examinations were the subject of two papers and a presentation. Appendices B and C are copies of these papers and Appendix D contains copies of the abstract and slides used in the invited lecture presented at the Fifth ASCE meeting referenced previously.

An experimental investigation of the local plastic deformation produced in a three-dimensional fracture specimen was initiated to validate the finite element results. A special LVDT probe was developed to measure the residual surface deformation remaining after a fracture specimen was unloaded. These measurements were compared quite favorably to the finite element predictions. A maximum deviation of 3% between the average experimental and finite element predictions was obtained. This is the first comparison between actual local deformation and finite element predictions known to the authors and validates the finite element approach. Average experimental measurements were used for comparison as the measured displacements exhibited considerable scatter due to material inhomogeneity, nonplanarity of the initial specimen surface and lack of symmetry in the initial fatigue crack. A complete summary of this work is presented in Appendix E and will be the subject of a future publication.

A new algorithm was developed for the computational modeling of slow, stable crack growth in elastic-plastic specimens. This algorithm convects the grid after each increment of crack growth updating both the local geometry and plastic state. The method has been applied quite successfully to thin sheet panels which can be modeled as two-dimensional plane-stress specimens. The results of this investigation were presented as an invited lecture at the 21st Annual Meeting of the SES referenced early. The abstract and slides used at that lecture are given in Appendix F. This work will be the subject of a future publication.

An experimental evaluation of surface crack growth in PMMA was initiated during this contract year. The main conclusions of that study are that (in the absence of back surface effects) arbitrary initial flaws will quickly obtain an approximately elliptic shape, back surface influence was not observed until the crack had traversed 50% of the specimen thickness, cracks under the influence of the back surface grew very rapidly and as the crack approached the back surface, typical through-crack characteristics were obtained (i.e., straight crack front, etc.). These results are elaborated upon in Appendix G and will be the subject of a future publication.

In summary, much work has been accomplished during the

current contract year. The results have been compiled and presented in both the open literature and as various invited papers and lectures. In addition, a review paper on Biaxial Loading Effects was prepared as an invited paper for a Special Issue of the Journal of the Aeronautical Society of India and is included as Appendix H. Further work is planned in the area of local-global load relations and surface crack growth characteristics. The majority of effort in the future, however, will be in the area of Creep Fracture Mechanics. This understanding of this field is vital to many areas of application and has not been sufficiently studied to date.

A P P E N D I C E S

APPENDIX A:

PUBLICATIONS - UNDER ONR CONTRACT #N00014-84-K-0027

Fiscal Year 1984

1] "Biaxial Load Effects in the Mechanics of Fracture," E. T. Moyer, Jr. and H. Liebowitz. An invited paper to appear in the Fracture Mechanics Special Issue of the Journal of the Aeronautical Society of India (March, 1985).

2] "Effect of Specimen Thickness on Crack Front Plasticity Characteristics in Three-Dimensions," E. T. Moyer, Jr. and H. Liebowitz. Presented at the Sixth International Conference on Fracture, New Delhi, India, December, 1984.

3] "A Mesh Adaptive Method for Modeling Slow Crack Growth," E. T. Moyer, Jr. and H. Liebowitz. An invited lecture presented at the 21st Annual Meeting of the SES, VPI&SU, Blacksburg, Virginia, October, 1984.

4] "The Effect of Biaxial Loading on Crack-Tip Yield Zones," E. T. Moyer, Jr. and H. Liebowitz. An invited lecture presented at the Fifth ASCE-EMD Specialty Conference, Laramie, Wyoming, August, 1984.

5] "Plastic Deformation and Hardening Characteristics in Three-Dimensional Fracture Specimens," E. T. Moyer, Jr. and H. Liebowitz. Proceedings of ICF International Symposium on Fracture Mechanics (Beijing), an invited lecture, Beijing, China, November, 1983.

APPENDIX B:

"Plastic Deformation and Hardening Characteristics in Three-Dimensional Fracture Specimens," E. T. Moyer, Jr. and H. Liebowitz. Proceedings of ICF International Symposium on Fracture Mechanics (Beijing), an invited lecture, Beijing China, November, 1983.

PLASTIC DEFORMATION AND HARDENING CHARACTERISTICS IN THREE-DIMENSIONAL FRACTURE SPECIMENS

By

E. Thomas Moyer, Jr.

and

H. Liebowitz

April 1983

School of Engineering and Applied Science
The George Washington University
Washington, D.C. 20052

ABSTRACT

The formulation for general three-dimensional small strain plasticity analysis is presented. A finite element computer code has been developed to carry out the analysis. General hardening characteristics are included as an input option to the program allowing for the study of a wide class of materials.

An example through crack problem is solved employing three different hardening assumptions (isotropic, kinematic and mixed). The plastic deformation in the region of the crack front predicted with each of the models is compared. While the predicted results are similar, several fundamental characteristics of each assumption can be observed. Residual deformation zones are also calculated as a measure of the extent of plastic deformation. The qualitative differences between hardening assumptions are consistent between the plasticity measures allowing for direct comparison with experimental observation.

INTRODUCTION

The study of ductile fracture processes has been widely discussed in the literature during the past decade. Theoretical, numerical, experimental and many combined studies have been presented. Fracture criteria have been proposed based on many controlling quantities (e.g., stress, strain, energy, displacements, etc.) both on global and local scale levels. Without exception, all of these criteria show a marked thickness and geometry dependence limiting their predictive capabilities. While some of the proposed criteria have been successful at predicting certain fracture phenomena for mildly ductile specimens, the geometry dependence of the controlling parameters makes application of these theories to practical specimens extremely difficult. The purpose of this study is to investigate the nature of the plastic deformation near a three-dimensional stationary crack front in a ductile material. Due to the three-dimensional nature of ductile fracture, it is essential to accurately model the stress-strain response for a general three-dimensional crack problem.

The majority of the studies on the plastic deformation near a crack are based on two-dimensional approximations. While these studies are a necessary first step in the study of ductile phenomena, several fundamental effects remain inadequately modeled. For specimens thick enough to be modeled by plane-strain, ductility effects are usually not

significant. Most engineering metals exhibiting significant plasticity effects are relatively thin. It is tempting, therefore, for many applications, to employ a plane-stress analysis. While the gross specimen behavior may be reasonably predicted with such an approach, the local effects near the crack will not be adequately modeled. For linear elastic materials it can be shown that the stress-strain state near a crack front in three-dimensions is essentially plane-strain except at the intersection of the crack with a free surface [1]. For problems involving plasticity, the incremental deformations during loading will exhibit the same characteristic behavior as an elastic body with an elastic modulus equal to the instantaneous tangent modulus [2]. The local, instantaneous response near an arbitrary crack front should be one of plane-strain independent of the specimen thickness. A fully three-dimensional analysis must be employed, therefore, to accurately model the local plastic response of a cracked medium.

To examine the local deformation response of a three-dimensional elastic-plastic crack specimen, a finite element code was developed. The formulation employs an incremental J_2 flow theory of plasticity with an arbitrary, "Mixed" hardening response. Two-dimensional studies have shown that different materials exhibit different hardening properties that can be load and geometry dependent. The generality of the hardening law employed allows for user determined hardening input. The

initial code generated for this study assumes infinitesimal displacements and strains. The formulation is easily modified, however, to account for finite strain effects. This will be the topic of a later study.

The program was tested on many problems of uniform expansion and simple geometric configurations with analytic (or quasi-analytic) solutions. These test runs facilitated the debugging of the convergence algorithms and iterative routines. The present study focuses on a center-cracked sheet made of an aluminum alloy similar in nature to 7075-T6751 aluminum. The response assuming kinematic hardening, isotropic hardening and a combined law is found. The results demonstrate that the local yield effects are moderately sensitive to the hardening law. For the range studied, however, there is not significant enough differences between the models to distinguish a preferred approach. Since reverse yield and cyclic loading have not been investigated, large distinction between hardening models is not anticipated. The similarity of the predicted results, however, serves as a strong indication of the numerical consistency of the solutions.

A comparison was made between the yield zones on the free surface predicted at maximum load with the von Mises stress yield criterion and the residual contractions predicted after unloading. Good correlation was obtained in that the yield characteristics predicted by both measures were

qualitatively similar. The predicted zones using the stress at maximum load were larger than the residual contraction zones as was expected. A contraction of 1.E-04 inches was the smallest contour plotted as this is on the order of resolution of both experimental techniques and the numerical results. While numerical correlations are purely qualitative without experimental calibration, they do serve to demonstrate the consistency and probable accuracy of the code and the mesh employed.

A companion experimental study is currently underway to compare the predicted yield characteristics with the experimentally observed deformations. The difficulty in any such study is the necessity of achieving significant plastic deformation without slow crack growth. The phenomena of slow crack growth is an effect which must be modeled independent of the deformation response. While slow growth is undoubtedly controlled by the local deformation state, the process is a fundamentally different physical failure mechanism. The validity of the plasticity model being employed must be ascertained independent of the fracture characteristics of the specimen.

CONTINUUM PLASTICITY FORMULATION

The goal of continuum plasticity theories is to provide a relationship between the incremental changes in deformation and stress as a material undergoes irreversible deformation. Due to the complex nature of the deformation fields generally produced in a solid, most mathematical theories attempt to extrapolate the phenomena observed in uniaxial tensile tests to more complex stress states. While many such formulations have been advanced, few provide constitutive relations which are practical for analysis of complex structures. Confining the discussion to incremental plasticity theories which are strain rate independent, essentially all the theories currently employed differ only in the hardening assumptions made and the choice of a yield criteria. The two most widely accepted yield criteria are the von Mises (J_2) criteria and the Tresca criteria. The Tresca criteria is mathematically simpler to employ, however, the yield surface exhibits singular points which are undesirable numerically. While these points can be handled with Lagrange multipliers [3], this approach renders the analysis as complex as the von Mises criteria. For most engineering fracture problems, it is generally agreed that the von Mises criteria more accurately models a wider class of materials in more practical applications than the Tresca criterion [4,5].

The incremental theory of plasticity employed in this

work is based on the classical rate proportionality assumptions and J_2 flow theory. While the mathematical details vary with the choice of yield criteria, the salient features of all incremental theories are the same. This discussion will, therefore, be confined to the specific theory employed in this work.

Assuming stress-strain rate proportionality and J_2 flow theory (which assumes the plastic deformations are incompressible) the stress-strain rate relations can be written as [6]

$$\dot{e}_{ij} = \begin{cases} \frac{1+\nu}{E}\dot{S}_{ij} + \frac{3}{2} f(\sigma_e) S'_{ij}\dot{\sigma}_e & \sigma_e = \sigma_y;\ \dot{\sigma}_e > 0 \\ \frac{1+\nu}{E}\dot{S}_{ij} & \text{Otherwise} \end{cases} \tag{1}$$

where:

$\dot{e}_{ij} = \dot{\varepsilon}_{ij} - \frac{1}{3}\dot{\varepsilon}_{pp}\delta_{ij}$ are the deviatoric strain rate components,

ν is Poisson's ratio,

E is Young's modulus,

$S_{ij} = \sigma_{ij} - \frac{1}{3}\sigma_{pp}\delta_{ij}$ are the deviatoric stress components,

a_{ij} are the coordinates in stress space of the yield surface center,

$S'_{ij} = S_{ij} - a_{ij}$ are the deviatoric stress components measured relative to the current yield center,

$\sigma_e = \sqrt{\frac{3}{2} S_{ij} S_{ij}}$ is the effective stress,

$\sigma'_e = \sqrt{\frac{3}{2} S'_{ij} S'_{ij}}$ is the effective stress relative to the current yield center,

σ_y is the current yield stress, and

$\cdot$ denotes time differentiation.

Due to the incompressibility condition, the hydrostatic strain rate is proportional to the mean stress rate and is given by

$$\dot{\varepsilon}_{pp} = \frac{1 - 2\nu}{E} \dot{\sigma}_{pp} \tag{2}$$

The function $f(\sigma_e)$ is dependent on the uniaxial stress-strain curve and will be discussed subsequently. For a von Mises (J_2) material, the center of the yield surface moves at a rate proportional to the projection of the stress rate vector onto the local normal to the current yield surface and can be written as

$$a_{ij} = \begin{cases} \frac{3}{2}(1 - \beta)\, S'_{k\ell}\dot{S}_{k\ell}S'_{ij}/\sigma_e'^2 & \sigma_e = \sigma_y;\ \dot{\sigma}_e > 0 \\ 0 & \text{Otherwise} \end{cases} \tag{3}$$

where β varying from 0 to 1 will model hardening behavior from kinematic ($\beta = 0$) to isotropic ($\beta = 1$).

The function $f(\sigma_e)$ is derived from the uniaxial stress-strain curve. For an uniaxial specimen, equation (1) reduces to

$$\frac{3}{2}(\dot{\varepsilon}_{axial} - \dot{\varepsilon}_{transverse}) = \frac{2}{3}\,\frac{(1 + \nu)}{E}\,\dot{\sigma}_e + f(\sigma_e)\,\sigma_e\dot{\sigma}_e \tag{4}$$

in the plastic range. Thus,

$$f(\sigma_e) = \frac{2}{3}(\dot{\varepsilon}_{axial} - \dot{\varepsilon}_{transverse})/\sigma_e\dot{\sigma}_e \tag{5}$$

Invoking incompressibility (i.e., $\dot{\varepsilon}_{transverse} = -\frac{1}{2}\,\dot{\varepsilon}_{axial}$), the function $f(\sigma_e)$ can be written as

$$f(\sigma_e) = \dot{\varepsilon}_{plastic}/\sigma_e\dot{\sigma}_e \tag{6}$$

If the uniaxial stress-strain curve is expressed in a multi-linear fashion as shown in Figure 1, the stress-strain relation is

$$\varepsilon = \frac{\sigma}{E} + \frac{\alpha_1}{E}(\sigma_1 - \sigma_y) + \frac{\alpha_2}{E}(\sigma_2 - \sigma_y) + \ldots + \frac{\alpha_m}{E}(\sigma - \sigma_m) \tag{7}$$

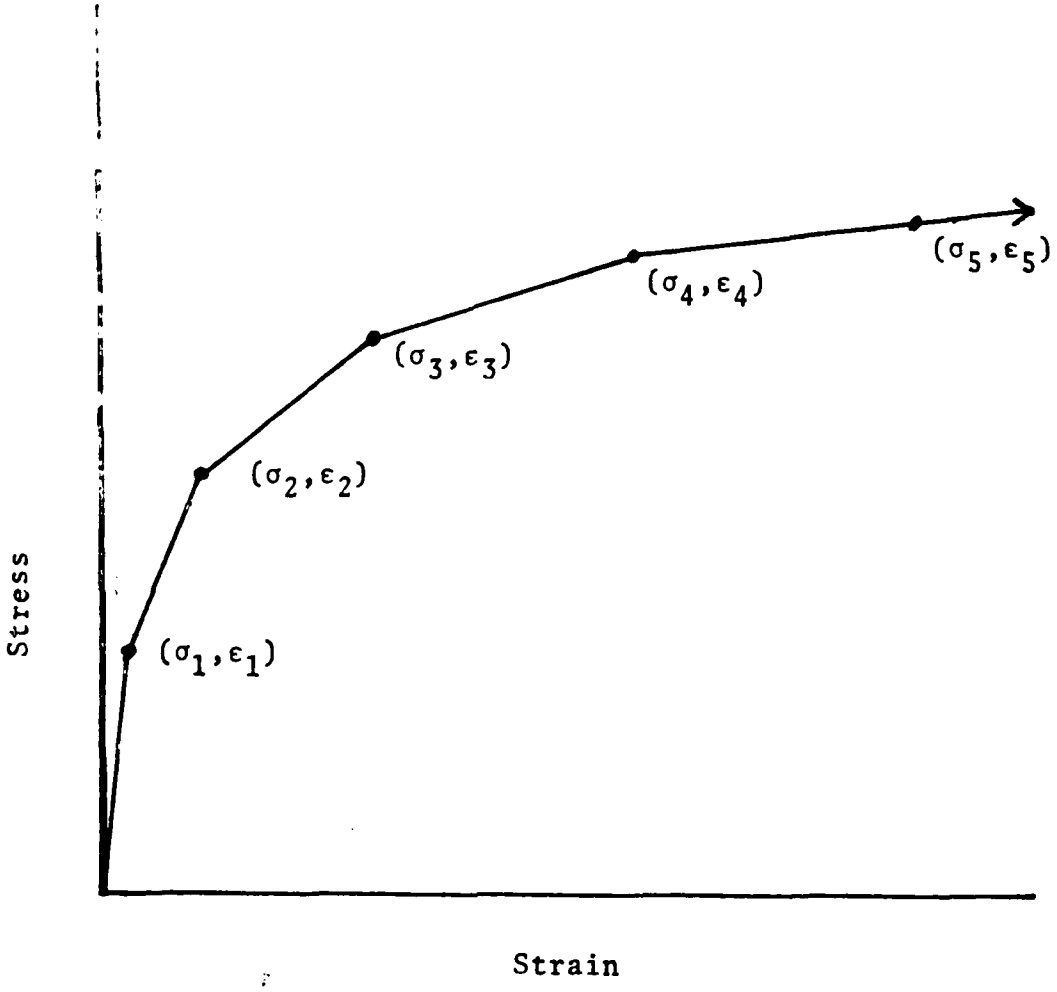

Figure 1: Multilinear Approximation For A Uniaxial Stress-Strain Curve With Hardening.

where $\sigma_{m-1} < \sigma < \sigma_m$ and α_m is given by

$$\alpha_m = \frac{E\Delta\epsilon_m - \Delta\sigma_m}{\Delta\sigma_m} \tag{8}$$

From equation (7), the plastic strain rate is given by

$$\dot{\epsilon}_{plastic} = \frac{\alpha_m \dot{\sigma}_e}{E} \tag{9}$$

and thus from (6)

$$f(\sigma_e) = \frac{\alpha_m}{E\sigma_e} \tag{10}$$

Equations (1), (2), (3) and (10) provide a complete set of elastic-plastic constitutive relations. Together with the equilibrium equations and the strain-displacement relations, a governing system will be formed. It is important to note that the constitutive formulation outlined above is acceptable for finite as well as infinitesimal strains. Also of importance is the fact that this formulation is strain-rate independent. This assumption appears to be realistic for most engineering metals at room temperature (or cooler). For high temperature problems a rate-independent formulation is dubious.

FINITE ELEMENT STRESS ANALYSIS

Equations (1), (2), (3) and (10) provide the fundamental relationships between stress and strain rates. The equilibrium conditions (governing equations) for a continuum body in the absence of body forces and inertia effects can be written as

$$\partial \dot{\sigma}_{ij}/\partial x_j = 0 \tag{11}$$

with the boundary conditions

$$\dot{\sigma}_{ij} n_j = \dot{T}_i \text{ on } S_T$$

and (12)

$$\dot{u}_i = \mathring{u}_i \text{ on } S_u$$

where $\dot{T}_i$ are the specified loading rates on the boundary experiencing applied tractions (S_T) and $\mathring{u}_i$ are the velocities specified on the remainder of the boundary (S_u). Utilizing the standard strain-displacement relations*

$$\epsilon_{ij} = \frac{1}{2}(\partial u_i/\partial x_j + \partial u_j/\partial x_i) \tag{13}$$

---

*The details of the analysis will be limited to infinitesimal strains for mathematical simplicity. The solution procedure with finite strains is identical, however, the notational complexities are considerable.

and either employing the Principle of Virtual Work for increments of displacement or by performing the standard Galerkin technique on the governing equations, (11) and (12), the finite element equations governing the nodal velocities, $\dot{\underset{\sim}{U}}$, can be written in terms of the loading rate vector, $\dot{\underset{\sim}{R}}$, in the form

$$\underset{\sim}{K}(\underset{\sim}{U}) \cdot \dot{\underset{\sim}{U}} - \dot{\underset{\sim}{R}} = 0 \tag{14}$$

The standard finite element assumptions made are given by

$$\begin{aligned} \underset{\sim}{u} &= \underset{\sim}{N} \cdot \underset{\sim}{U} \\ \dot{\underset{\sim}{\varepsilon}} &= \underset{\sim}{B} \cdot \dot{\underset{\sim}{U}} \\ \dot{\underset{\sim}{\sigma}} &= \underset{\sim}{D}(\underset{\sim}{U}) \cdot \dot{\underset{\sim}{\varepsilon}} \end{aligned} \tag{15}$$

$$\underset{\sim}{K}(\underset{\sim}{U}) = \sum_{\text{elements}} \int_{\text{element area}} \underset{\sim}{B}^T \underset{\sim}{D}(\underset{\sim}{U}) \underset{\sim}{B} \, dA$$

where $\underset{\sim}{N}$ are the shape functions and two dimensional analysis has been assumed (as implied by the area integral). The set of rate equations (14) will be integrated one load increment ($\Delta\underset{\sim}{R}$) at a given time to determine the corresponding new displacement increment, $\Delta\underset{\sim}{U}$. The Newton-Raphson or tangent stiffness solution procedure is employed. At load increment $L + 1$, the initial solution $\Delta\underset{\sim}{U}^i_{L+1}$ is found from

$$\underset{\sim}{K}(\underset{\sim}{U}_L) \cdot \Delta\underset{\sim}{U}^i_{L+1} = \Delta\underset{\sim}{R}_{L+1} \tag{16}$$

The "new" displacement is then used in the stiffness matrix, $K(U_L + \sum_{i=1}^{m} \Delta U^i_{L+1})$, and a new correction is obtained from

$$\underset{\sim}{K}\left[\underset{\sim}{U}_L + \sum_{i=1}^{m} \Delta\underset{\sim}{U}^i_{L+1}\right] \cdot \Delta\underset{\sim}{U}^{m+1}_{L+1} = \Delta\underset{\sim}{R}_{L+1} - \int_{U_L}^{U_L + \sum_{i=1}^{m} \Delta U^i_{L+1}} \underset{\sim}{K}(\underset{\sim}{U}) \, d\underset{\sim}{U} = \underset{\sim}{F}^{i+1}_{L+1} \tag{17}$$

where the integral is approximated using Simpson's rule. The procedure is repeated until two convergence criteria are met:

$$\left|\underset{\sim}{F}^{i+1}_{L+1}\right|^2 / \left|\Delta\underset{\sim}{R}_{L+1}\right|^2 \leq C_1$$

and (18)

$$\left|\underset{\sim}{F}^{i+1}_{L+1}\right|^2 / \left|\underset{\sim}{R}_{L+1}\right|^2 \leq C_2$$

where $\underset{\sim}{R}_{L+1}$ is the total load at step L + 1.

In this study, 20-node quadratic isoparametric elements were employed exclusively. All integration was carried out utilizing 3 x 3 x 3 Gauss-Legendre quadrature formulae. Strains were calculated at the Gauss integration points in each element from the strain-displacement relations of (13). Stresses were cumulatively calculated at the Gauss points from the stress-strain relations.

Directly calculating strains and stresses from the finite element relations (15) at points on element boundaries inherently yields poor results. This is especially true when C^0 shape functions are employed. A superior approach is to calculate the stresses and strains at the Legendre quadrature points and to extrapolate or smooth them to the boundaries. This approach has been shown to yield very accurate results for a wide variety of geometric mappings. In this study the smoothing technique as developed in [7] is employed for all stress and strain evaluations.

Currently, four methods of accounting for the crack tip singularity are widely employed. Each of these methods is based on an established technique in LEFM (Linear Elastic Fracture Mechanics). The first method, the enriched element approach (where the shape functions are modified with the asymptotic crack solution vanishing at the nodes) has been employed both for the multilinear stress-strain models and for power law hardening models [8]. Enriched elements based on the power law hardening model assume that the enriched

element is fully yielded. This assumption is physically unrealistic, especially behind the crack tip. The singular solution employed for the power law hardening case also assumes a circular yield zone which is far from realistic. The solutions generated using enriched elements and a multilinear stress-strain assumption are reasonably accurate providing a judicious choice of enriched element size and surrounding grid characteristics is made. The major drawback to the use of enriched elements is the computation time required to obtain convergence due to element incompatibility. The second method, the most basic approach, uses a very fine mesh near the crack tip and employs only conventional elements. This method produces reasonable results far from the crack region but questionable local results. Convergence is usually rapid, therefore, gross specimen behavior can be obtained quickly. With unrealistically fine grids, good local results can be obtained (except in the elements bordering the crack tip) but only at the expense of computer time [9]. The third method is based on the fact that if isoparametric elements are chosen with midside nodes, judicious choice of the placement of these nodes results in the inducement of a $\sqrt{r}$ term in the displacement shape functions [10, 11]. These elements are essentially equivalent to enriching the shape functions, however, element compatibility is preserved resulting in faster convergence. The fourth technique of modeling crack tip behavior is through the use of hybrid elements where elements bordering a surface

with traction boundary conditions are forced to satisfy those conditions exactly and the elements bordering a surface with displacement boundary conditions are also forced exactly. The element boundaries are then matched by using Lagrange multipliers in the variational equations to ensure element equilibrium and continuity in an approximate sense. Little work has been done on comparisons of hybrid methods to conventional methods in elastic-plastic crack problems, however, the technique was applied with questionable success in [12]. The preferred method in the literature is still to use a very fine mesh and standard elements. Complete discussions of the above methods can be found in [13-15].

In this study, only conventional 20-node elements are employed. Studies on linear elastic through-crack specimens has demonstrated the accuracy of this approach for predicting local stress responses. Since the details of the local singularity are unknown in the plasticity case, this approach is the most likely to delineate the characteristics of the numerical solution without the influence of singularity assumptions. The grid employed is shown in Figures 4a, 4b and 4c. The accuracy of the results predicted by this grid are discussed in [16] for the linear elastic case. The choice of grid characteristics is based on the convergence study cited above. Since there are no known three-dimensional elastic-plastic bench mark solutions available for comparison, linear convergence studies appear to be the most reliable

indicator of mesh accuracy. Few numerical solutions have been presented in the literature for three-dimensional elastic-plastic crack problems. The studies that have been done have been limited to initial stress approaches (e.g., [17]) or deformation theory approaches (e.g., [18]). These were severely limited in grid density due to computational restrictions, therefore, no comparison has been attempted. The computational requirements of the present approach are extreme and will be discussed subsequently.

PROBLEM DESCRIPTION AND FINITE ELEMENT MODELING

The problem chosen for study is that of a center-cracked plate with a through crack. The plate has dimensions of 7 inches in length, 3.5 inches in width with a thickness of .5 inches. The applied load is assumed to be normal to the crack orientation as shown in Figure 2 (i.e., Mode I loading). The material properties chosen are typical of many aluminum alloys. The assumed elastic properties are

$$E = 10.5\ E + 06\ PSI$$

$$\nu = 0.3$$

$$\sigma_y = 59.00\ E + 03\ PSI$$

The uniaxial stress-strain curve models the behavior of 7075-T7651 aluminum. A trilinear approximation is employed in the analysis. Both a typical experimental curve and the trilinear approximation are shown in Figure 3. The effect of hardening behavior modeling is studied by varying the hardening parameter β, defined in equation (3). Isotropic hardening ($\beta = 0$), kinematic hardening ($\beta = 1$) and a mixed state ($\beta = 0.5$) were modeled.

The finite element grid employed consists of 96 20-node isoparametric elements with quadratic shape functions. No "singular" elements are employed due to the unknown nature of the crack front singularity in plasticity. The grid is shown in Figures 4a, 4b and 4c. Computationally this grid is

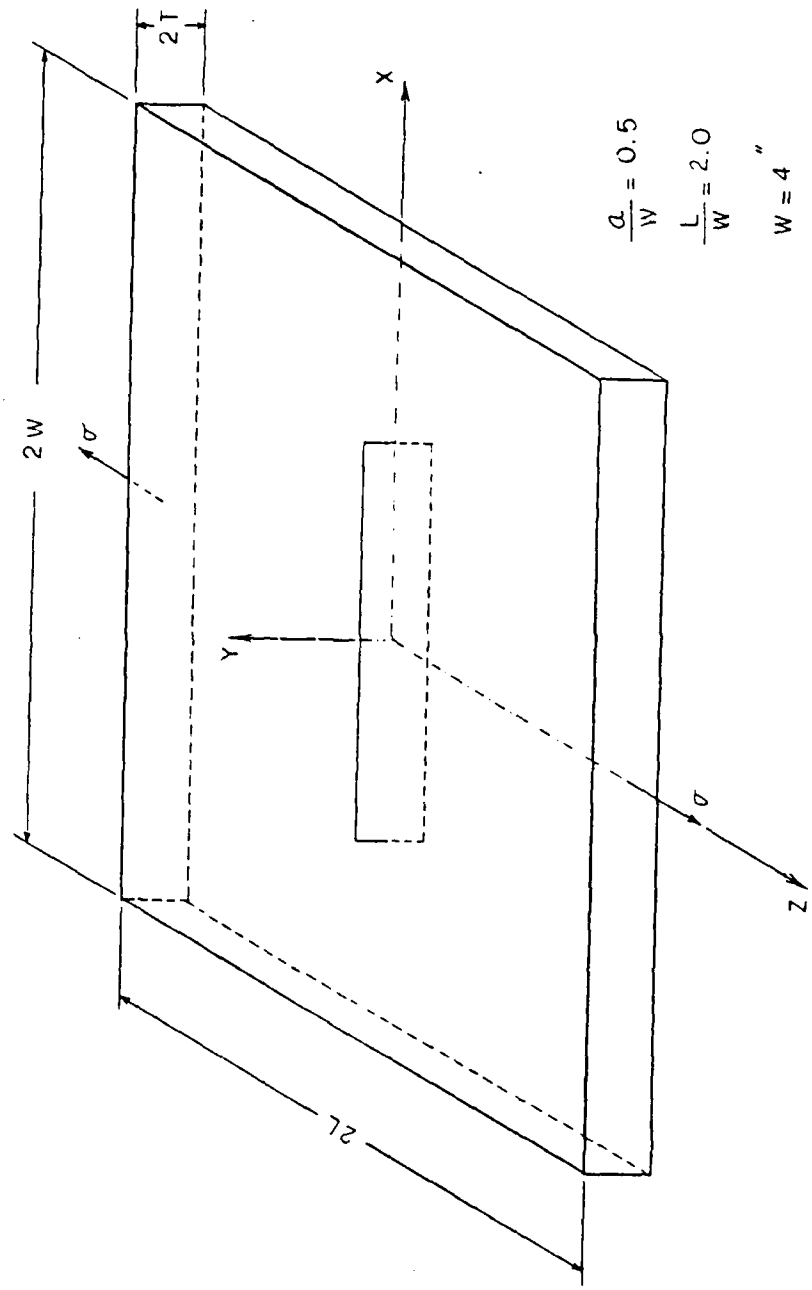

Figure 2: Through Crack Geometry And Loading.

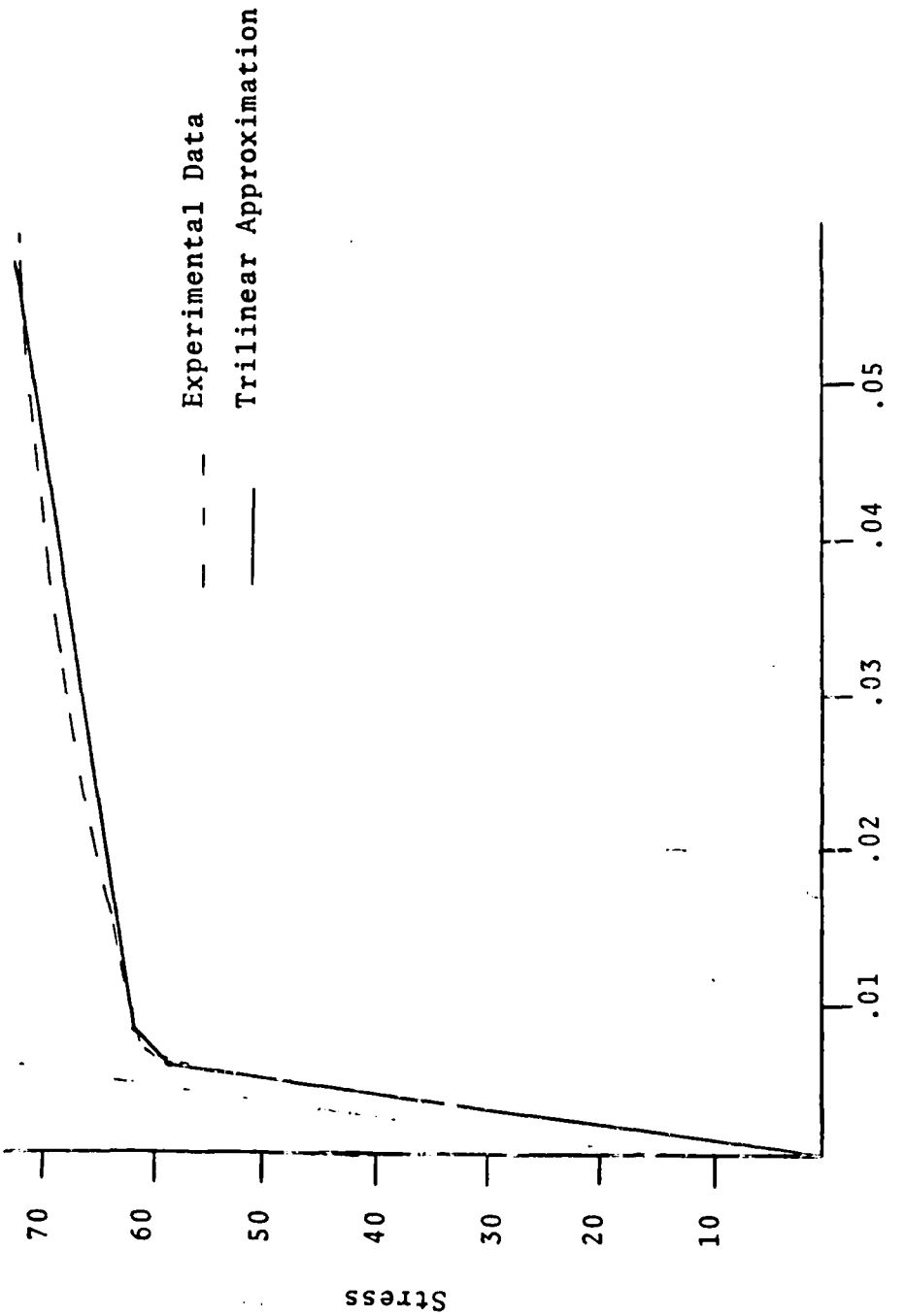

Figure 3: Uniaxial Stress-Strain Curve For 7075-T6751 Aluminum.

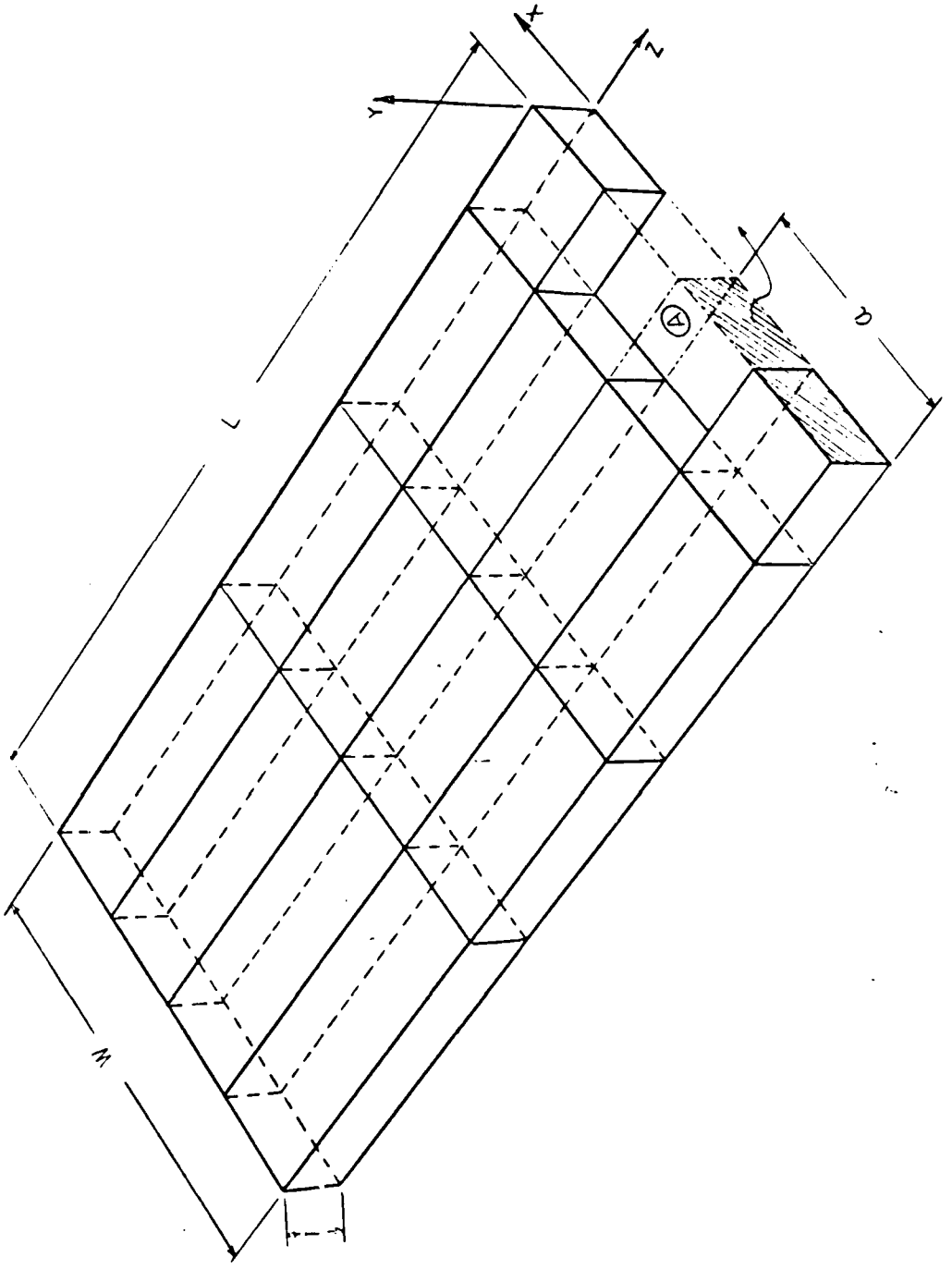

Figure 4a: Finite Element Grid - Coarse Outer Region.

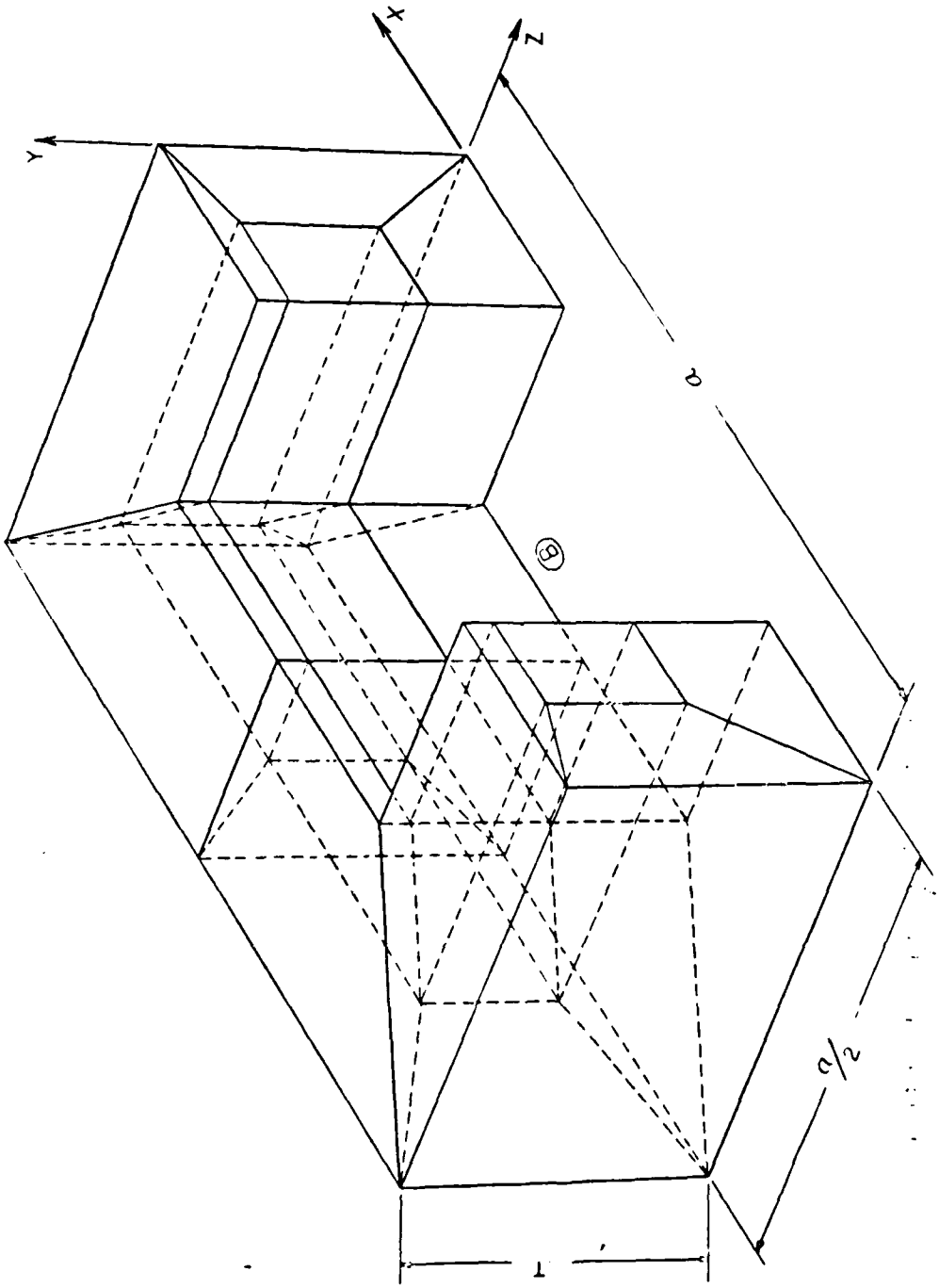

Figure 4b: Finite Element Grid - Blowup Of Region A.

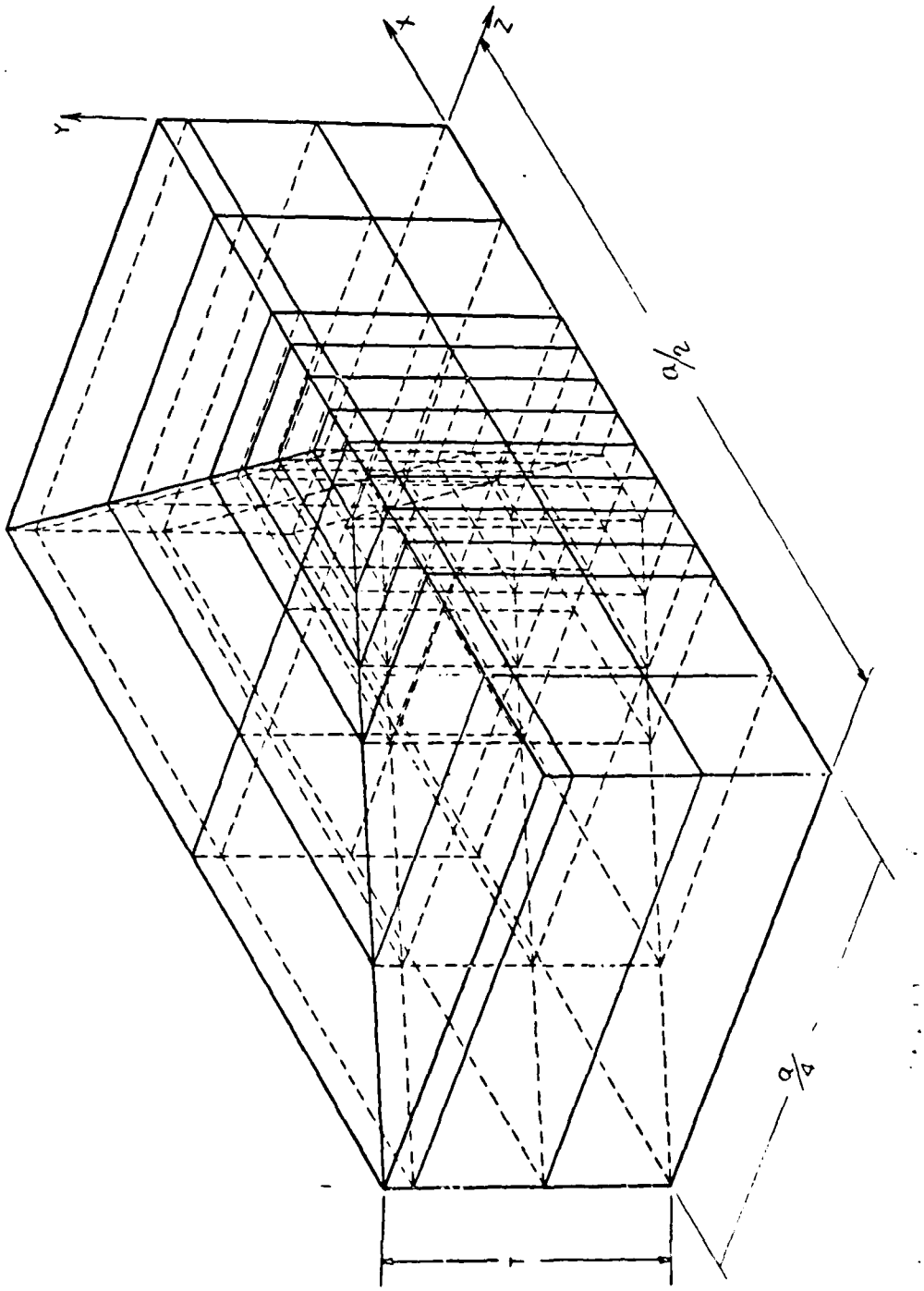

Figure 4c: Finite Element Grid - Near Tip Region B.

extremely expensive. The convergence studies cited previously have demonstrated the advantages and desirability of this approach. The grid has 1872 total degrees of freedom and requires approximately 1 hour and 13 minutes of CPU time on a VAX-11/780 to complete each iteration. Where significant plasticity occurred, extreme runtimes where required (often on the order of several days). While the current approach is believed to be very accurate and reproducing the necessary resolution to accurately describe the three-dimensional elastic-plastic crack phenomena, the complexity of the calculation and extreme computational requirements should be appreciated at the outset. Three-dimensional elastic studies have indicated that these computational requirements are necessary for accurate solution [7]. It is dubious that simpler approaches will be able to predict the local fields with any degree of confidence.

RESULTS AND DISCUSSION

The yield zones predicted at the maximum load for each of the three hardening models were calculated and plotted both on the free surface and on the midplane. The stress components were calculated in each element at the quadrature points and interpolated to the surfaces using the technique discussed previously.

Figure 5 is a plot of the von Mises stress contours predicted on the free surface at the maximum load assuming an isotropic hardening law. The maximum plastic radius predicted is 0.541 inches. The extent of the plastic zone ahead of the crack tip is 0.169 inches, predicting a fairly rotund zone. Figure 6 is a plot of the von Mises stress contours predicted on the free surface with a kinematic hardening model. The maximum plastic radius of 0.524 inches and crack line extent of 0.148 inches are both significantly less than predicted with isotropic hardening. The results assuming a mixed hardening model are shown in Figure 7. The maximum plastic radius of 0.544 inches is almost identical to the isotropic model. The crack line extent predicted, however, is much less than those predicted with either a kinematic or isotropic model. The predicted zone is much narrower than the other models demonstrate. It is unknown whether this phenomena is due to the inaccuracies of the numerical results or the physical assumptions. The narrower predicted yield zone is consistent

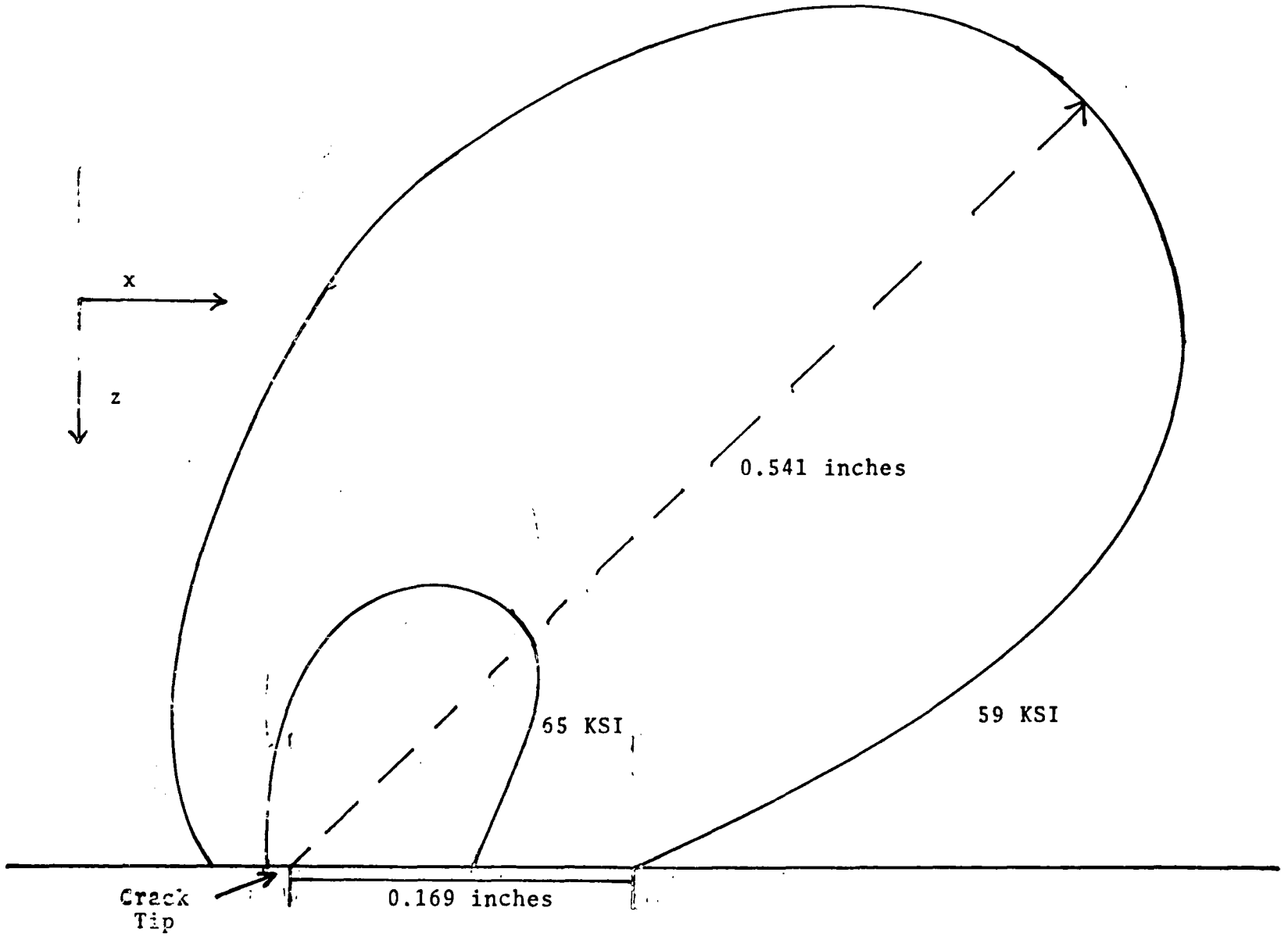

Figure 5: von Mises Stress Contours Near The Crack Tip On Specimen Surface At Maximum Load - Isotropic Hardening.

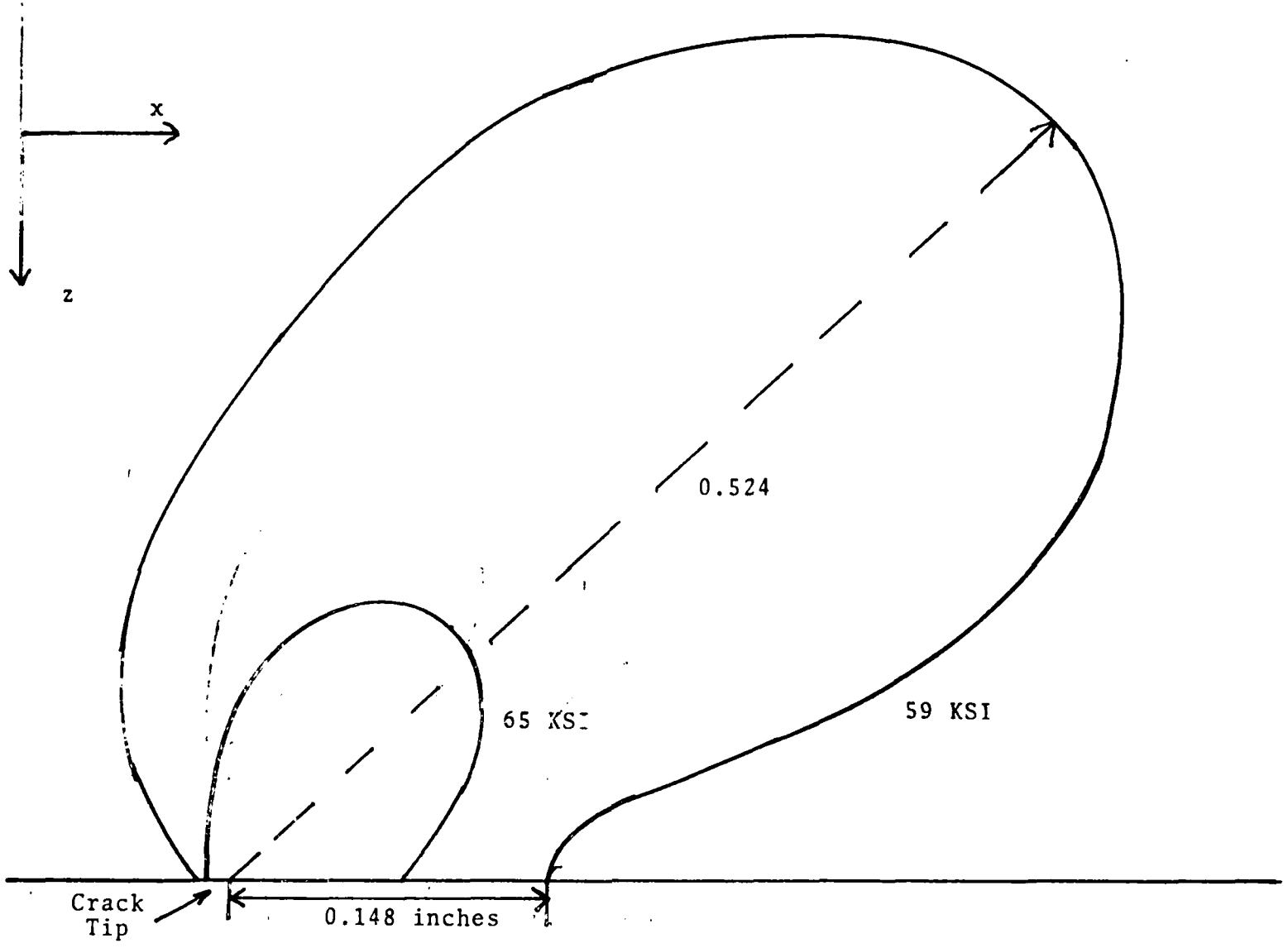

Figure 6: von Mises Stress Contours Near The Crack Tip On Specimen Surface At Maximum Load - Kinematic Hardening.

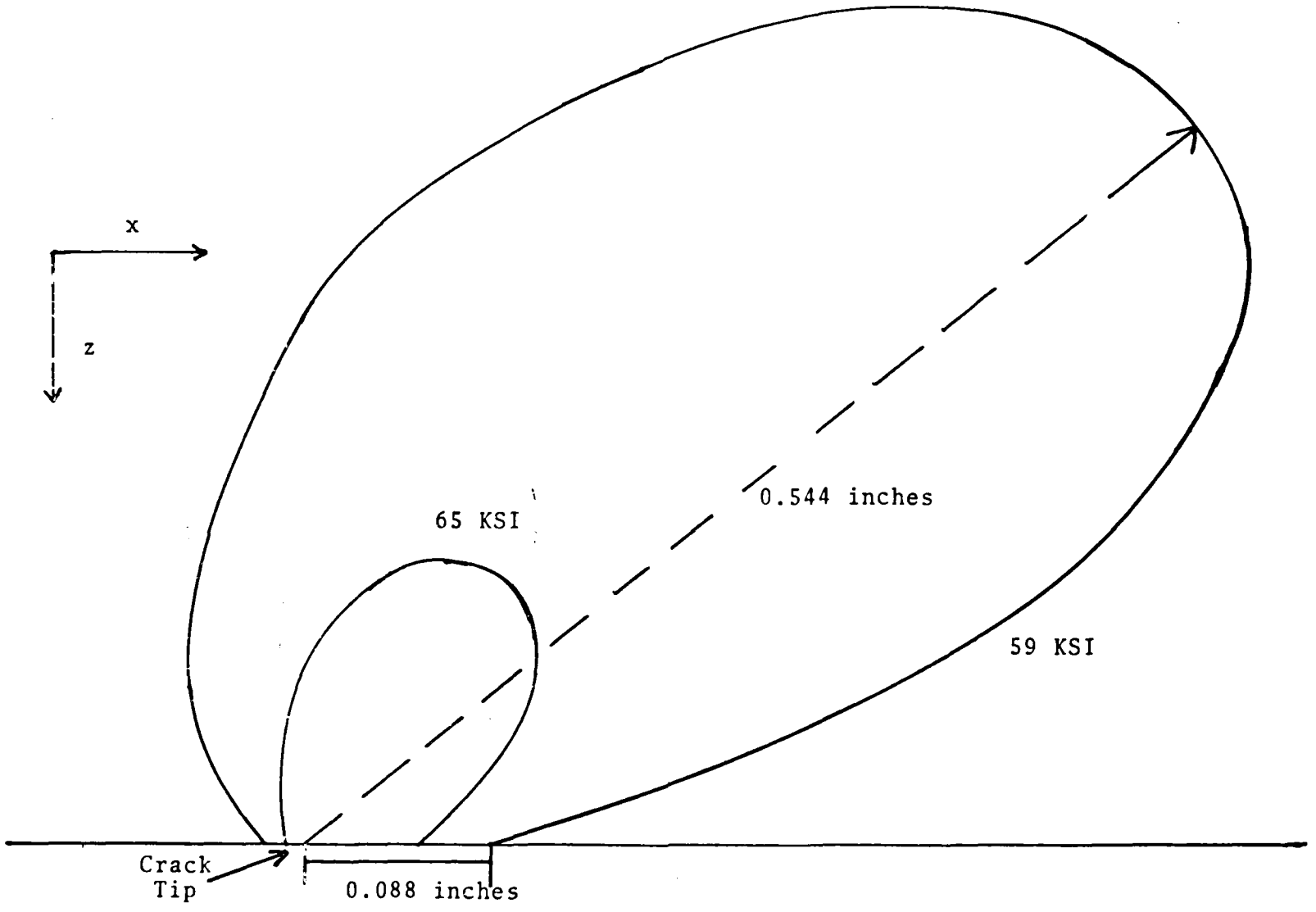

Figure 7: von Mises Stress Contours Near The Crack Tip On Specimen Surface At Maximum Load - Mixed Hardening.

with the dilatant stress field anticipated in front of the crack.

Figure 8 is a plot of the von Mises contours predicted on the midplane at the maximum load with an isotropic hardening model. As expected, the zone is smaller than the surface zone. The yielding along the crack line is, however, almost identical to the surface prediction. Figures 9 and 10 show the predicted midplane zones for the kinematic and mixed hardening assumptions. In both cases, the yielding extent ahead of the crack tip is very close to that predicted on the surface. The differences between the maximum radii of the predicted midplane zones are less than the surface zones. This phenomena is consistent with the smaller amount of plasticity and the nearly plane-strain conditions on the midplane.

One approach to predicting the extent of plastic deformation is to measure or calculate the amount of surface contraction or residual deformation on the surface after the specimen has been unloaded. Inside the plastic region measurable residual deformation should exist. Figure 11 is a plot of the surface contraction predicted after the specimen was unloaded to zero applied load assuming a kinematic hardening model. Contraction contours of 1.E-04 inches to 5.E-04 inches are shown. The lowest contour plotted (1.E-04 inches) is on the order of the deformation resolvable in the laboratory and is also on the anticipated accuracy of the finite element method being employed. The predicted plastic region is smaller than

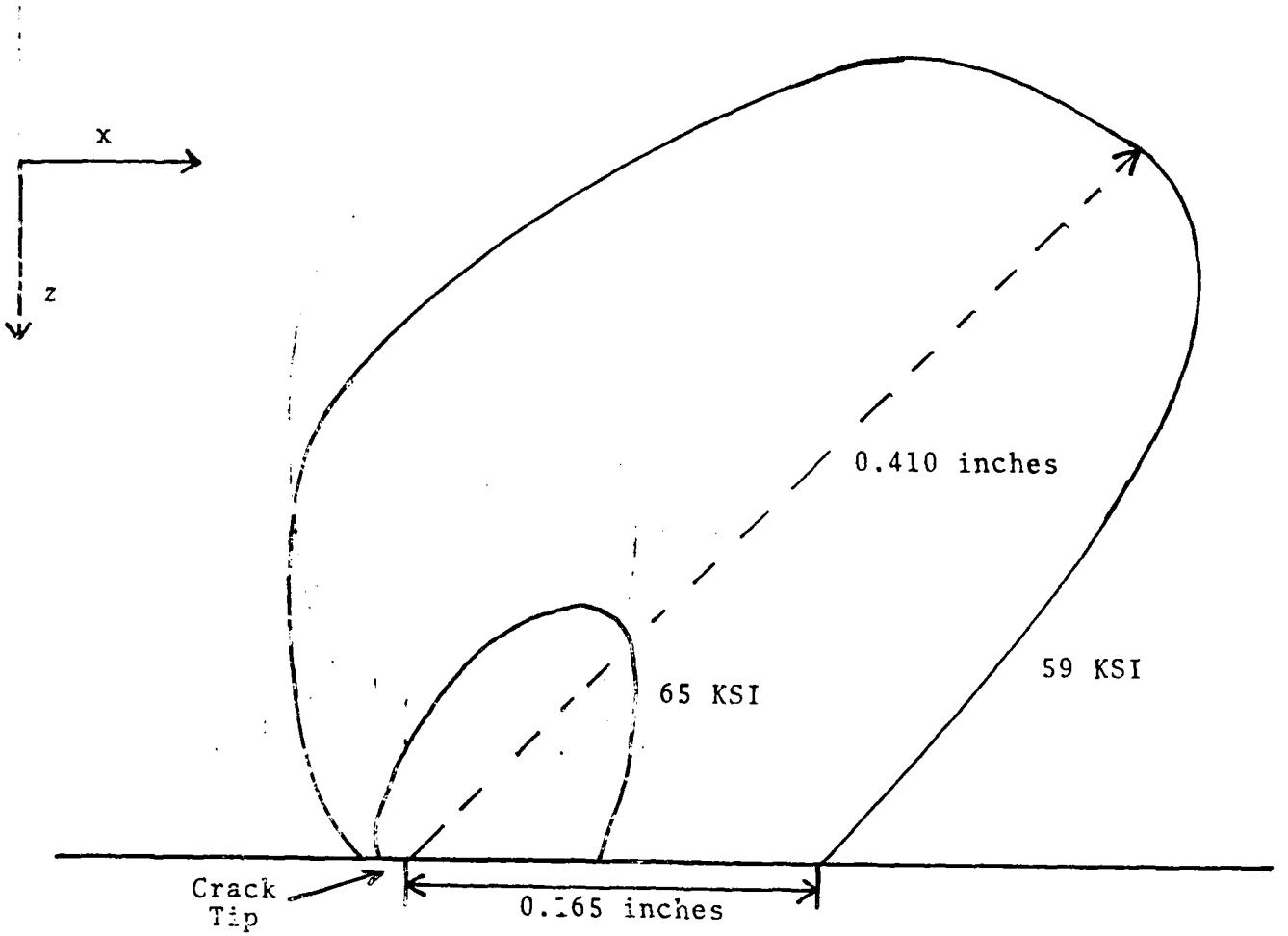

Figure 8: von Mises Stress Contours Near The Crack Tip On Specimen Midplane At Maximum Load - Isotropic Hardening.

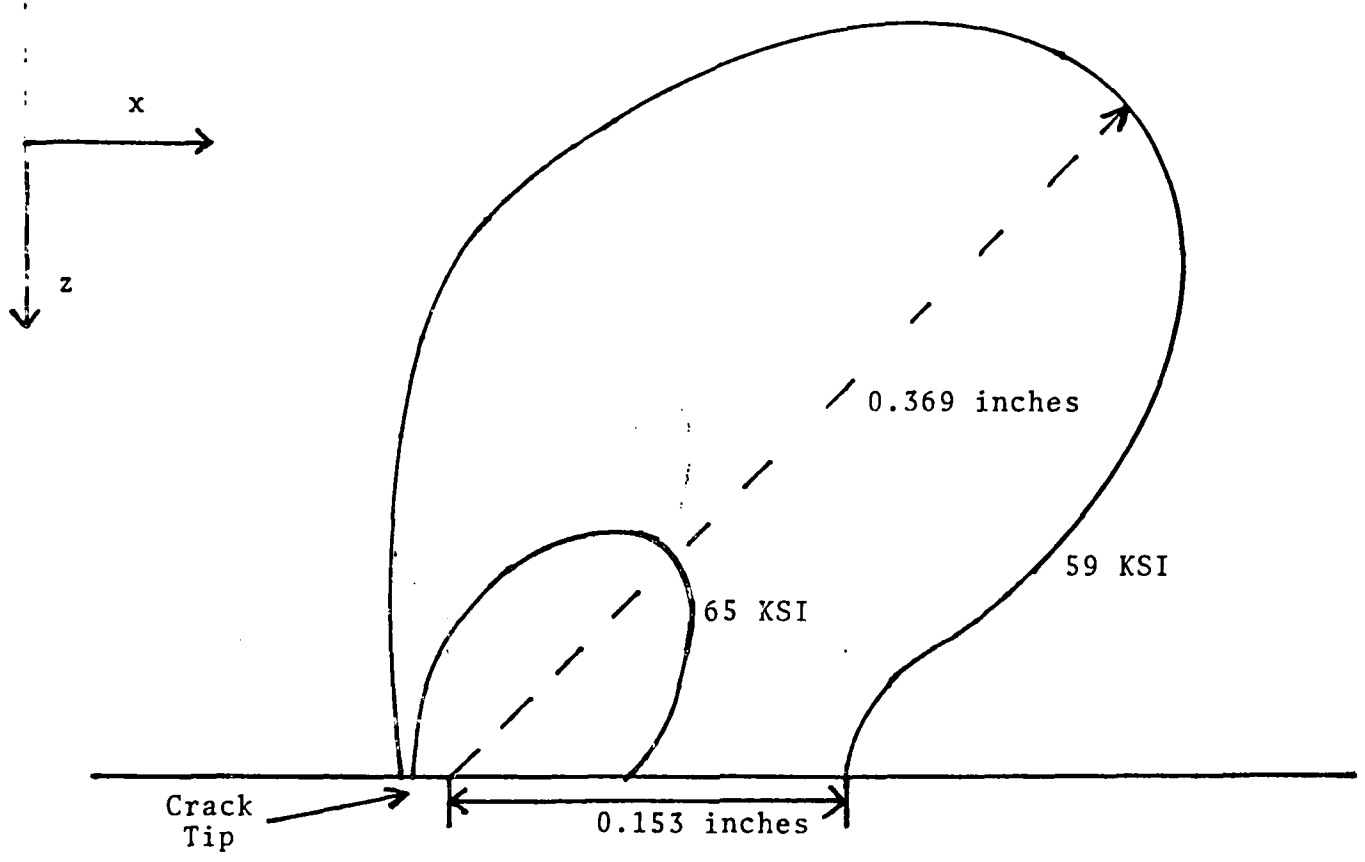

Figure 9: von Mises Stress Contours Near The Crack Tip On Specimen Midplane At Maximum Load - Kinematic Hardening.

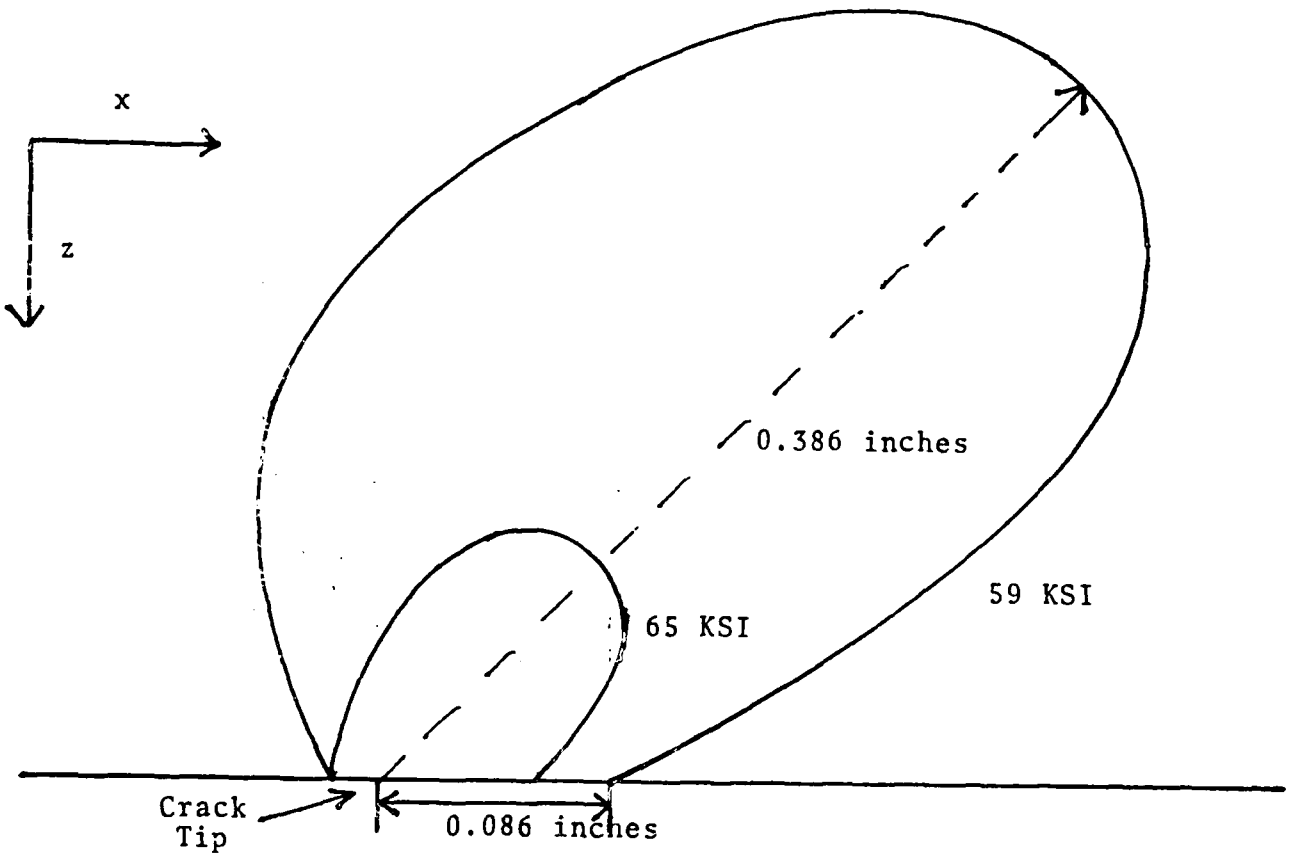

Figure 10: von Mises Stress Contours Near The Crack Tip On Specimen Midplane At Maximum Load - Mixed Hardening.

Figure 11: Surface Contractions Near Crack Tip After Unloading - Kinematic Hardening ($\times 10^{-4}$ inches).

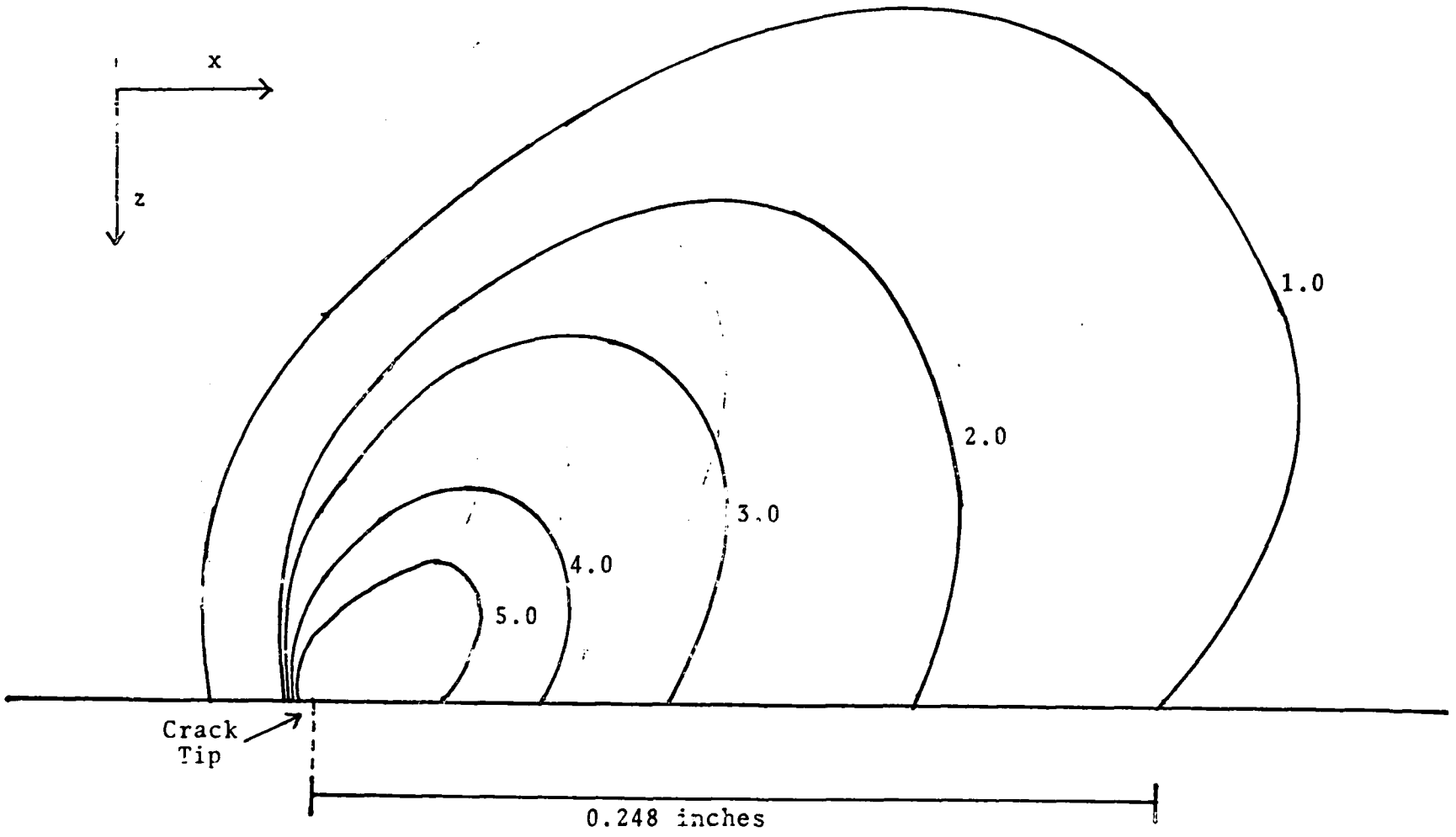

that predicted by the von Mises stress measure discussed above (Figure 6). This is not unexpected as the stress criterion is more sensitive to minimal plastic deformation. The yielded extent predicted ahead of the crack tip is larger, however, than predicted above. The deviation from a dilatational stress state ahead of the tip will be detected sooner by the residual deformation than by the effective stress (a large deviatoric stress field must be present to create a von Mises stress larger than the yield stress whereas any deviation in the neighborhood of a significant residual field will cause surface contractions). Figures 12 and 13 are plots of the surface contours predicted with isotropic and mixed hardening models. Consistent with the von Mises stress predictions, the zones with an isotropic model are larger than those predicted with any of the other models. The mixed hardening model predicts zones which are similar to the isotropic zones with less yielding directly ahead of the crack tip. All three models demonstrate more residual deformation ahead of the tip than would be expected from the stress results.

Figure 12: Surface Contractions Near Crack Tip After Unloading - Isotropic Hardening ($\times 10^{-4}$ inches).

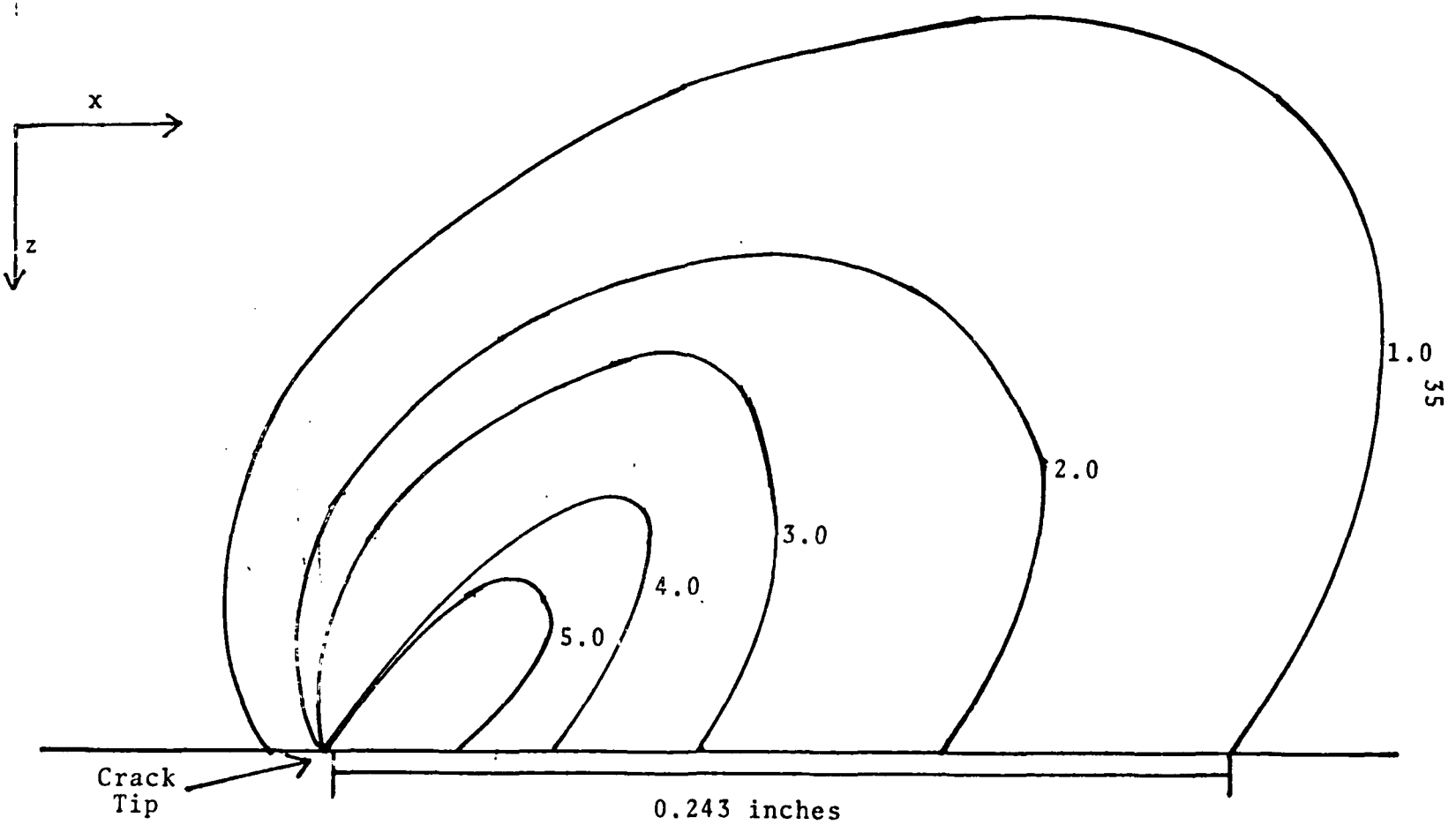

Figure 13: Surface Contractions Near Crack Tip After Unloading - Mixed Hardening ($\times 10^{-4}$ inches).

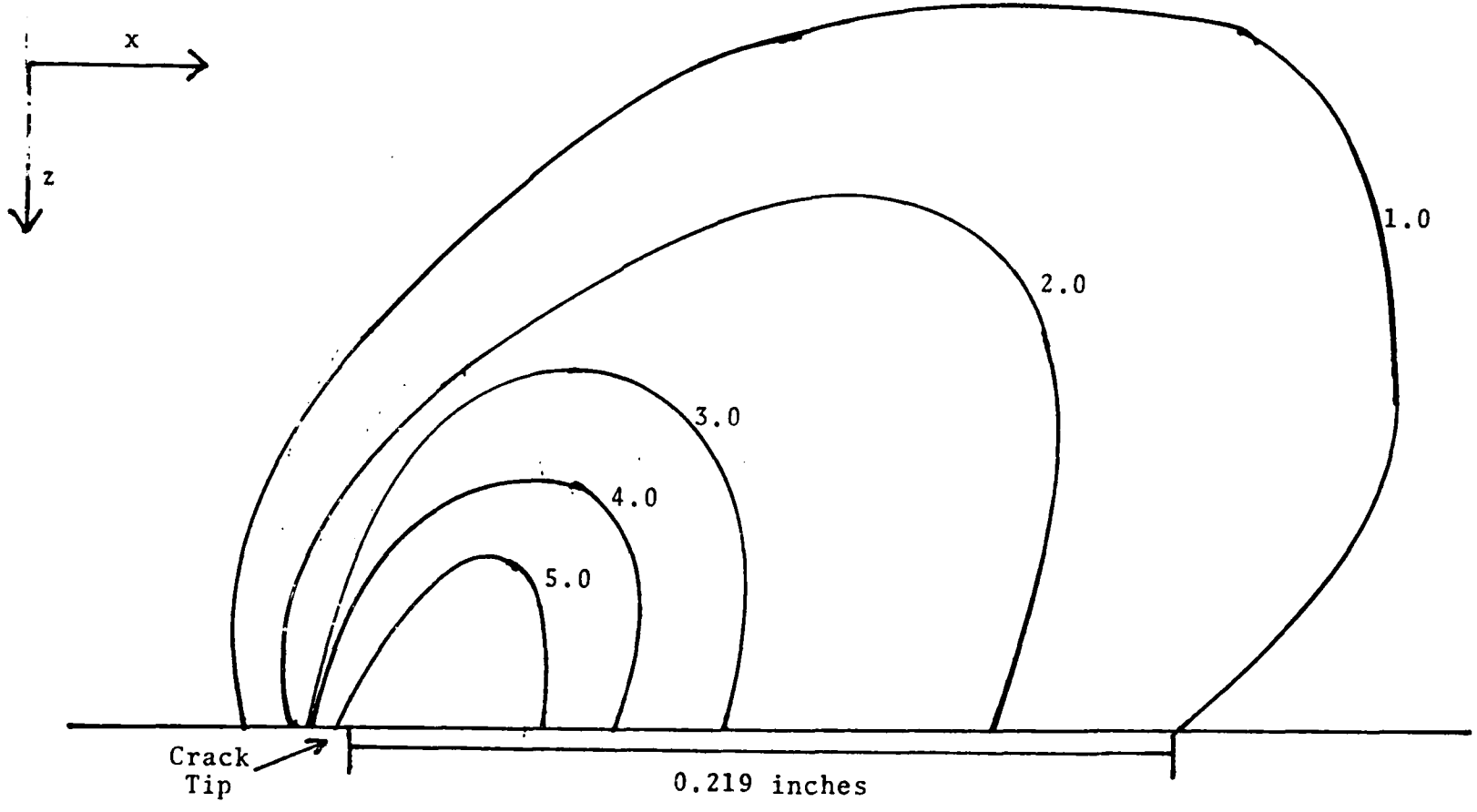

CONCLUSIONS

The finite element formulation for general three-dimensional elastic-plastic bodies undergoing infinitesimal deformation has been presented. A computer code has been developed and an example crack problem was solved with three widely employed hardening models. The crack front yield zones predicted are very similar in size and shape. For many applications, the differences may be negligible. Significant variation in crack line extent yielding and surface curvature was discovered. It is unknown at present as to which model will more accurately describe different metals of interest to engineers. The predicted differences are so slight, however, that full three-dimensional experimental studies will be needed to discern a valid model for specific applications.

To compare theoretical and experimental predictions, it is proposed to measure the residual deformation on the surface of the specimen in the unloaded state. The theoretical study presented above demonstrates that the finite element predictions are qualitatively realistic and sensitive to hardening characteristics. Comparison with experimental results will delineate the grid characteristics and hardening models which best model specific geometric and material applications. After successful "tuning" of the finite element model, a complete description of the stress and energy state in a cracked body can be predicted with confidence. Once fully three-

dimensional stress fields are predicted, ductile failure theories can be tested and skeptically compared without the bias of unrealistic analytical approximations.

ACKNOWLEDGEMENTS

This work was sponsored by the Office of Naval Research under Contract Number: N00014-75-C-0946.

REFERENCES

[1] G. C. Sih and R. J. Hartranft, "The Use Of Eigen-Function Expansions In The General Solution Of Three-Dimensional Crack Problems," Journal of Mathematics and Mechanics, Vol. 19, No. 2, 1969, pp. 123-138.

[2] S. W. Key, "A Finite Element Procedure For Large Deformation Dynamic Response Of Axisymmetric Solids," Computer Methods In Applied Mechanics And Engineering, Vol. 4, 1974, pp. 195-218.

[3] W. T. Koiter, "Stress-Strain Relations, Uniqueness, And Variational Theorems For Elastic-Plastic Materials With Singular Yield Surface," Quarterly Applied Mathematics, Vol. 11, 1953, pp. 350-354.

[4] P. G. Hodge and G. N. White, "A Quantitative Comparison Of Flow And Deformation Theories Of Plasticity," Journal of Applied Mechanics, Vol. 17, 1950, pp. 180-184.

[5] D. G. H. Latzgo (ed.), Post Yield Fracture, Applied Science, Ltd., New York, 1979.

[6] L. M. Kachanov, Foundations Of The Theory Of Plasticity, North-Holland Publishing Co., 1971.

[7] E. T. Moyer, Jr., "A Brief Note On The 'Local Least Squares' Stress Smoothing Technique," Accepted For Publication in Engineering Fracture Mechanics, 1982.

[8] P. D. Hilton and L. N. Gifford, "Evaluation Of Some Crack Tip Finite Elements For Elastoplastic Fracture Analysis," DTNSRDC Report 79/052, July 1979.

[9] W. K. Wilson and J. O. Osias, "A Comparison Of Finite Element Solutions For An Elastic-Plastic Crack Problem," International Journal Fracture, Vol. 14, 1978, R95-R108.

[10] S. L. Pu and M. A. Hussain, "The Collapsed Cubic Isoparametric Element As A Singular Element For Crack Problems," International Journal Numerical Methods Of Engineering, Vol. 12, 1978, pp. 1727-2742.

[11] S. E. Benzley, "Nonlinear Calculations With A Quadratic Quarter-Point Crack Tip Element," International Journal Fracture, Vol. 12, 1976, pp. 475-477.

[12] S. N. Atluri and K. Katherisan, "3-D Analysis Of Surface Flaws In Thick Walled Reactor Pressure-Vessels Using Displacement-Hybrid Finite Element Method," Nuclear Engineering Design, Vol. 51, 1979, pp. 163-176.

[13] O. C. Zienkiewicz, The Finite Element Method, McGraw-Hill, New York, 1977.

[14] J. T. Oden, Finite Elements Of Nonlinear Continua, McGraw-Hill, New York, 1972.

[15] A. J. Fawkes, D. R. J. Owen and A. R. Luxmoore, "An Assessment Of Crack Tip Singularity Models For Use With Isoparametric Elements," Engineering Fracture Mechanics, Vol. 11, 1979, pp. 143-159.

[16] E. T. Moyer, Jr. and H. Liebowitz, "Comparative Study On Three-Dimensional Crack Tip Modeling Methodology." To be presented at the International Conference on Application Of Fracture Mechanics To Materials And Structures, Freiburg, Germany, June 20-24, 1983.

[17] G. C. Sih and B. V. Kiefer, "Nonlinear Response Of Solids Due To Crack Growth And Plastic Deformation," International Nonlinear And Dynamic Fracture Mechanics, ASME AMD, Vol. 35, 1979, pp. 135-156.

[18] O. C. Zienkiewicz, "Viscoplasticity, Plasticity, Creep, And Viscoplastic Flow." Proceedings of the International Conference On Computational Methods of Nonlinear Mechanics, University of Texas, 1974.

APPENDIX C:

"Effect of Specimen Thickness on Crack Front Plasticity Characteristics in Three-Dimensions," E. T. Moyer, Jr. and H. Liebowitz. Presented at the Sixth International Conference on Fracture, New Delhi, India, December, 1984.

EFFECT OF SPECIMEN THICKNESS ON CRACK FRONT PLASTICITY CHARACTERISTICS IN THREE-DIMENSIONS

E. Moyer, Jr. and H. Liebowitz

School of Engineering and Applied Science, The George Washington University, Washington, D.C.

ABSTRACT

A finite element investigation of the effect of thickness on plastic deformation and yielding characteristics in three-dimensional cracked bodies is presented. It is shown that the fundamental deformation modes and extent of plastic deformation are significantly influenced by the specimen thickness. The results show the transition from a local plane strain to plane stress response near the crack front as the specimen thickness is decreased. While the results are generated for a specific aluminum alloy (7075-T7651), the predictions for other hardening materials would be qualitatively the same.

KEYWORDS

Nonlinear finite-element calculations, plastic deformation, three-dimensional crack specimens, incremental analysis.

INTRODUCTION

Of fundamental importance to the accurate fracture assessment of components and structures made of metals is the study of ductile fracture processes and the plastic response near a crack. The basic deformation response near the crack front must be resolved accurately for reliable predictions. Fracture criteria have been proposed based on many controlling quantities (e.g., stress, strain, energy, displacements, etc.) both on global and local scale levels. Without exception, all of these criteria require accurate local deformation modeling.

To understand the scale shifting effects from the laboratory specimen to the structural component, it is imperative to discover the effects of specimen thickness on the deformation response. This problem is an essentially three-dimensional one and must be investigated accordingly.

The purpose of this investigation is to delineate the effect of specimen thickness on local crack front yielding characteristics in a cracked specimen. The three-dimensional elastic plastic finite element code developed in [1] is employed for the analysis. Specimen thicknesses investigated range

from well beyond ASTM plane-strain requirements to thin sheet dimensions. The yield zones calculated in this work demonstrate the transition from dilatational to distortional dominance ahead of the crack tip as a function of thickness (equivalent to a transition from plane strain to plane stress). The magnitude as well as the extent of yielding is shown to be highly thickness dependent. The results of this study also demonstrate that two-dimensional analysis based on plane strain (for thick specimens) or plane stress (for thin specimens) can fail to accurately model the local response when simple standards would dictate otherwise.

PLASTICITY FORMULATION

The incremental theory of plasticity employed in this work is based on the classical rate proportionality assumptions and J_2 flow theory. While the mathematical details vary with the choice of yield criteria, the salient features of all incremental theories are the same. This discussion will, therefore, be confined to the specific theory employed in this work.

Assuming stress strain rate proportionality and J_2 flow theory (which assumes the plastic deformations are incompressible) the stress-strain rate relations can be written as [2]

$$\dot{e}_{ij} = \begin{cases} \frac{1+\nu}{E}\dot{S}_{ij} + \frac{3}{2} f(\sigma_e)\, S'_{ij}\dot{\sigma}_e & \sigma_e = \sigma_y;\ \dot{\sigma}_e > 0 \\ \frac{1+\nu}{E}\dot{S}_{ij} & \text{Otherwise} \end{cases} \tag{1}$$

where:

$\dot{e}_{ij} = \dot{\varepsilon}_{ij} - \frac{1}{3}\dot{\varepsilon}_{pp}\,\delta_{ij}$ are the deviatoric strain rate components,
ν is Poisson's ratio,
E is Young's modulus,
$S_{ij} = \sigma_{ij} - \frac{1}{3}\sigma_{pp}\,\delta_{ij}$ are the deviatoric stress components,
a_{ij} are the coordinates in stress space of the yield surface center
$S'_{ij} = S_{ij} - a_{ij}$ are the deviatoric stress components measured relative to the current yield center,
$\sigma_e = \sqrt{\frac{3}{2} S_{ij}S_{ij}}$ is the effective stress,
$\sigma'_e = \sqrt{\frac{3}{2} S'_{ij}S'_{ij}}$ is the effective stress relative to the current yield center,
σ_y is the current yield stress, and
$\dot{}$ denotes time differentiation.

Due to the incompressibility condition, the hydrostatic strain rate is proportional to the mean stress rate and is given by

$$\dot{\varepsilon}_{pp} = \frac{1-2\nu}{E}\dot{\sigma}_{pp} \tag{2}$$

The function $f(\sigma_e)$ is dependent on the uniaxial stress-strain curve and will be discussed subsequently. For a von Mises (J_2) material, the center of the yield surface moves at a rate proportional to the projection of the stress rate vector onto the local normal to the current yield surface and can be written as

$$a_{ij} = \begin{cases} \frac{3}{2}(1-\beta)\, S'_{kl}\dot{S}_{kl}S'_{ij}/\sigma_e'^2 & \sigma_e = \sigma_y;\ \dot{\sigma}_e > 0 \\ 0 & \text{Otherwise} \end{cases} \tag{3}$$

where β varying from 0 to 1 will model hardening behavior from kinematic ($\beta = 0$) to isotropic ($\beta = 1$).

The function $f(\sigma_e)$ is derived from the uniaxial stress-strain curve. For a uniaxial specimen, equation (1) reduces to

$$\frac{3}{2}(\dot{\varepsilon}_{axial} - \dot{\varepsilon}_{transverse}) = \frac{2}{3}\left(\frac{1+\nu}{E}\right)\dot{\sigma}_e + f(\sigma_e)\,\sigma_e\dot{\sigma}_e \tag{4}$$

in the plastic range. Thus,

$$f(\sigma_e) = \frac{2}{3}(\dot{\varepsilon}_{axial} - \dot{\varepsilon}_{transverse})/\sigma_e\dot{\sigma}_e \tag{5}$$

Invoking incompressibility (i.e., $\dot{\varepsilon}_{transverse} = -\frac{1}{2}\dot{\varepsilon}_{axial}$), the function $f(\sigma_e)$ can be written as

$$f(\sigma_e) = \dot{\varepsilon}_{plastic}/\sigma_e\dot{\sigma}_e \tag{6}$$

If the uniaxial stress-strain curve is expressed in a multilinear fashion, the stress-strain relation is

$$\varepsilon = \frac{\sigma}{E} + \frac{\alpha_1}{E}(\sigma_1-\sigma_y) + \frac{\alpha_2}{E}(\sigma_2-\sigma_y) + \ldots + \frac{\alpha_m}{E}(\sigma-\sigma_m) \tag{7}$$

where $\sigma_{m-1} < \sigma < \sigma_m$ and α_m is given by

$$\alpha_m = \frac{E\Delta\varepsilon_m - \Delta\sigma_m}{\Delta\sigma_m} \tag{8}$$

From equation (7), the plastic strain rate is given by

$$\dot{\varepsilon}_{plastic} = \frac{\alpha_m\dot{\sigma}_e}{E} \tag{9}$$

and thus from (6)

$$f(\sigma_e) = \frac{\alpha_m}{E\sigma_e} \tag{10}$$

Equations (1), (2), (3) and (10) provide a complete set of elastic-plastic constitutive relations. Together with the equilibrium equations and the strain-displacement relations, a governing system will be formed. It is important to note that the constitutive formulation outlined above is acceptable for finite as well as infinitesimal strains. Also of importance is the fact that this formulation is strain-rate independent. This assumption appears to be realistic for most engineering metals at room temperature (or cooler). For high temperature problems a rate-independent formulation is dubious.

Equations (1), (2), (3) and (10) provide the fundamental relationships between stress and strain rates. The equilibrium conditions (governing equations) for a continuum body in the absence of body forces and inertia effects can be written as

$$\partial \dot{\sigma}_{ij}/\partial x_j = 0 \tag{11}$$

with the boundary conditions

$$\dot{\sigma}_{ij} n_j = \dot{T}_i \text{ on } S_T$$

and (12)

$$\dot{u}_i = \dot{\hat{u}}_i \text{ on } S_u$$

where $\dot{T}$ are the specified loading rates on the boundary experiencing applied tractions (S_T) and $\dot{\hat{u}}_i$ are the velocities specified on the remainder of the boundary (S_u). Utilizing the standard infinitesimal strain-displacement relations

$$\varepsilon_{ij} = \frac{1}{2}(\partial u_i/\partial x_j + \partial u_j/\partial x_i) \tag{13}$$

and either employing the Principle of Virtual Work for increments of displacement or by performing the standard Galerkin technique on the governing equations, (11) and (12), the finite element equations governing the nodal velocities, $\dot{\underset{\sim}{U}}$ can be written in terms of the loading rate vector, $\dot{\underset{\sim}{R}}$, in the form

$$\underset{\sim}{K}(\underset{\sim}{U}) \cdot \dot{\underset{\sim}{U}} - \dot{\underset{\sim}{R}} = 0 \tag{14}$$

The standard finite element assumptions made are given by

$$\begin{aligned} \underset{\sim}{u} &= \underset{\sim}{N} \cdot \underset{\sim}{U} \\ \dot{\underset{\sim}{\varepsilon}} &= \underset{\sim}{B} \circ \dot{\underset{\sim}{U}} \\ \dot{\underset{\sim}{\sigma}} &= \underset{\sim}{D}(\underset{\sim}{U}) \cdot \dot{\underset{\sim}{\varepsilon}} \end{aligned} \tag{15}$$

$$\underset{\sim}{K}(\underset{\sim}{U}) = \sum_{\text{elements}} \int_{\text{element volume}} \underset{\sim}{B}^T \underset{\sim}{D}(\underset{\sim}{U}) \underset{\sim}{B} \, dA$$

where N are the shape functions. The set of rate equations (14) will be integrated one load increment (ΔR) at a given time to determine the corresponding new displacement increment, ΔU. The Newton-Raphson or tangent stiffness solution procedure is employed as described in [3].

PROBLEM DESCRIPTION

To study the effects of specimen thickness on the yielding characteristics of typical fracture specimens, a finite center-cracked plate was chosen for investigation. The standard mode I configuration shown in Fig. 1 was analyzed for total thicknesses of

2T = 2.54 cm 2T = 1.27 cm
2T = 6.35 mm 2T = 3.175 mm

The material investigated was a 7075-T7651 aluminum alloy with elastic properties

$E = 7.24 \text{ E+04 MPa}$

$\nu = 0.3$

$\sigma_y = 4.07 \text{ E+02 MPa}$

The uniaxial stress-strain curve is shown in Fig. 2.

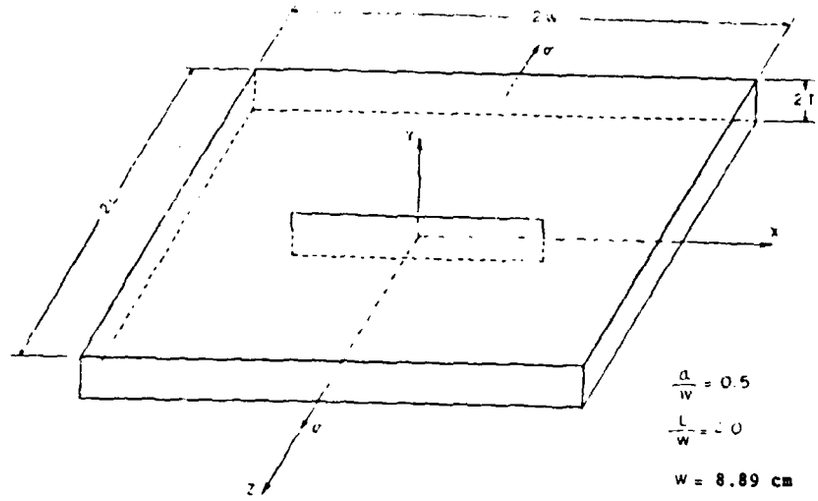

Fig. 1. Through crack geometry and loading.

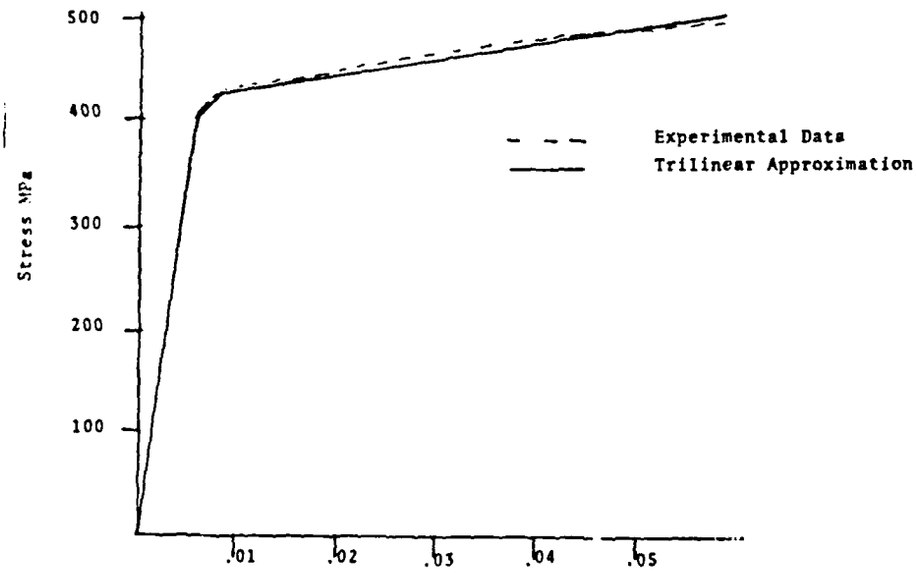

Fig. 2. Uniaxial stress-strain curve for 7075-T6751 aluminum.

The finite element discretization employed in the analysis utilizes 20-Node quadratic isoparametric elements exclusively. A fine mesh near the crack front is employed for accurate modeling. The grid characteristics and convergence properties are discussed in [1,4]. The maximum load applied was

$$\sigma_{max} = 1.77\ E{+}02\ MPa$$

A hardening parameter of $\beta = 0.5$ was also assumed in the analysis.

RESULTS AND DISCUSSION

The yield zones predicted at the maximum load for each of the four thicknesses studied were calculated and plotted both on the surface and midplane of the specimen. The results demonstrate the significant influence thickness has both on the nature and extent of the yielding.

Figure 3a is a plot of the von Mises stress contour corresponding to the specimen yield stress calculated at the maximum load on the surface of the 2.54 cm thick specimen. As expected for a thick specimen, this zone has the characteristic form of a plane strain yield zone (i.e., minimal yielding ahead of the crack tip and a very upright yield zone). The maximum extent of yielding is 30.7% of the half crack length which is consistent with the small strain assumptions made in the analysis requiring contained yielding. Figure 3b is a plot of the surface zones for a specimen with total thickness of 1.27 cm. The yield zone is slightly wider (more rounded) with this thickness. The maximum radius is now 32.7% of the half crack length and the yielding ahead of the tip has increased (though it is still small). The zone still maintains the basic plane strain characteristics at this thickness.

Figure 3c shows the surface yield zone for a specimen with thickness of 6.35 mm. The zone is now much wider with a larger maximum radius and yield extent ahead of the tip. The zone no longer exhibits the plane strain characteristics but is in transition between plane strain and plane stress. Figure 3d is a plot of the surface yield zone for a specimen with total thickness of 3.175 mm. The zone is significantly more rounded than any of the previous zones with a larger maximum radius and yield extent. The maximum yield radii and extent of yielding ahead of the crack tip for the four thickness surface zones are given in Table 1a. These yield parameters both increase with decreasing thickness as was expected. The final zone at a thickness of 3.175 mm has the rounded characteristic of a plane stress yield zone. The direction of maximum yielding, however, is still a fairly large angle relative to the crack line suggesting some influence of dilatation. Though for this problem (with a relatively small amount of plastic deformation present) the difference between the maximum radii is not large, the nature and extent of yielding ahead of the crack tip show a large dependence on the specimen thickness.

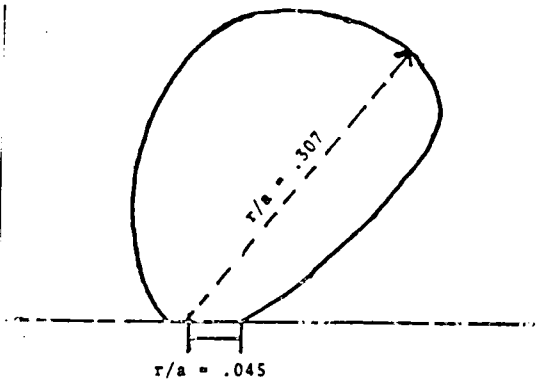

Fig. 3a. Surface yield zones for specimen with 2T = 2.54 cm.

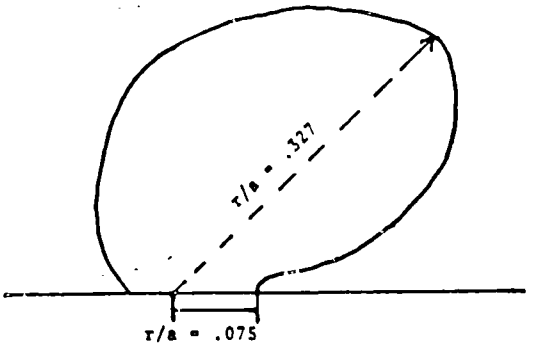

Fig. 3b. Surface yield zones for specimen with 2T = 1.27 cm.

Figure 4a is a plot of the von Mises stress contour corresponding to the material yield stress on the midplane of the 2.54 cmm thick specimen. The zone is typical of plane strain zones and is smaller than the surface zone for the same thickness specimen. The shape of the zone with a minimal extent of yielding ahead of the crack tip suggests high dilatation in that region. The midplane zone for the 1.27 cm thick specimen is shown in

Fig. 4b. The zone is larger than that of the thicker specimen, however, there is still minimal yielding ahead of the tip. The angle of maximum yielding is more acute than in the thicker specimen. The stress state, however, would still be characterized by plane strain.

Figure 4c shows the midplane yield zone for the 6.35 mm thick specimen. The zone is considerably wider and more rounded than for the thicker specimens. It shows characteristics of both plane strain and plane stress zones suggesting a region of transition. Figure 4d is a plot of the midplane yield zone for the 3.175 mm thick specimen. The zone is basically a plane stress zone and is larger than for the thicker specimens. The maximum yield radii and radius of yielding ahead of the crack tip on the specimen mid-planes are given in Table 1b. Both increase with decreasing thickness as was expected. In all cases, the midplane yield zones are smaller than the surface zones.

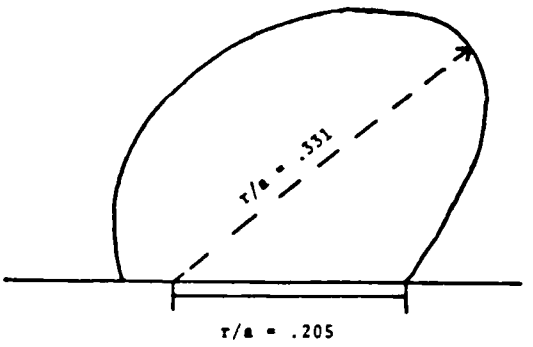

Fig. 3c. Surface yield zones for specimen with 2T = 6.35 mm.

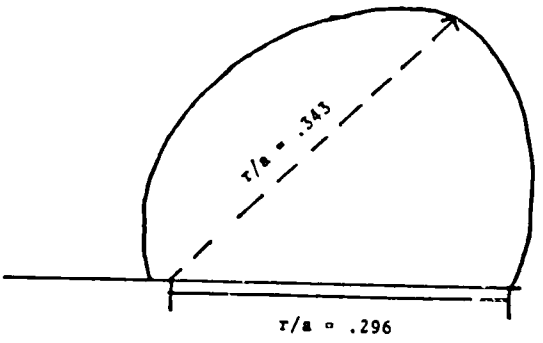

Fig. 3d. Surface yield zones for specimen with 2T = 3.175 mm.

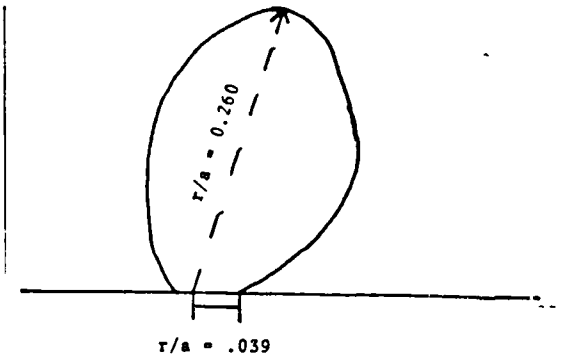

Fig. 4a. Midplane yield zones for specimen with 2T = 2.54 cm.

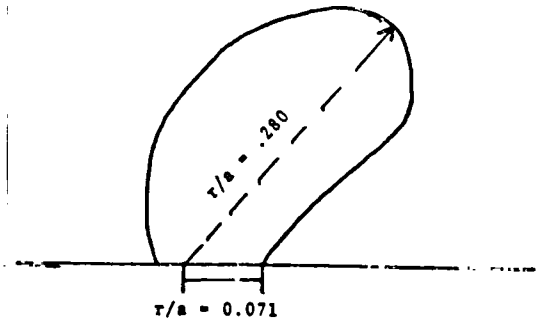

Fig. 4b. Midplane yield zones for specimen with 2T = 1.27 cm.

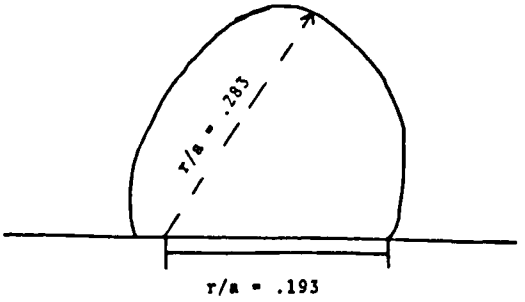

Fig. 4c. Midplane yield zones for specimen with 2T = 6.35 mm.

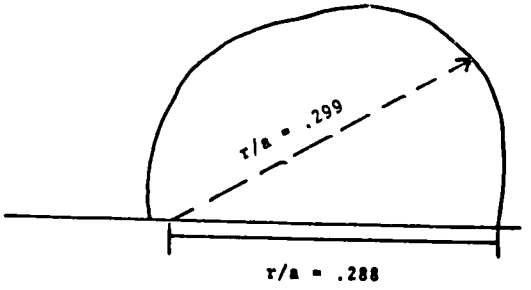

Fig. 4d. Midplane yield zones for specimen with 2T = 3.175 mm.

TABLE 1a Yield Radii as a function of Thickness for Surface Yield Zones.

Thickness	$r_{max/a}$	$r_{o/a}$
T = 2.54 cm	0.307	0.045
T = 1.27 cm	0.327	0.075
T = 6.35 mm	0.331	0.205
T = 3.175 mm	0.343	0.296

r_{max} → maximum yield radius

TABLE 1b Yield Radii as a Function of Thickness for Midplane Yield Zones.

Thickness	$r_{max/a}$	$r_{o/a}$
T = 2.54 cm	0.260	0.039
T = 1.27 cm	0.280	0.071
T = 6.35 mm	0.283	0.193
T = 3.175 mm	0.299	0.288

r_o → yield radius along crack line

CONCLUSIONS

The results of this study demonstrate the thickness dependence of the yield zones near a crack front on specimen thickness. It is shown that both the extent of plastic deformation and the dominance of deformation type (i.e., dilatation or distortion) are controlled by the thickness. The nature of the deformation is fundamental to the understanding of the incipient fracture processes. The delineation of the fundamental deformation response near a three-dimensional crack front is an imperative first step in the understanding and accurate prediction of ductile fracture processes.

To further the understanding of ductile fracture, it is necessary to compare theoretical and experimental deformation predictions local to the crack front. Only through such comparisons can an assessment be made of the accuracy and reliability of the numerical methods for plastic analysis. Toward this goal, it is proposed to measure the residual deformation on the surface of the specimen in the unloaded state. The theoretical study presented above demonstrates that the finite element predictions are qualitatively realistic and sensitive to specimen thickness. Comparison with experimental results will delineate the grid characteristics and hardening models which best model specific geometric and material applications. After successful "tuning" of the finite element model, a complete description of the stress and energy state in a cracked body can be predicted with confidence. Once fully three-dimensional stress fields are predicted, ductile failure theories can be tested and skeptically compared without the bias of unrealistic analytical approximations.

REFERENCES

Moyer, Jr., E. T. and H. Liebowitz (1983). Plastic deformation and hardening characteristics in three-dimensional fracture specimens. Presented at the ICF International Symposium on Fracture Mechanics, Beijing, China, November 22-25.

Kachanov, L. M. (1971). Foundations of the Theory of Plasticity, North-Holland Publishing Co.

Zienkiewicz, O. C. (1977). The Finite Element Method, McGraw-Hill, New York.

Moyer, Jr., E. T. and H. Liebowitz (1983). Comparative study on three-dimensional crack tip modeling methodology. Presented at the International Conference on Application of Fracture Mechanics to Materials and Structures, Freiburg, Germany, June 20-24.

ACKNOWLEDGMENT

This work was sponsored by the Office of Naval Research under Contract Number: N00014-75-C-0946.

APPENDIX D:

"The Effect of Biaxial Loading on Crack-Tip Yield Zones," E. T. Moyer, Jr. and H. Liebowitz. An invited lecture presented at the Fifth ASCE-EMD Specialty Conference, Laramie, Wyoming, August, 1984.

THE EFFECT OF BIAXIAL LOADING ON CRACK TIP YIELD ZONES

E. Thomas Moyer, Jr.* and Harold Liebowitz**

The existence of a biaxial far-field stress component has been the subject of much research in the past. Its influence on crack growth characteristics, fracture strength and ultimate load capacity has been investigated both theoretically and experimentally for thin sheet specimens made of relatively brittle material [1]. The purpose of this study is to investigate the influence of a biaxial load component on the crack tip yield zones in a relatively ductile, plane strain specimen. Many applications require an understanding of the deformation in a relatively thick specimen made of ductile materials.

The problem chosen for investigation is a square, center-cracked panel shown in Figure 1. The crack-length to width ratio is 0.5. The material properties chosen model a class of very ductile aluminums in the 6061 family. The true stress-strain curve and the associated material properties are shown in Figure 2. A bi-linear approximation has been assumed for the hardening features of the curve. The normal applied stress ($\sigma_{y\infty}$) was held constant in the analysis and biaxial load ratios ($k = \frac{\sigma_{x\infty}}{\sigma_{y\infty}}$) of 0.0, 0.2, 0.4, 0.6, and 0.8 were investigated. Two values of the normal applied stress were tested, $\sigma_{y\infty} = S_y/3$ and $\sigma_{y\infty} = 0.45 \times S_y$.

The analysis employed a two-dimensional incremental plasticity approach which accounts for large plastic strains, finite deformations and mixed hardening. J-2 Flow theory plasticity with a von Mises yield criterion was assumed. A Newton-Raphson finite element solution was generated using the code developed in [2]. Convergence was assured by employing local and global force balances and by using an Updated-Lagrangian approach for the finite displacements.

Figure 3 shows the von Mises stress corresponding to the initial yield stress for an applied normal stress of $\sigma_{y\infty} = S_y/3$ and a biaxial load factor k = 0.0. It is typical of plane strain yield zones. Figures 4-7 show the near tip yield zone with the same applied normal stress due to increasing biaxial load factor (k = 0.2,0.4,0.6,0.8). The increasing biaxial load has the effect of reducing the amount of local plastic deformation. This will cause a more brittle global response.

*Senior Research Engineer
**Dean, School of Engineering and Applied Science, The George Washington University, Washington, D.C. 20052.

The same effect can be observed for larger applied normal stress values. Figure 8 shows the near tip yield zone for an applied normal stress of $\sigma_{y\infty}$=.45 x S_y and a biaxial load factor k = 0.0. Figures 9-12 show the near tip yield zones with this larger applied normal stress due to increasing biaxial load factors (k = 0.2,0.4,0.6,0.8).

The decrease of plastic deformation with increasing biaxial load factor should be expected since the addition of biaxial loading will increase the local dilatational component of the stress field and decrease the distortional component which causes plasticity. Since the response to larger biaxial load factors is more brittle, specimens under biaxial loading should fail at lower load levels than those without biaxial loading. The ductility of a cracked specimen, therefore, is strongly dependent on the nature of the loading. Increased biaxial loading tend to render a specimen more brittle.

References

[1] G. C. Sih and E. T. Moyer, Jr., "Path Dependent Nature of Fatigue Crack Growth," Journal of Engineering Fracture Mechanics, Vol. 17, No. 3, pp. 269-280, 1983.

[2] E. Thomas Moyer, Jr. and H. Liebowitz, "A Review of the Effects of Biaxial Loading on Fracture Properties and Characteristics of Engineering Materials." To be published in the Journal of the Aeronautical Society of India, 1984.

Acknowledgement

This work was sponsored by the Office of Naval Research under Contract Number: N00014-84-K-0027.

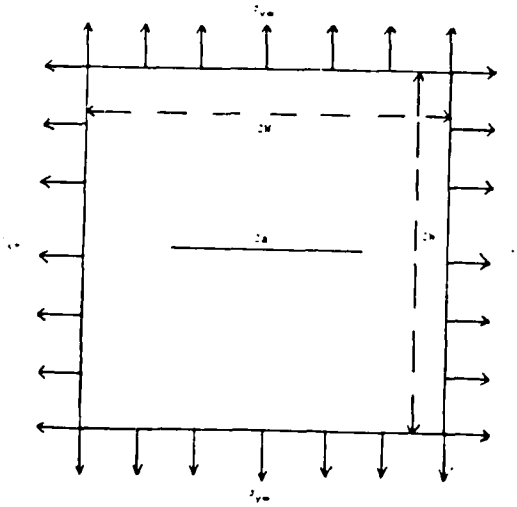

Figure 1 Specimen Geometry and Loading

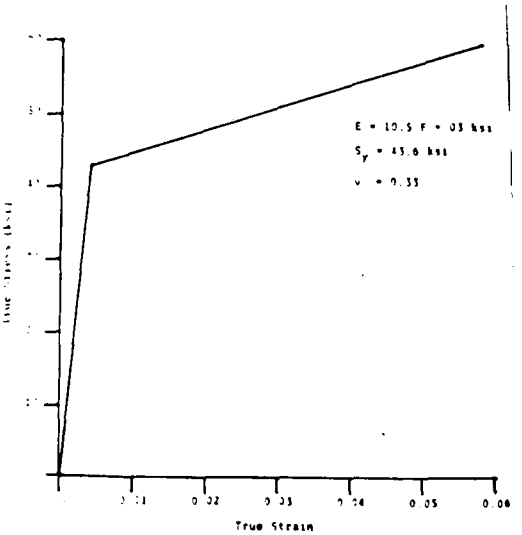

Figure 2 Material Response And Properties.

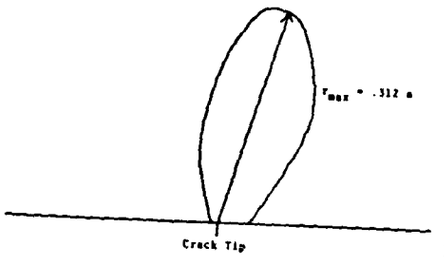

Figure 3: Near Tip Yield Zone For $\sigma_{ym} = S_y/3$ and $k = 0.0$.

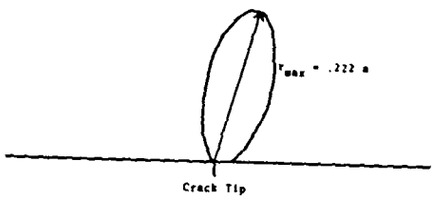

Figure 4: Near Tip Yield Zone For $\sigma_{ym} = S_y/3$ and $k = 0.2$.

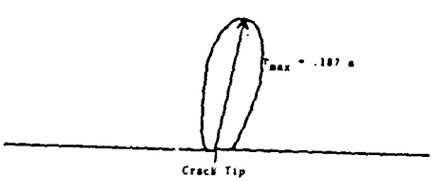

Figure 5: Near Tip Yield Zone For $\sigma_{ym} = S_y/3$ and $k = 0.4$.

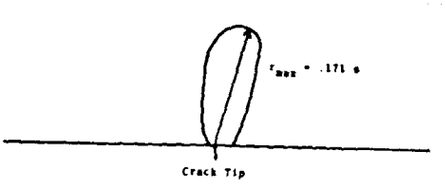

Figure 6: Near Tip Yield Zone For $\sigma_{ym} = S_y/3$ and $k = 0.6$.

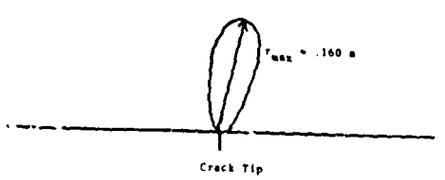

Figure 7: Near Tip Yield Zone For $\sigma_{ym} = S_y/3$ and $k = 0.8$.

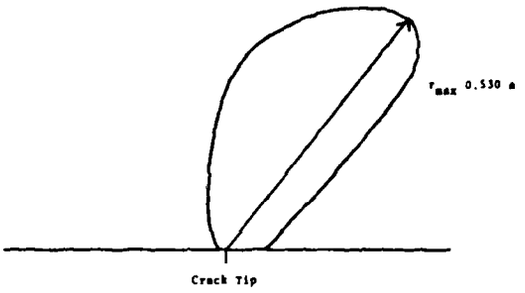

Figure 8: Near Tip Yield Zone For $\sigma_{ym} = 0.45 \times S_y$ and $k = 0.0$.

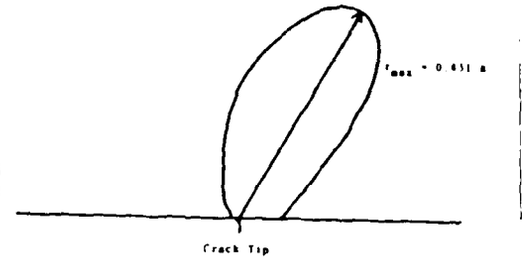

Figure 9 Near Tip Yield Zone For $\sigma_{ym} = 0.45 \times S_y$ and $k = 0.2$.

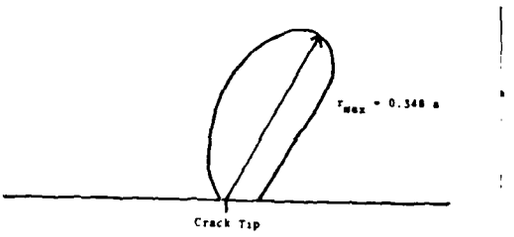

Figure 10: Near Tip Yield Zone For $\sigma_{ym} = 0.45 \times S_y$ and $k = 0.4$.

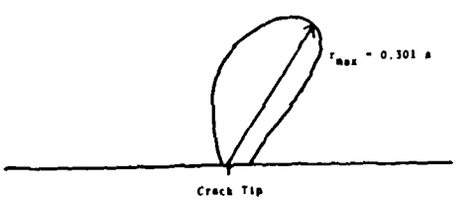

Figure 11: Near Tip Yield Zone For $\sigma_{ym} = 0.45 \times S_y$ and $k = 0.6$.

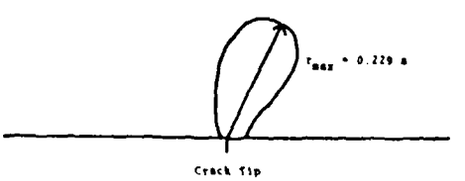

Figure 12: Near Tip Yield Zone For $\sigma_{ym} = 0.45 \times S_y$ and $k = 0.8$.

PLASTIC AREAS (A/A_{MAX})

	$\sigma_{y\infty} = S_y/3$	$\sigma_{y\infty} = 0.45\ S_y$
k = 0.0	0.564	1.000
k = 0.2	0.256	0.641
k = 0.4	0.205	0.385
k = 0.6	0.179	0.308
k = 0.8	0.154	0.205

$$A_{MAX} = 6.314 \times 10^{-2}\ a^2$$

$\sigma_{y\infty} = S_y/3$

	k = 0.	k = 0.2	k = 0.4	k = 0.6	k = 0.8
r_{max}/a	0.312	0.222	0.187	0.171	0.160
θ	73°	73°	77°	73°	76°

$\sigma_{y\infty} = 0.45\ S_y$

	k = 0.0	k = 0.2	k = 0.4	k = 0.6	k = 0.8
r_{max}/a	0.530	0.431	0.348	0.301	0.229
θ	51°	60°	62°	63°	65°

MAXIMUM YIELD RADII AND ORIENTATION

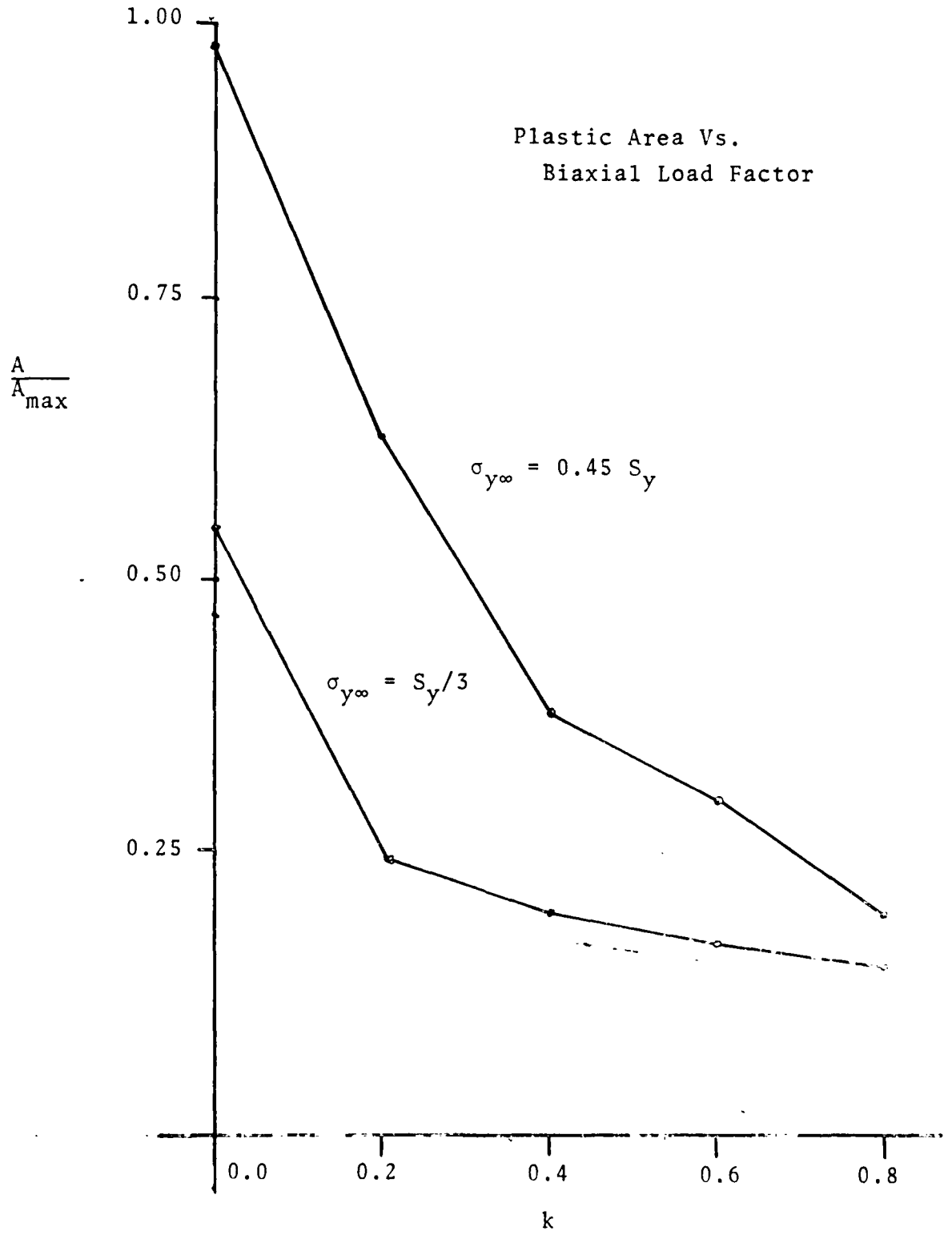
Plastic Area Vs.
Biaxial Load Factor
1.00
0.75
0.50
0.25
A / A_max
σ_y∞ = 0.45 S_y
σ_y∞ = S_y/3
0.0
0.2
0.4
0.6
0.8
k

MATERIAL → 6061 ALUMINUM

$E = 10.5 \times 10^6$ PSI

$S_y = 43.6$ KSI

$\nu = 0.33$

ANALYSIS

1] J_2 Flow Theory

2] Incremental Solution

3] Newton-Raphson Iteration

4] Updated Lagrangian Approach

5] Finite Strain Theory

6] Model Convergence By Mesh Reduction

$$k \equiv \frac{\sigma_{x\infty}}{\sigma_{y\infty}}$$

APPENDIX E:

PLASTIC ZONE MEASUREMENTS AND COMPARISON WITH FINITE ELEMENT RESULTS

The size and the shape of the plastic zone at the crack tip was measured on a center-cracked specimen with width 8.89cm and crack length-to-width ratio 0.5. The material used was an aluminum alloy 7075 in overaged condition (T7651). The zone size was determined by measuring the permanent reduction in thickness after the specimen was unloaded. The contours of the plastic zones were determined using a surface profile measuring device. The sensor of which consisted of a stylus attached to a thin litanium alloy sheet on which strain gauges were mounted to form a four arm bridge circuit.

The specimen was also studied by the finite element method. The grid described in Appendices B and C was used to predict the local crack front deformation on unloading. The program described in these papers was utilized. It employs 20-node isoparametric elements as the main structural element, J-2 Flow Theory Plasticity and an iterative Newton-Raphson computational procedure. The results are compared with the experimental measurements below.

The results of the measurement on the four crack-tip regions on the surfaces are shown in Figures 1 to 4 for depths 0.0051, 0.0102, 0.0152 and 0.0203mm respectively. The results show that there is scatter in the data obtained from the four zones; however, the averaged values agree

well with the results obtained from the finite element analysis (shown as a solid line in the Figures).

Although the resolution of the sensor is very high and is limited only by the extent of amplification of the signal, errors can be introduced due to any nonplanarity of this initial specimen surface and slight variations in the pressure applied on the micrometer screws while advancing manually. The variation in pressure can cause an error of approximately 0.0001in. The planarity of the surface was checked initially before deforming the specimen. The size may not be indentical for all the four zones measured in one specimen. This may be caused by the lack of perfect symmetry in the fatigue crack growth on both sides and by the nonhomogeneity of the material. The measurement of the four zone sizes and averaging the results reduced the errors introduced by these factors.

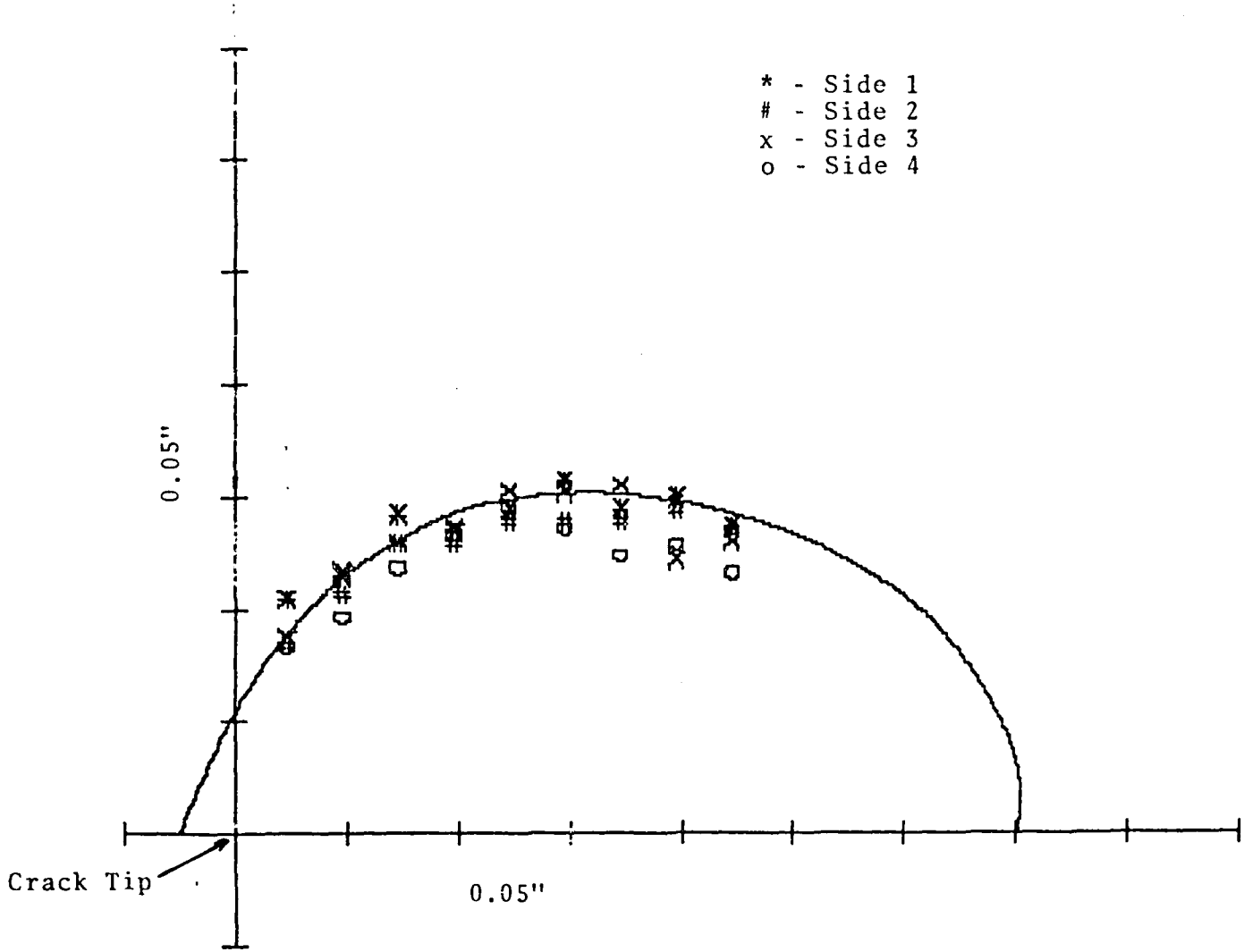

Figure 1. Plastic Zone Shape - Contour Lines of Depth - 0.0002"

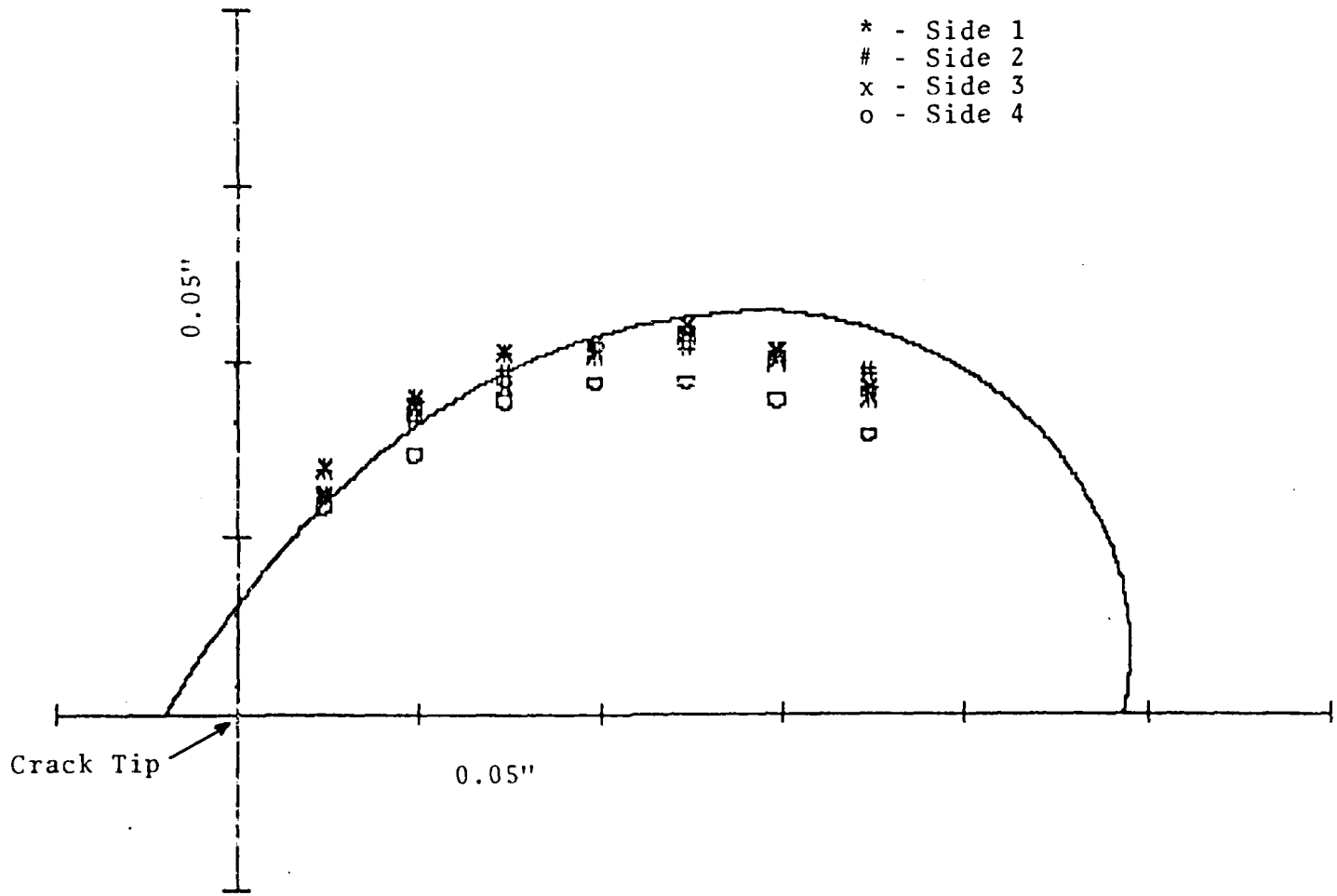

Figure 2. Plastic Zone Shape - Contour Lines of Depth 0.0004"

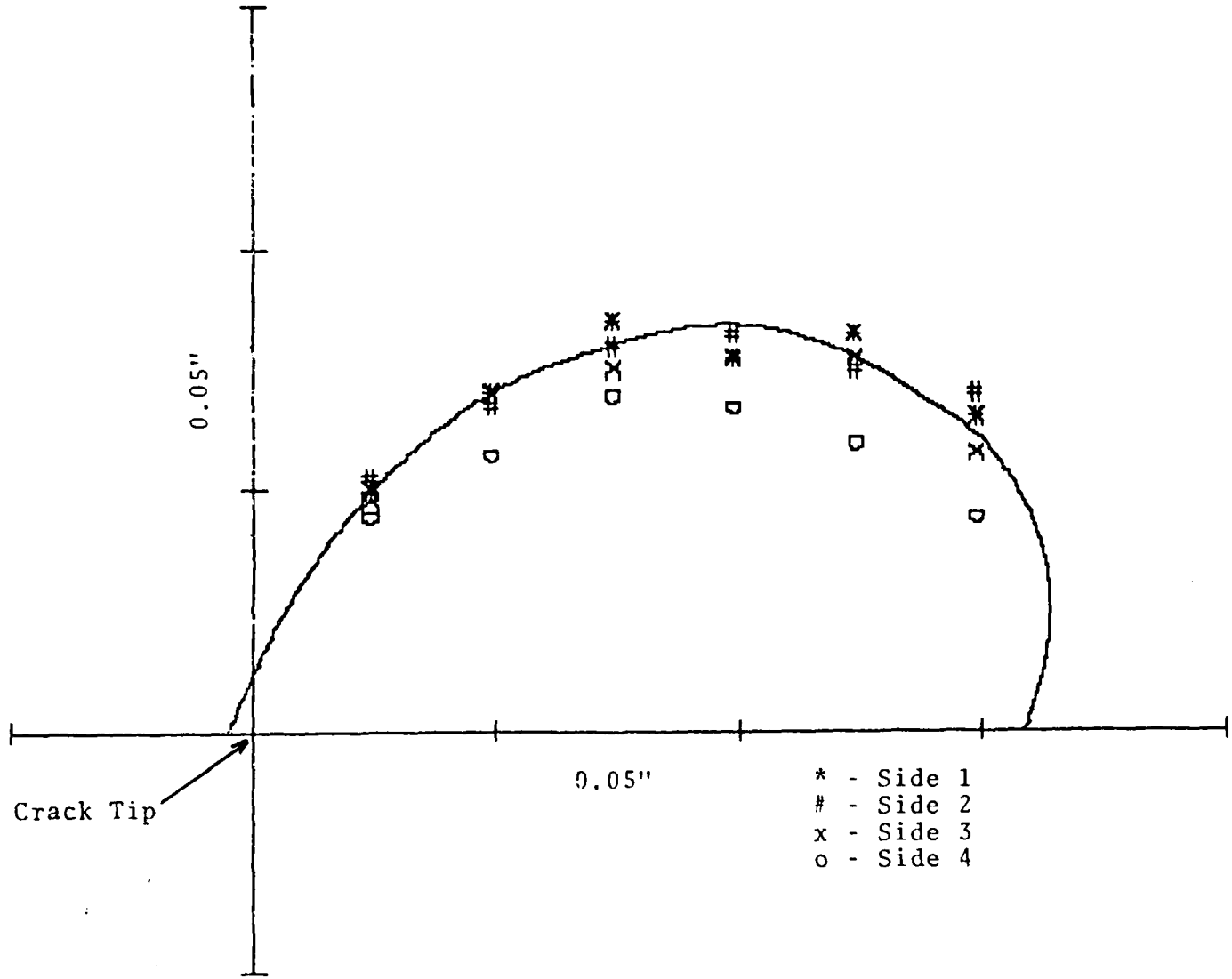

Figure 3. Plastic Zone Shape - Contour Lines of Depth 0.0006"

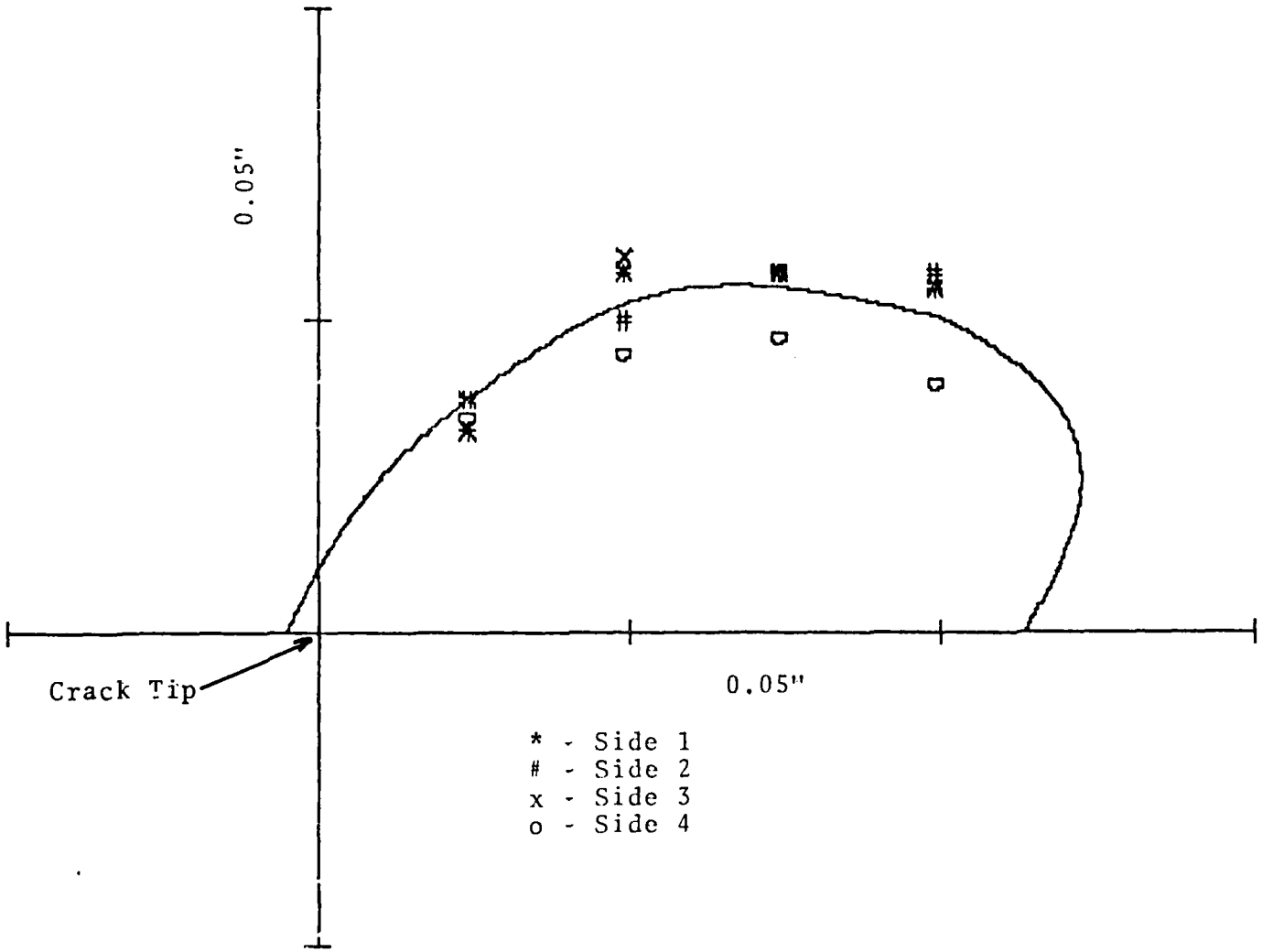

Figure 4. Plastic Zone Shape - Contour Lines of Depth 0.0008"

APPENDIX F:

"A Mesh Adaptive Method for Modeling Slow Crack Growth," E. T. Moyer, Jr. and H. Liebowitz. An invited lecture presented at the 21st Annual Meeting of the SES, VPI&SU, Blacksburg, Virginia, October, 1984.

A MESH ADAPTIVE METHOD FOR MODELING SLOW CRACK GROWTH

by

E. Thomas Moyer, Jr. and Harold Liebowitz
School of Engineering and Applied Science
The George Washington University
Washington, D.C. 20052

The accurate modeling of slow crack growth requires the coalition of a careful stress analysis, a consistent crack growth criterion (or constitutive relation) and a numerical scheme which continually redefines the crack position and size. The numerical scheme employed must account for the local unloading and stress redistribution near the crack during the growth process.

Traditionally, the numerical schemes used to simulate crack growth either did not address the local unloading [1] (accurate for very low load levels only) or required a mesh density such that the crack tip element size corresponded exactly to one growth step (e.g., [2]). Other, more recent models employ springs at nodal points whose stiffness can be relaxed during the growth process (e.g., [3]). This approach has yielded extremely limited success and requires a nodal spacing consistent with the growth incrementation. The major drawback the methods employed to date is that the growth incrementation must be known a priori. Much of the work also couples the crack growth criterion and the mesh spacing into the same model making assessment of the validity of either impossible.

A new method is presented in this work which alleviates the drawbacks of the schemes described above. A standard elastic-plastic stress analysis is performed to the load at the initiation of crack growth. The load is then increased slightly. The amount of crack growth is then predicted corresponding to the current load level (the method will work with any fracture criterion). The near crack mesh is convected to the new location of the crack tip. The stress along the new section of crack is relaxed to zero and an update is made in the stress analysis. Finally, the new stress state is extrapolated to the current grid geometry. The process is repeated for each increment of crack growth.

An example problem in 2-dimensions is considered. A thin (.0625 inch) 2024 aluminum panel with a central crack is loaded uniaxially. The experimental Load vs Crack Growth curve is used to dictate the crack growth incrementation (this approach tests the validity of the numerical method independent of the fracture criterion). The load-displacement relation is predicted by the numerical method and compared to the experimental record. Three refinements of crack incrementation are employed to assure convergence. The

results show good agreement with the experimental load-displacement record.

By employing the technique described above, it is possible to test various fracture criteria for slow crack growth. These studies (to be reported subsequently) allow for a separation of numerical and mechanical growth modeling which is essential for delineating the validity of predicted results.

While the example presented in this work is 2-dimensional, the method will apply equally well in three-dimensions. Since larger, high order elements are employed, crack growth studies in 3-dimensions should be possible with current computer resources. The extension of nodal force release techniques to 3-dimensions requires far to many elements (for accurate modeling) to be solved with today's resources.

ACKNOWLEDGMENT

This work was sponsored by the Office of Naval Research under Contract #N00014-84-K-0027.

REFERENCES

[1] Sih, G. C. and Moyer, Jr., E. T., "Path Dependent Nature of Fatigue Crack Growth", J. of Eng. Frac. Mech., Vol. 17, No. 3, 1983, pp. 269-280.

[2] Lee, James D. and Liebowitz, Harold, "Considerations of Crack Growth and Plasticity in Finite Element Analysis", J. of Comp. and Struc., Vol. 8, No. 3/4, 1978, pp. 401-403.

[3] Gifford, L. N. and Hilton, p. D., "Preliminary Documentation of PAPST - Nonlinear Fracture and Stress Analysis By Finite Elements", NDW-DTNSRDC 3960/43b, Feb. 1981.

A MESH ADAPTIVE METHOD FOR MODELING SLOW CRACK GROWTH

By

E. Thomas Moyer, Jr.

and

Harold Liebowitz

This study was sponsored under
ONR Contract #N00014-84-K-0027

School of Engineering and Applied Science
The George Washington University
Washington, D.C. 20052

CRACK GROWTH ALGORITHM - MODEL 2

1] RELEASE NODAL FORCES ON NEW CRACK SURFACE.

2] SAVE QUADRATURE POINT YIELD SURFACE AND DEFORMATION INFORMATION.

3] GEOMETRICALLY REDEFINE GRID.

4] INTERPOLATE/EXTRAPOLATE NEW QUADRATURE INFORMATION.

5] LOAD AGAIN AND REPEAT.

CRACK TIP REGION GRID - MODEL 1

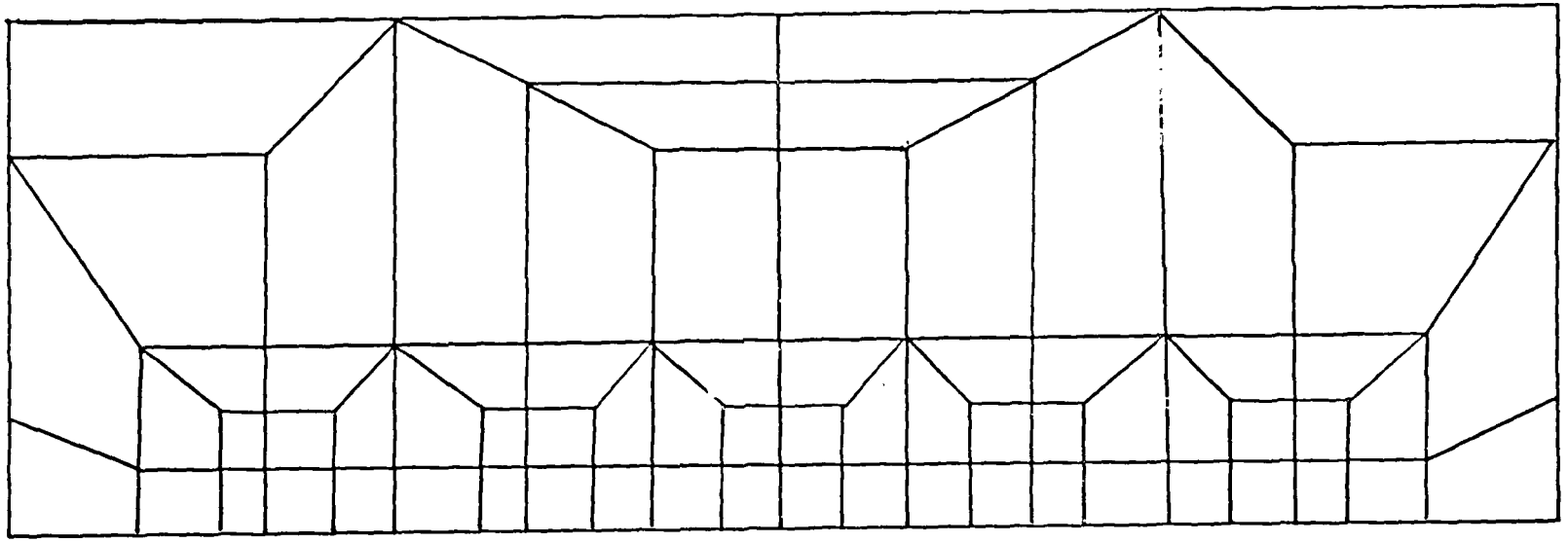

GRID FOR MODEL 1

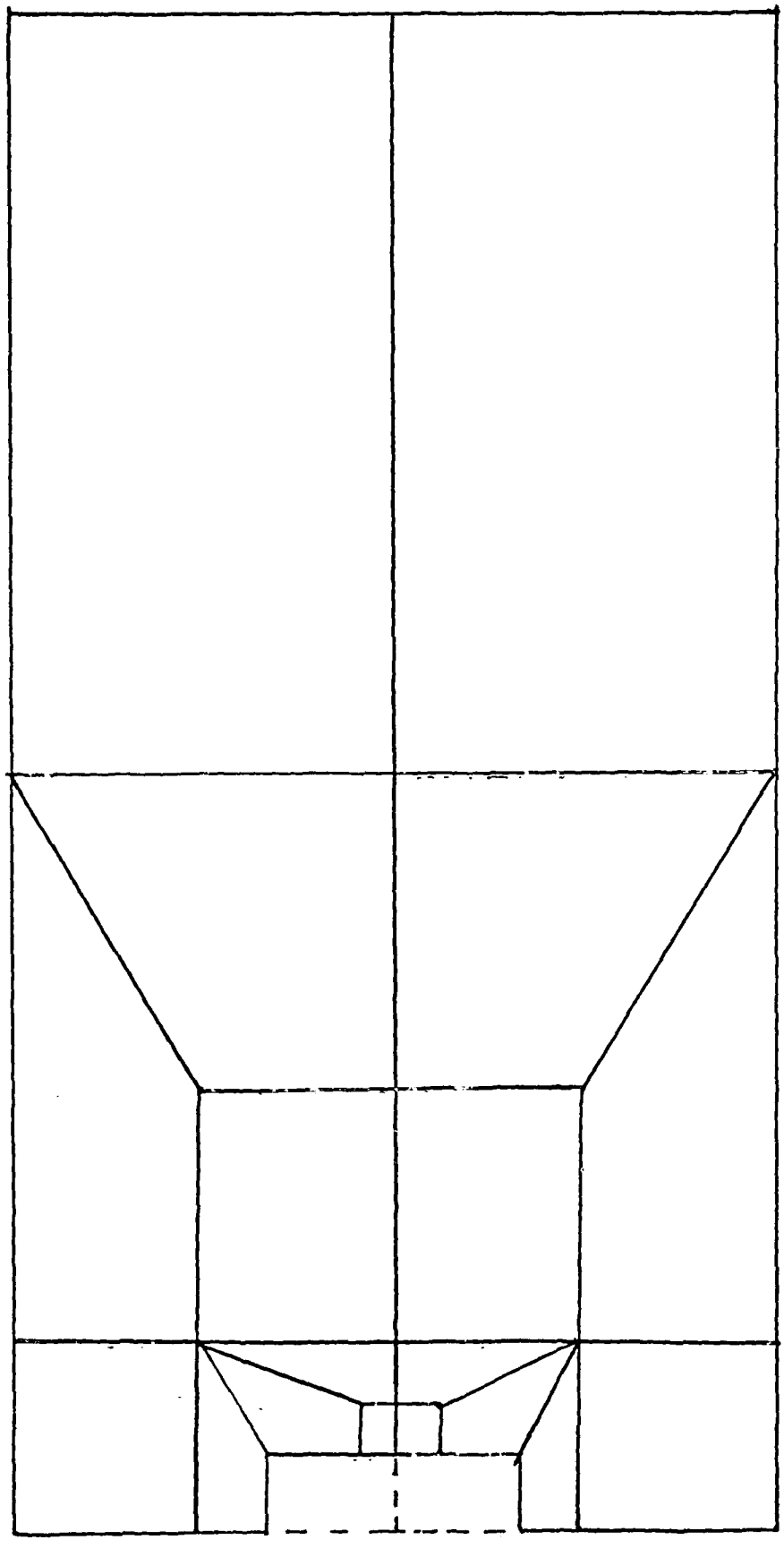

REGION 2 - MODEL 1

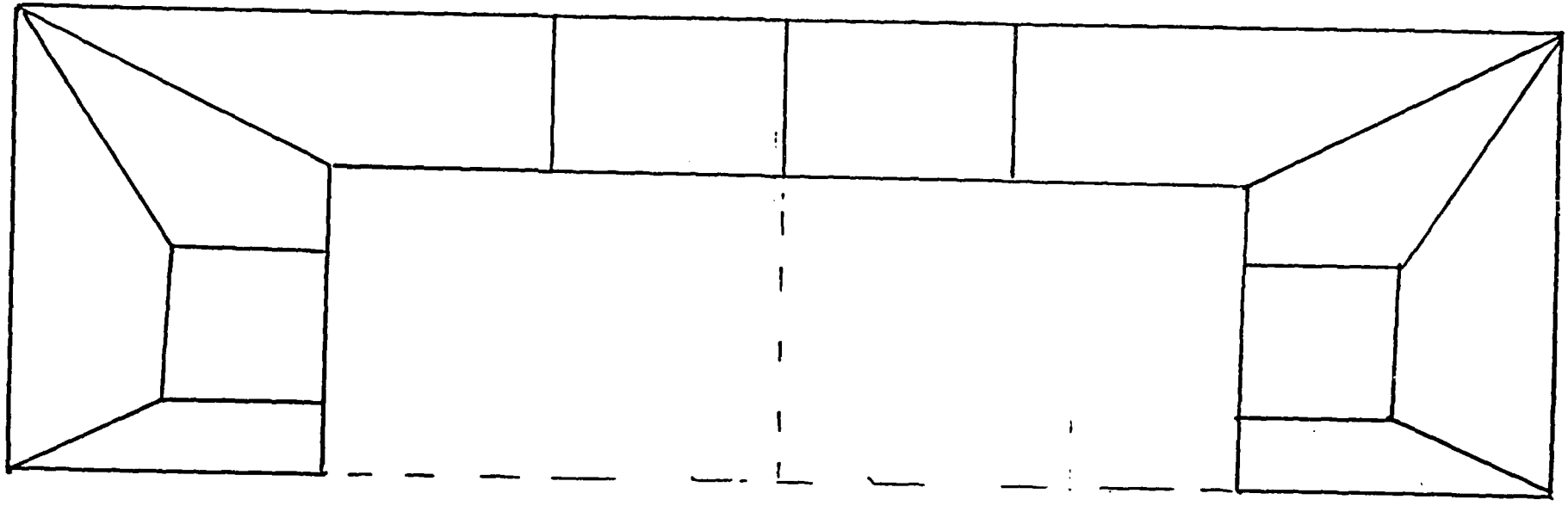

CRACK REGION FOR MODEL 2

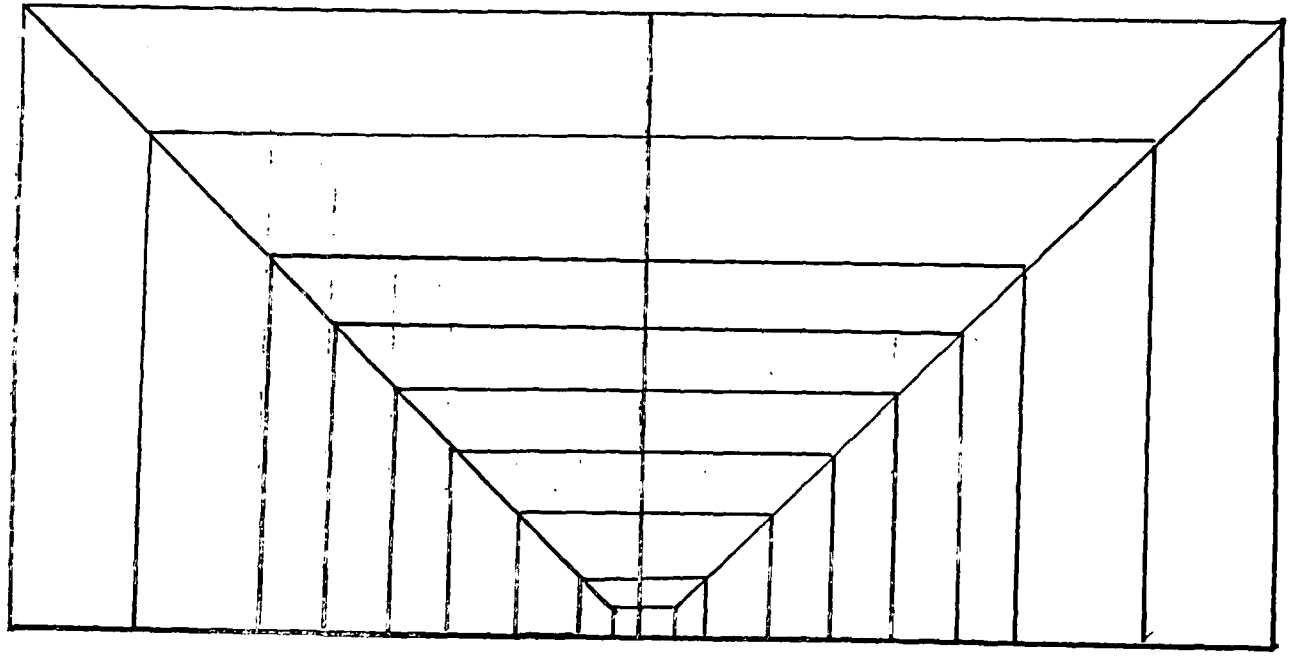

GRID FOR MODEL 2

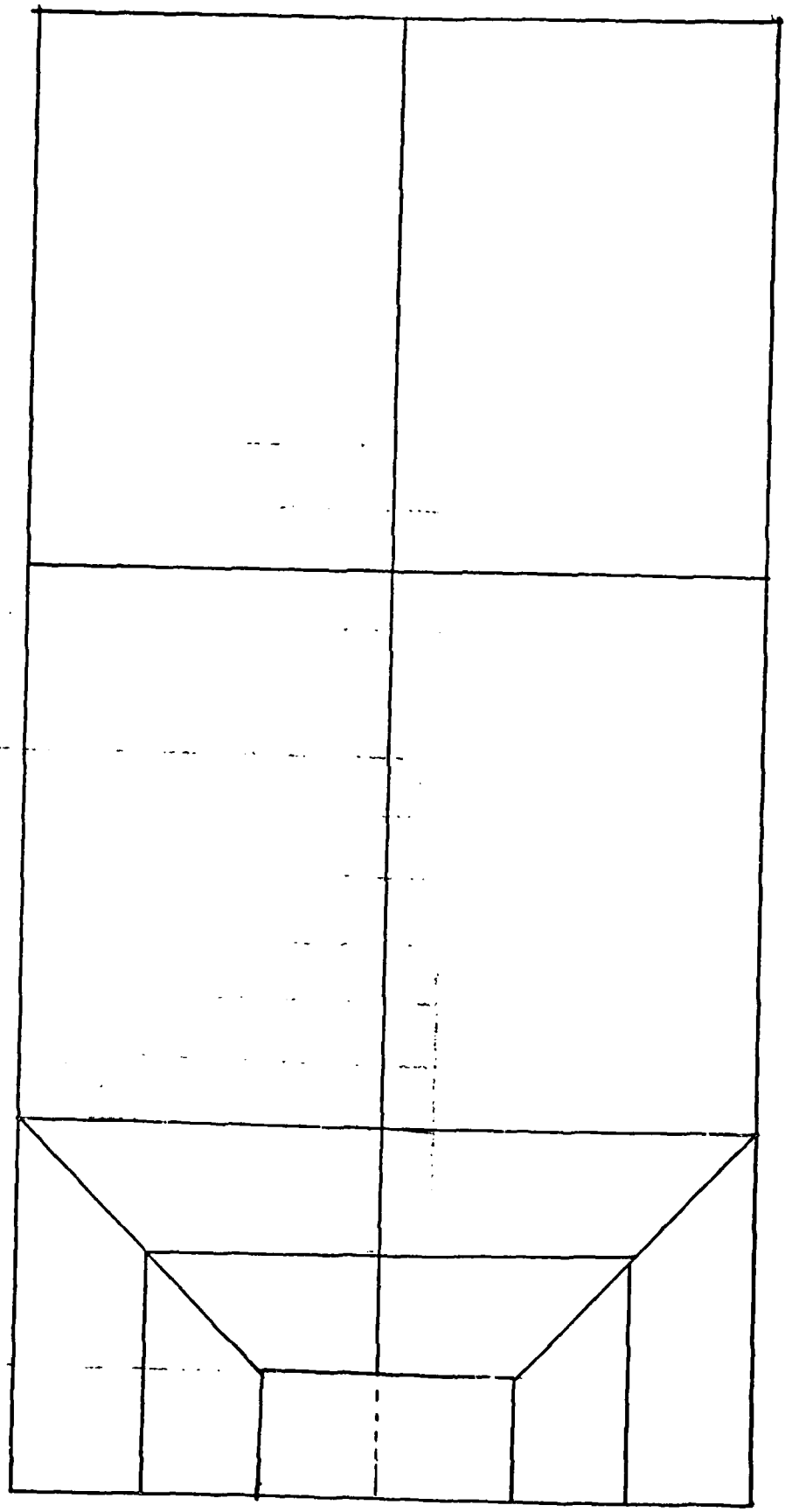

MAXIMUM DISTORTION IN GRID - MODEL 2

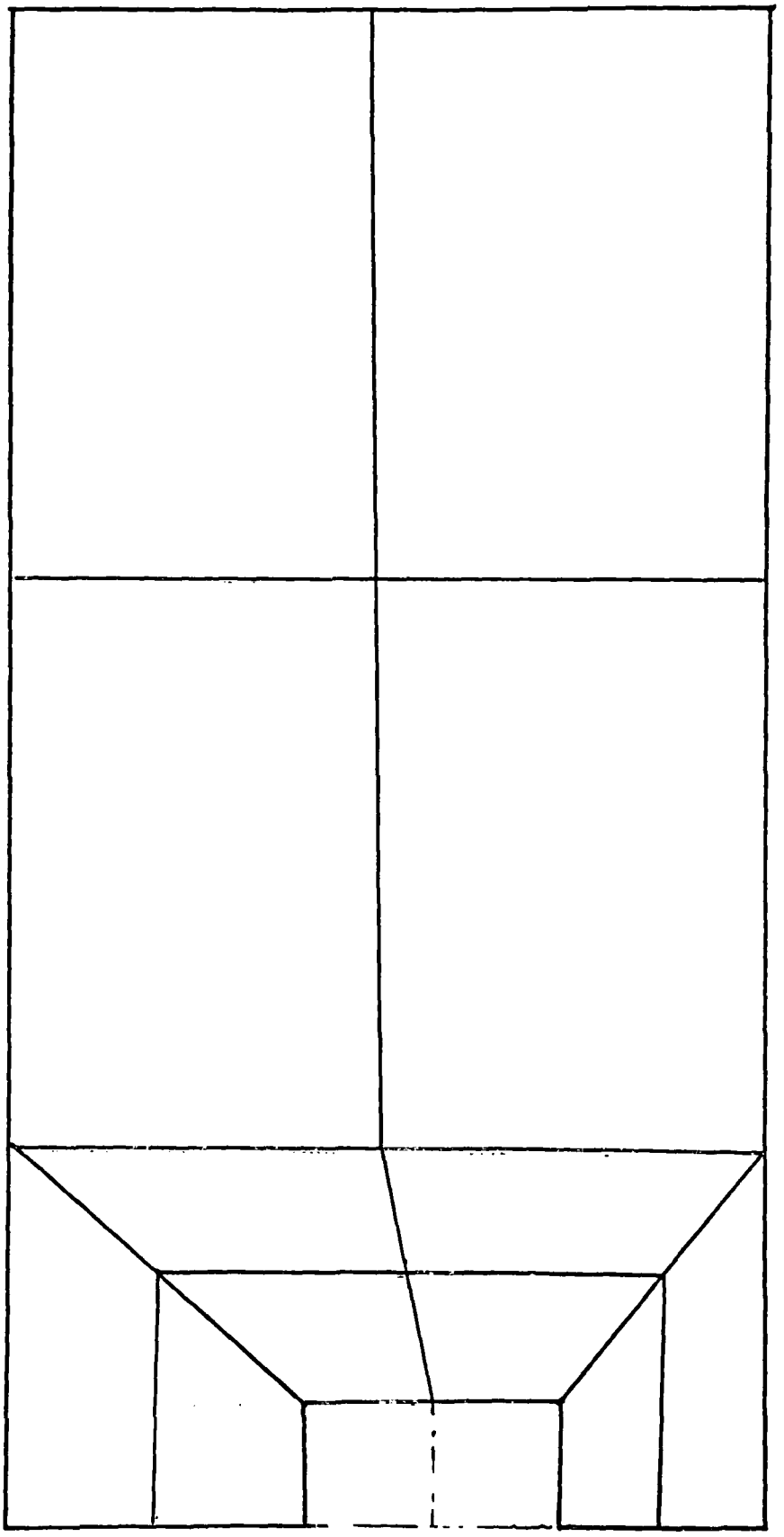

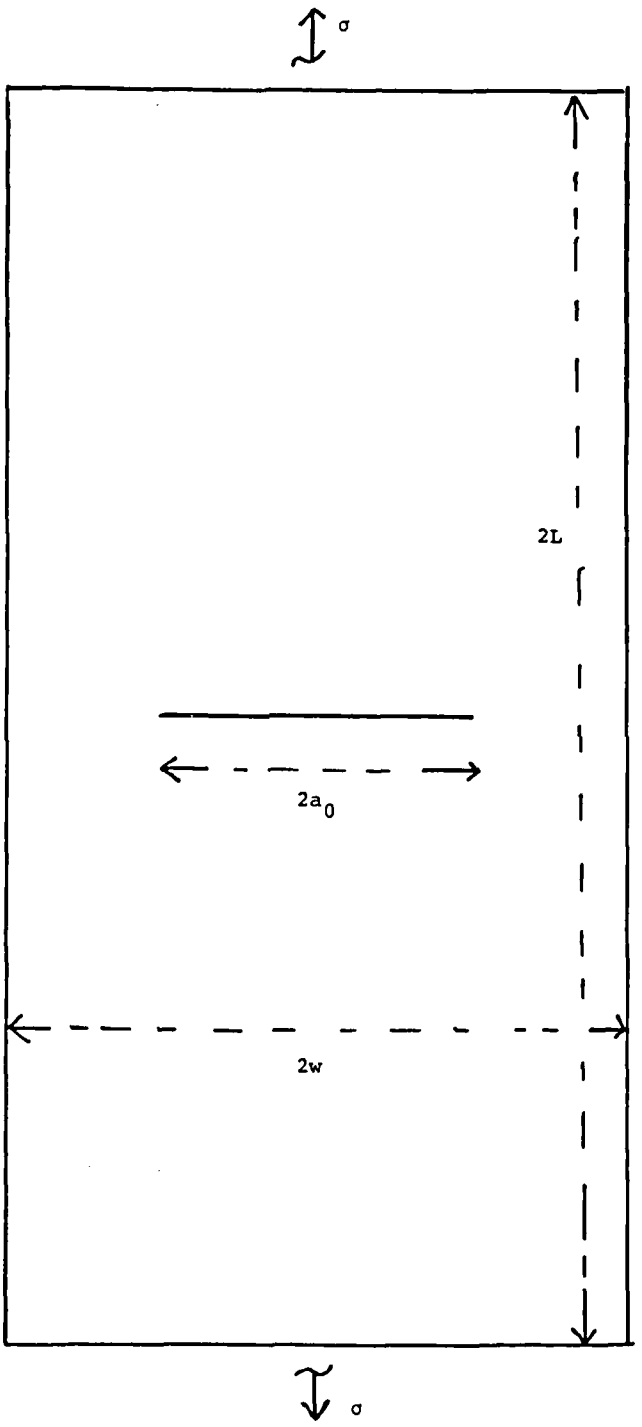
σ
2L
2a0
2w
σ

TRUE STRESS-STRAIN CURVE
2024-T3 Aluminum

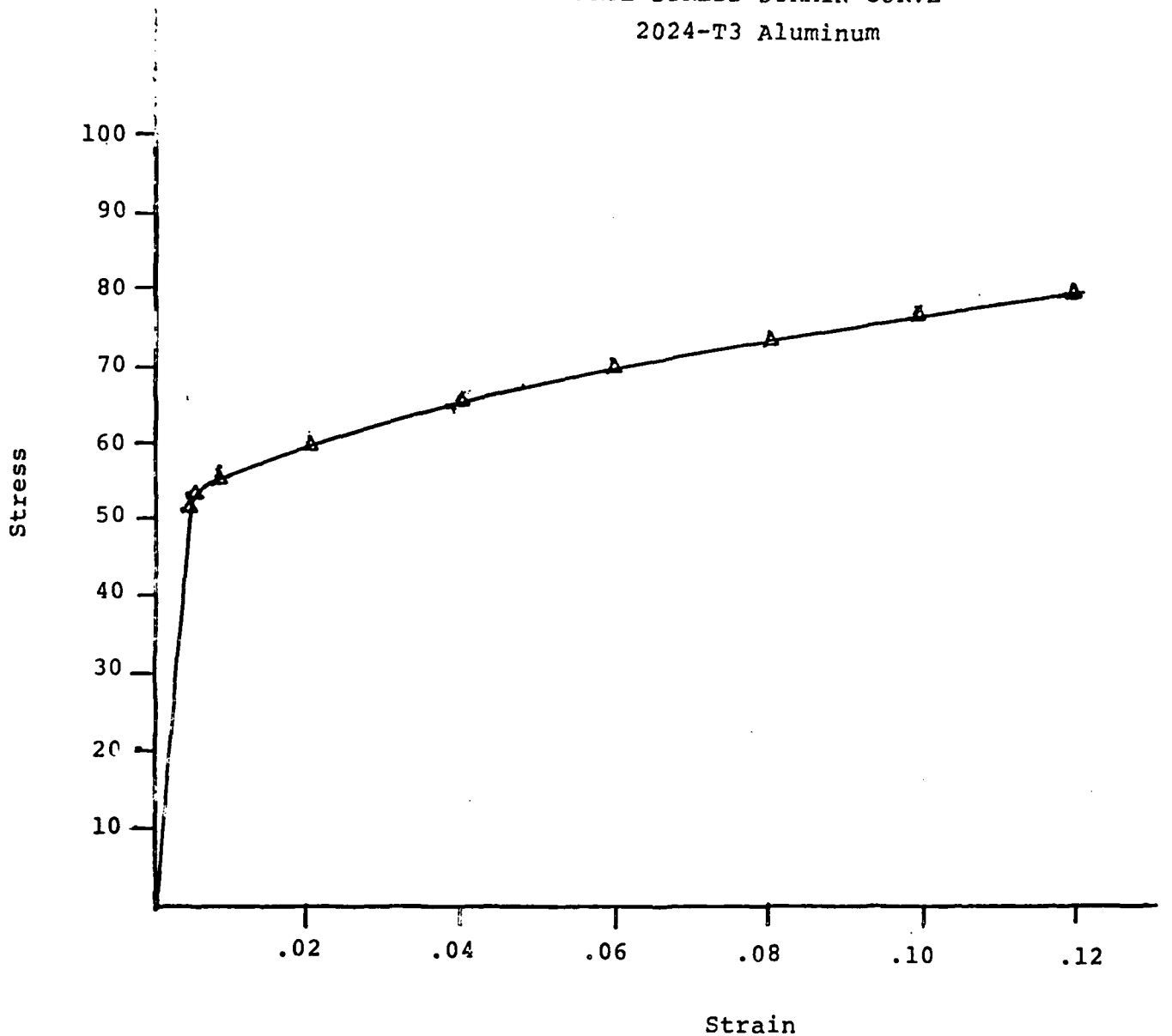

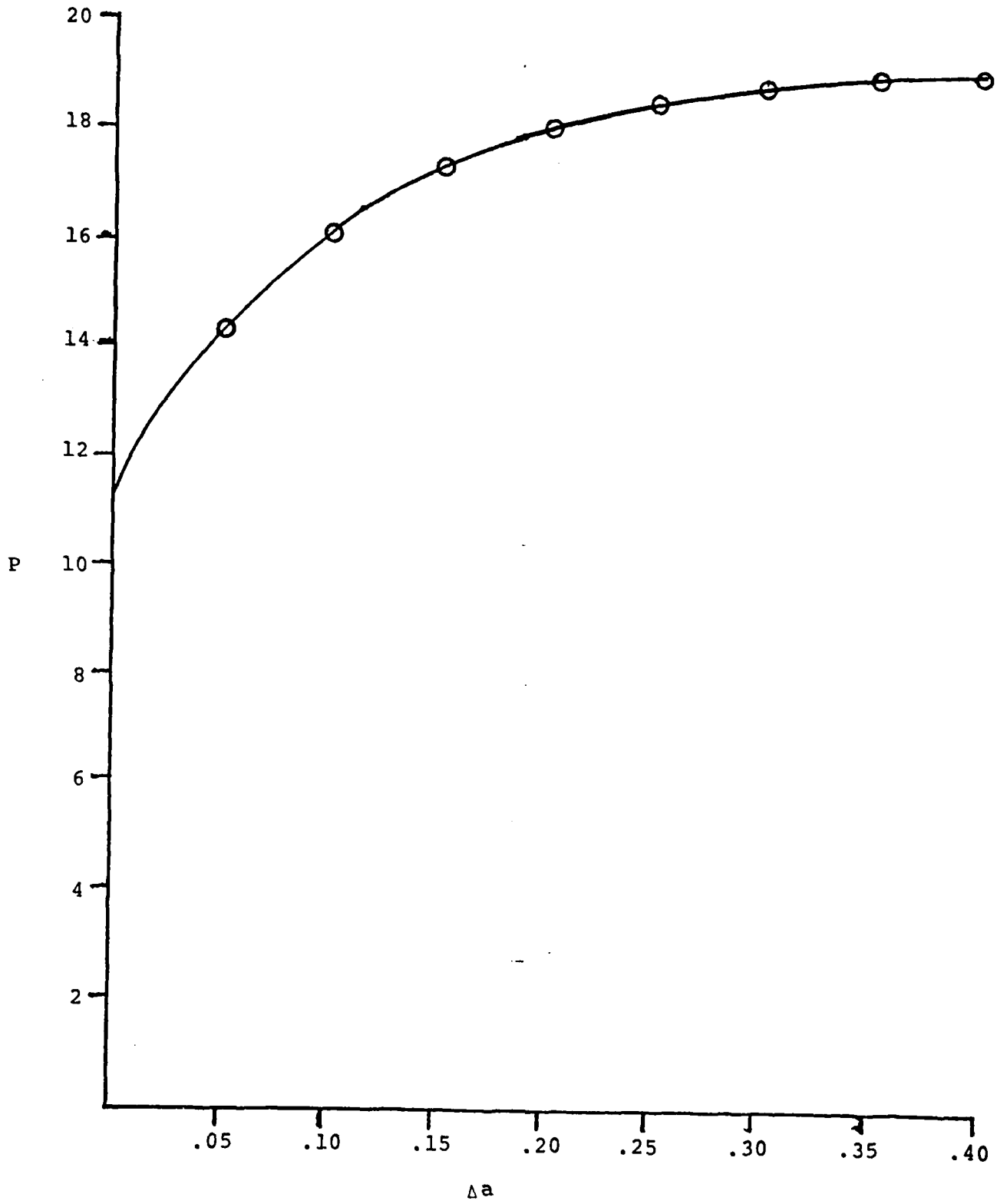

Load vs. Crack Extension

LOAD-DISPLACEMENT CURVE

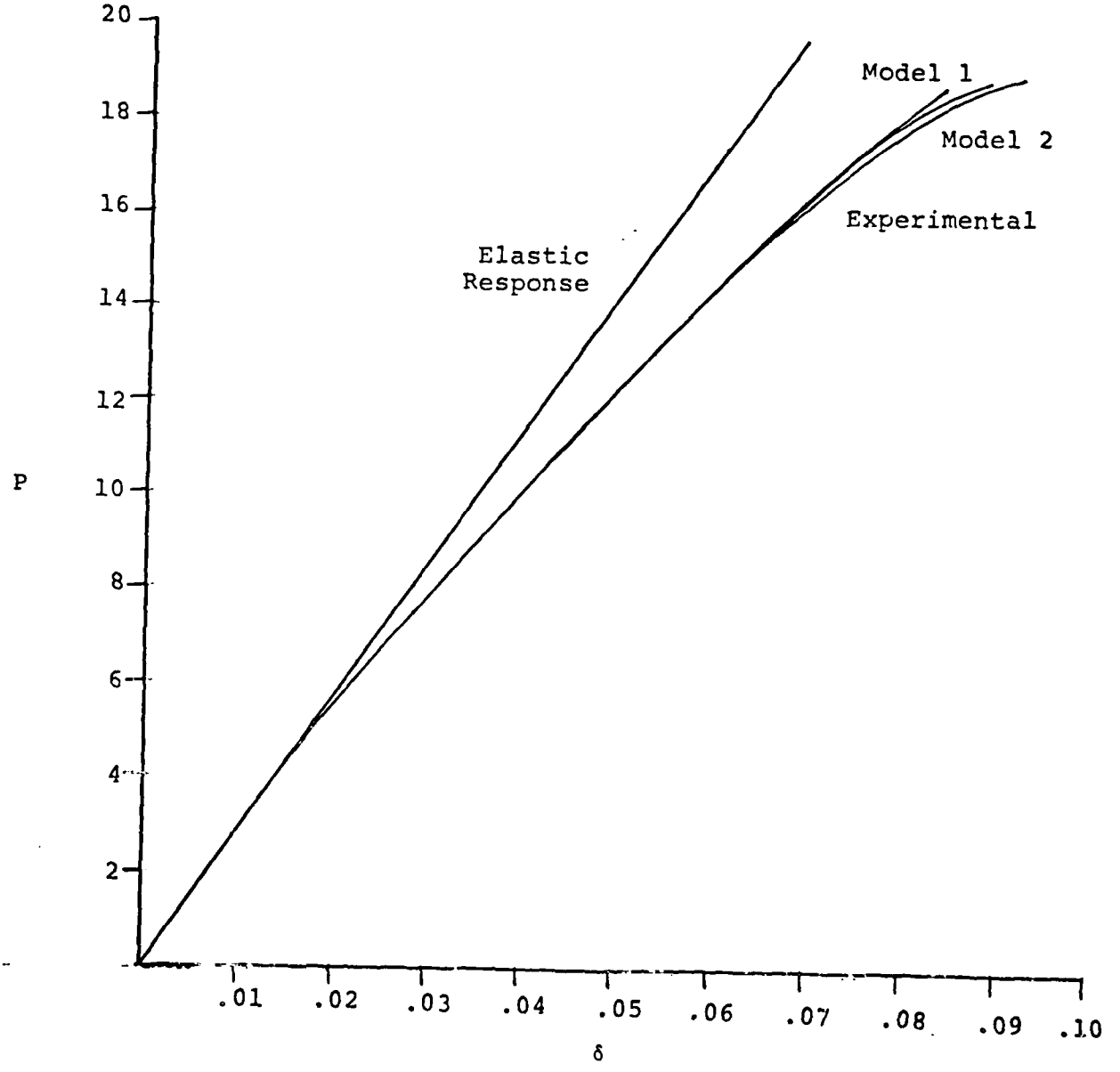

LOAD-DISPLACEMENT CURVE

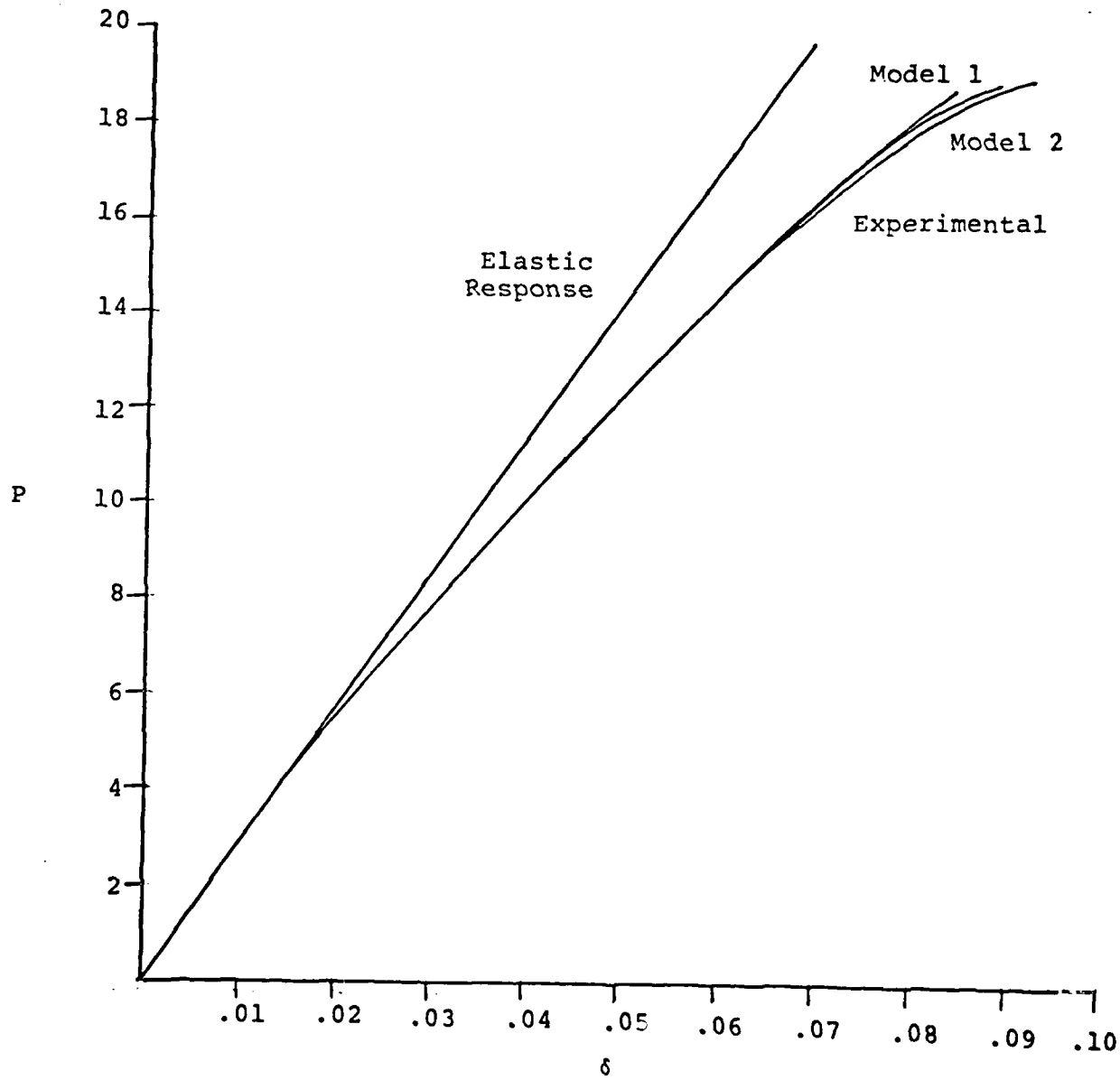

APPENDIX G:

SURFACE CRACK GROWTH IN FATIGUE

An experimental evaluation of the surface crack growth in PMMA (Plexiglass) in tensile fatigue loading has been made. Fatigue crack growth in specimens of thickness ranging from 12.52mm to 25.4mm and width ranging from 50.8mm to 88.9mm was measured. The changes in the rate of growth and the shape of a crack when initiated from a flow and their dependence on the specimen width and thickness were studied.

From the test results (Figures 1-3) the following characteristics of crack growth were observed:

1. Regardless of the shape of the initial flaw, the crack grew into an approximately elliptical shape before the influence of the back surface affected crack growth.

2. The influence of the back surface was not observed until after the crack grew through 50% of thickness, after which the crack growth in the direction normal to the surface slowed down rapidly distorting the elliptical shape of the crack front. This trend was common to all thickness studied.

3. Once the crack penetrated the back surface, it grew rapidly at the back surface approaching the shape of a straight through crack. However, the acceleration did not occur until it had grown through about 95% of the thickness.

4. The pattern of crack growth suggests that the determination of stress intensity in the thickness direction alone or the assumption of the equivalency of a through crack for fatigue life prediction (as done by several investigations) in insufficient in crack growth estimation.

5. Unlike in ductile metallic materials, in PMMA the crack front near the surface was essentially perpendicular to the surface.

6. No effect of the width change was observed in the ranges examined.

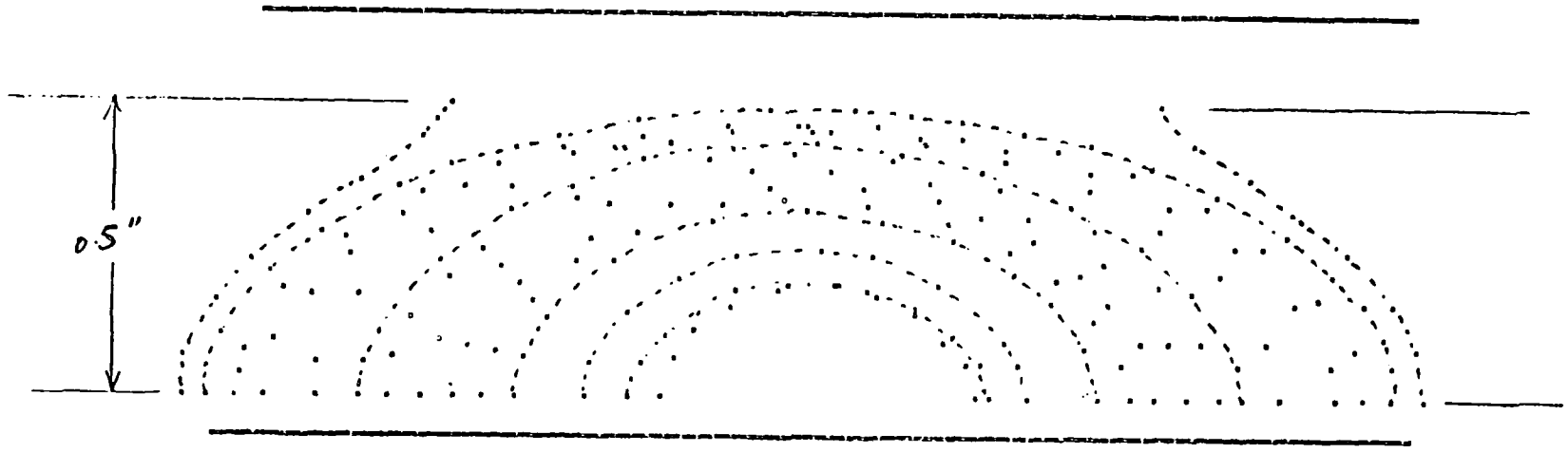

Figure 1. Change of Crack Profile with Crack Growth in a 0.5" Thick Specimen

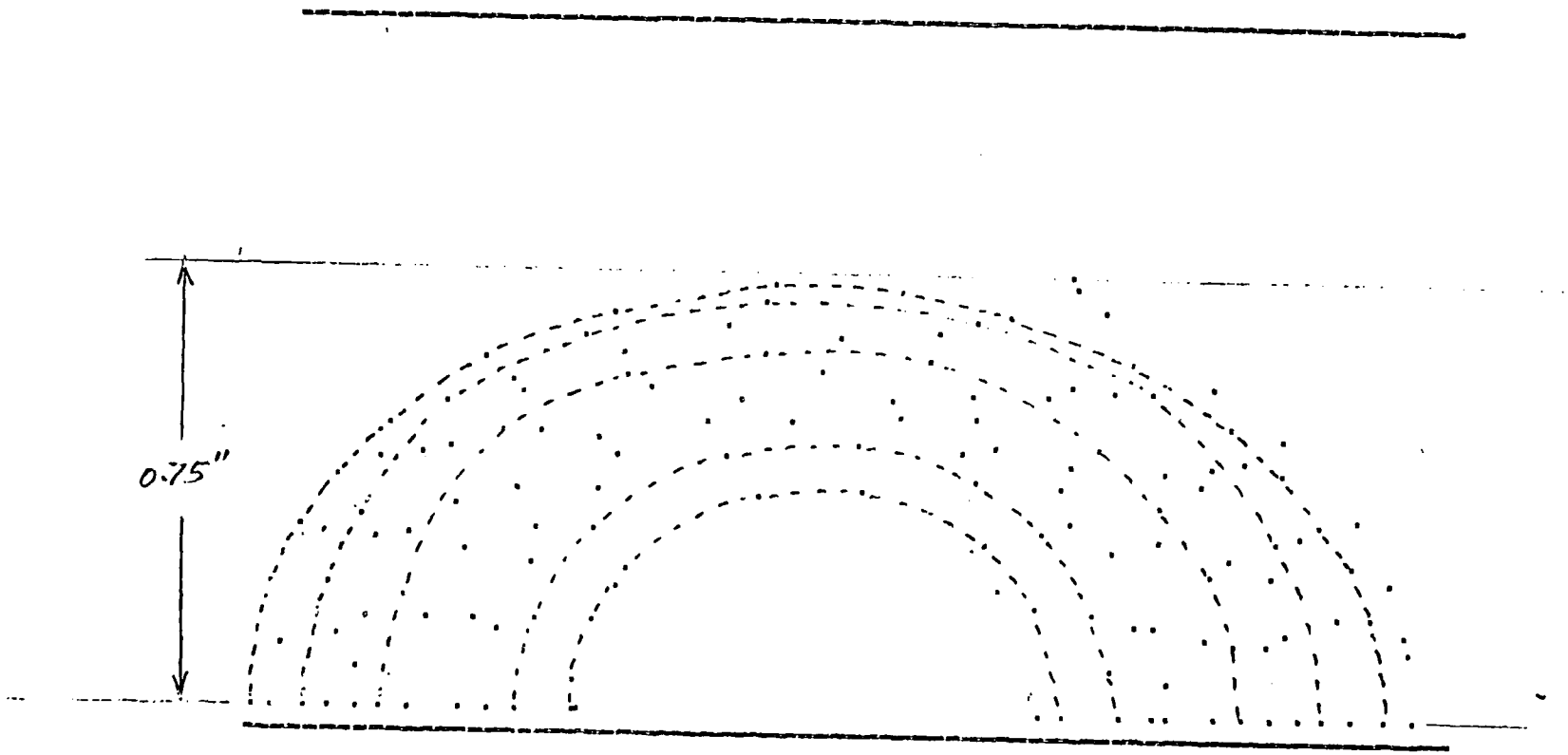

Figure 2. Change of Crack Profile with Crack Growth in a 0.75" Thick Specimen

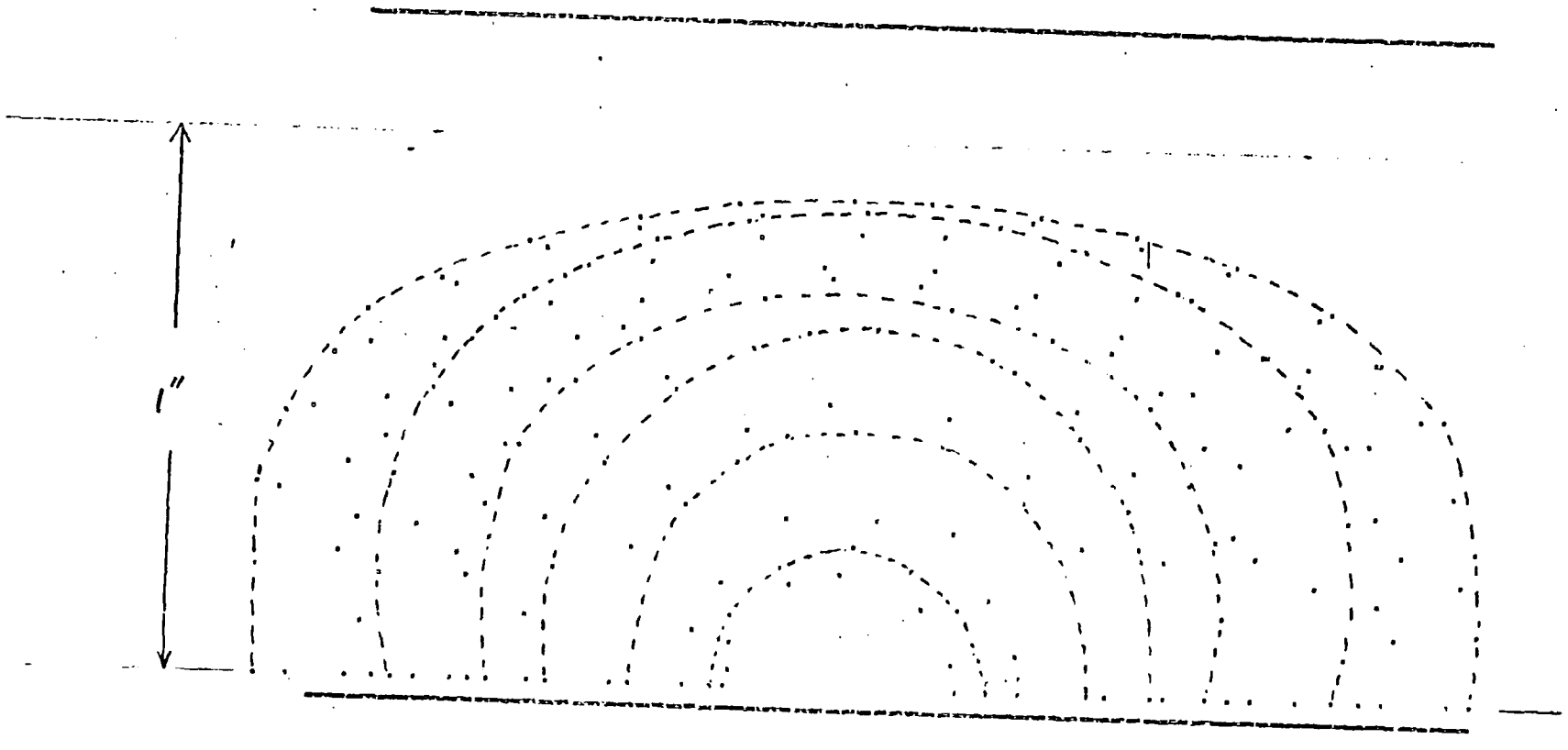

Figure 3. Change of Crack Profile with Crack Growth in a 1" Thick Specimen

APPENDIX H:

"Biaxial Load Effects in the Mechanics of Fracture," E. T. Moyer, Jr. and H. Liebowitz. An invited paper to appear in the Fracture Mechanics Special Issue of the Journal of the Aeronautical Society of India (March, 1985).

AD-A152 073 DETERMINATION OF FAILURE CHARACTERISTICS OF MATERIALS AND STRUCTURES(U) GEORGE WASHINGTON UNIV WASHINGTON DC SCHOOL OF ENGINEERING AN.. H LIEBOWITZ 14 DEC 84 2/2

UNCLASSIFIED N00014-84-K-0027 F/G 20/11 NL

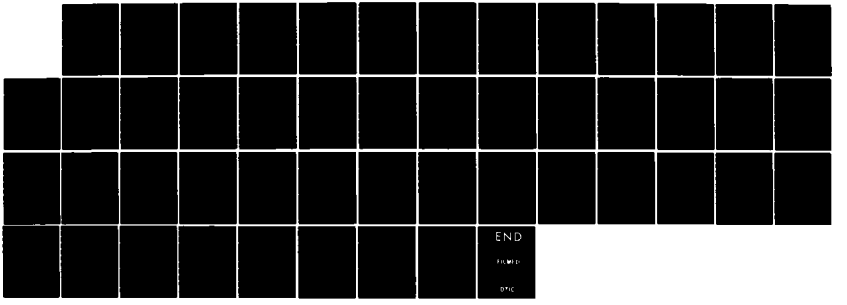

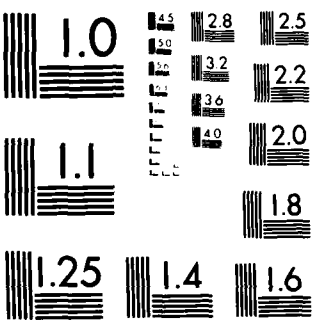

MICROCOPY RESOLUTION TEST CHART
NATIONAL BUREAU OF STANDARDS 1964-A

BIAXIAL LOAD EFFECTS IN THE MECHANICS OF FRACTURE

By

E. Thomas Moyer, Jr.

and

Harold Liebowitz

December 1983

School of Engineering and Applied Science

The George Washington University

Washington, D.C. 20052

ABSTRACT

This paper reviews the current literature on the effects of biaxial loading on the fracture behavior of materials and structures. Emphasis is given to the fundamental results found in the literature (both theoretical and experimental). A brief survey of the applications literature is also made. Areas where further research is needed are delineated and recommendations for future studies are proposed.

LIST OF SYMBOLS

t_{xx}, t_{yy}, t_{xy}, t_{ij}	Cartesian Stress Tensor Components
K_I, K_{II}, K_{III}	Elastic Stress Intensity Factors
u_x, u_y	Cartesian Displacement Components
K_σ, K_ε	Nonlinear Stress and Strain Intensity Factors
ε_{ij}	Strain Components
k	Biaxial Load Ratio
μ	Shear Modulus
ν	Poisson's Ratio
κ	Material Parameter
n	Power-Law Hardening Exponent
x, y	Cartesian Coordinates
r, θ	Polar Coordinates
G	Energy Release Rate
J	Rice's Path Independent Integral
α	Angle Of Crack Inclination
a, b	Elliptical or Parabolic Crack Shape Parameters
K(k), E(k)	Complete Elliptic Integrals
A_p	Area Of Crack Tip Plastic Zones

INTRODUCTION

The importance of studying the effects of biaxial loading on the fracture behavior of materials and structures has been recognized for many years. Most problems of interest in application involve at best a biaxial load condition and usually extremely comlex loadings and geometries. An important first step in understanding fracture behavior is the study of Mode I uniaxial loading as first investigated by Griffith [1] and clarified and expounded upon by Irwin [2]. An important second step is the study of biaxial load effects. All the fracture parameters and specimen characteristics (i.e., crack growth properties, energy release rate, fracture toughness, fatigue properties) are known to be dependent on load biaxiality to some extent.

The purpose of this paper is to present a review of the literature involving biaxial load effects which has evolved over the years. The literature base is far too large for a single review to encompass. This paper will concentrate on summarizing the most fundamental and important results which have been discovered (as determined by their use in applied studies and their acceptance over time).

The paper starts out with a brief review of the experimental findings which demonstrate the importance of biaxial load effects. Basic studies on the effects of biaxial loading on fracture toughness, non-self-similar growth problems, fatigue crack propagation and subcritical growth properties are presented and summarized.

The third section discusses the fundamental analytic solutions for problems of cracks in an elastic solid under biaxial loading. The basic asymptotic field representations are presented along with several stress-intensity factor solutions of both practical and theoretical interest.

The fourth section looks at the effects of biaxial loading on problems involving plastic deformation. Early asymptotic solutions for nonlinear elastic as well as recent numerical results are presented. The emphasis is on the solution of problems with significant plastic deformation and the discussion of stable crack growth.

The fifth section provides a survey of the applications literature for the design and development of engineering structures. For conciseness, only the problems studied and the references are presented.

The final section summarizes the need for biaxial studies and presents suggestions for future research. For further details the reader is referred to the references cited and to reviews [3, 4] which emphasize basic theoretical and experimental findings for stationary cracks and modeling of practical problems and nonlinear behavior respectively.

EXPERIMENTAL STUDIES

During the past two decades, several experimental investigations have been carried out to determine the effects of biaxial loading on the fracture characteristics of test specimens and structures. Of primary interest is the effect on fracture toughness, crack growth trajectory and crack growth rate characteristics. Many of the early investigations showed large discrepancies in results. Much of the difference can be attributed to the use of test specimens which did not preclude load interaction effects. Typical fracture specimens for use in biaxial studies are reviewed in [5]. A specimen geometry and grip configuration which has proven to be consistent and relatively free of load interaction effects is shown in Figure 1. While this is not the only specimen which can be validly employed for biaxial studies, it is a commonly employed and useful specimen.

Examining the remaining literature on biaxial effects on fracture characteristics several qualitative trends can be found common to most experimental investigations. Several investigators have found the fracture toughness of engineering materials to be dependent on the biaxial load factor. The magnitude of the effect, however, is not consistent among the published studies. The results of Kibler and Roberts [6] demonstrate significant influence of the biaxial load factor on the fracture toughness (K_{Ic} value) of 6061-T4, T6 aluminum alloys. Similar studies on plexiglass were carried out by Levers, et al. [7], whose results show negligible influence of biaxial load factor on fracture toughness. Kibler and Roberts had performed similar tests on plexiglass and had found significant influence on fracture toughness. The results of these studies are shown in Figures 2-4.

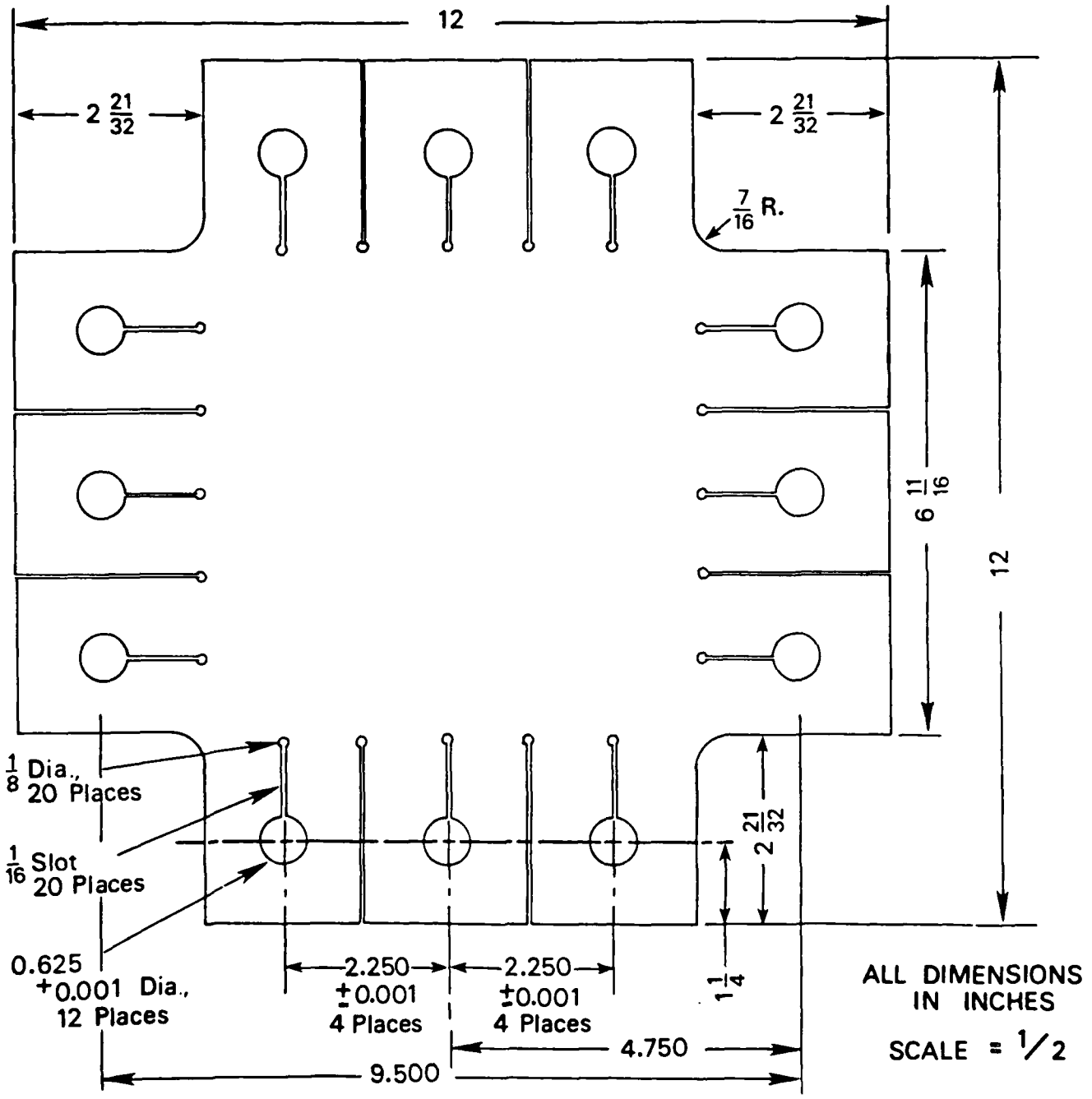

Figure 1: Biaxial Specimen Design.

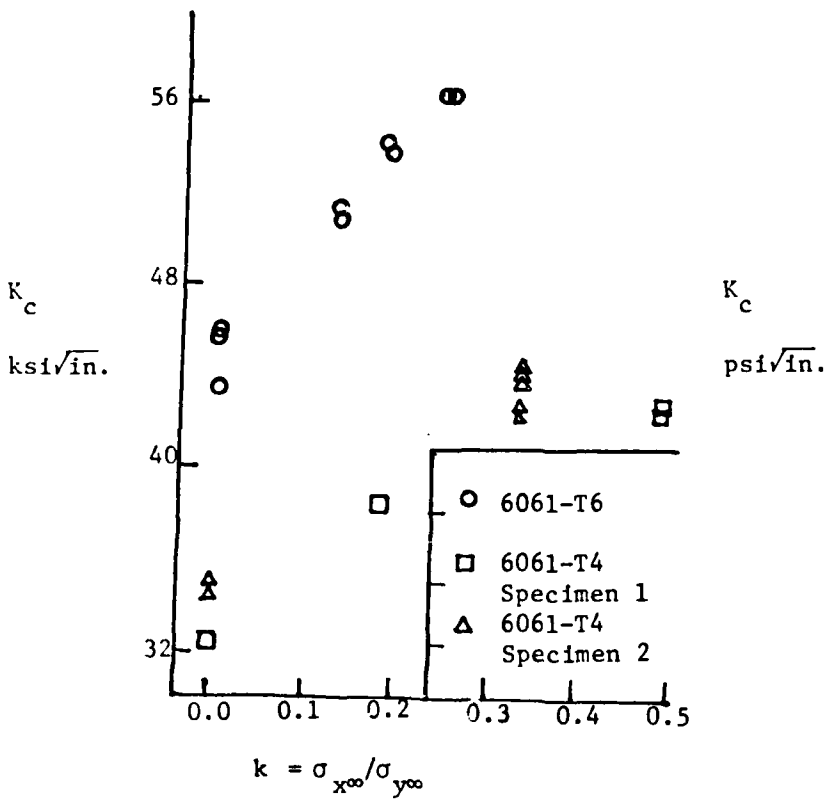

Figure 2: Effect Of Load Biaxiality On K_c In 6061 Aℓ.

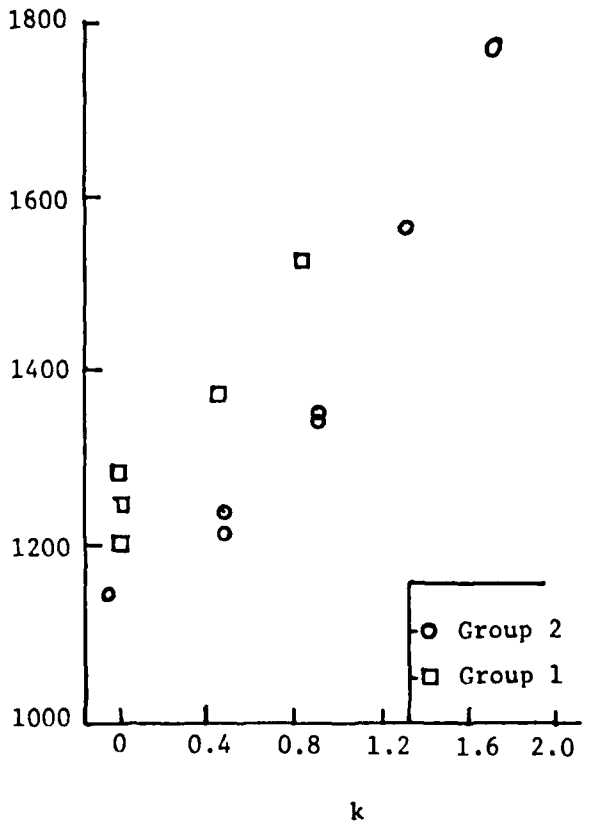

Figure 3: Effect Of Load Biaxiality On K_c In Plexiglass.

Tests performed by Jones and Eftis [8] show a minimal amount of biaxial load dependence of the fracture load for 7075-T6 and 2024-T3 aluminums. Qualitatively, both show slight increases in fracture load with increasing biaxial load factor, however, in many of the tests the experimental scatter is larger than the demonstrated effect. Representative results are shown in Figures 5 and 6.

Recent tests performed on PMMA by Ueda et al. [9] show negligible influence of biaxial loading on fracture load (fracture toughness). Their tests show only slightly stronger dependence for mixed mode problems (i.e., a slanted crack in a biaxial field). The results for a horizontal, Mode I crack in a biaxial stress field are summarized in Table 1.

TABLE 1: Fracture Toughness As A Function Of Load Biaxiality In Plexiglass

	σ_x/σ_y	0.0	0.2	0.5	0.8	1.0
Test 1:	K_f/K_{Ic}	1.01	0.97	0.93	0.91	0.89
Test 2:	K_f/K_{Ic}	1.03	1.01	0.99	0.98	0.95

One feature which has been demonstrated by many authors is that a straight horizontal crack in a biaxial stress field will deviate from self-similar growth at high biaxial load factors. This phenomena is documented in the results of [9, 10, 11]. An example from [10] is shown in Figure 7. This effect can be predicted theoretically from elastic analysis using either the Strain Energy Density Criterion [12] or The Maximum Tearing Stress Criterion [13] (to be discussed in a subsequent section).

A few studies have been done on the influence of biaxial loads on fatigue crack propagation rates. The results from [14] on RR58 alloy show a significant influence on fatigue crack propagation rates by the biaxial load factor

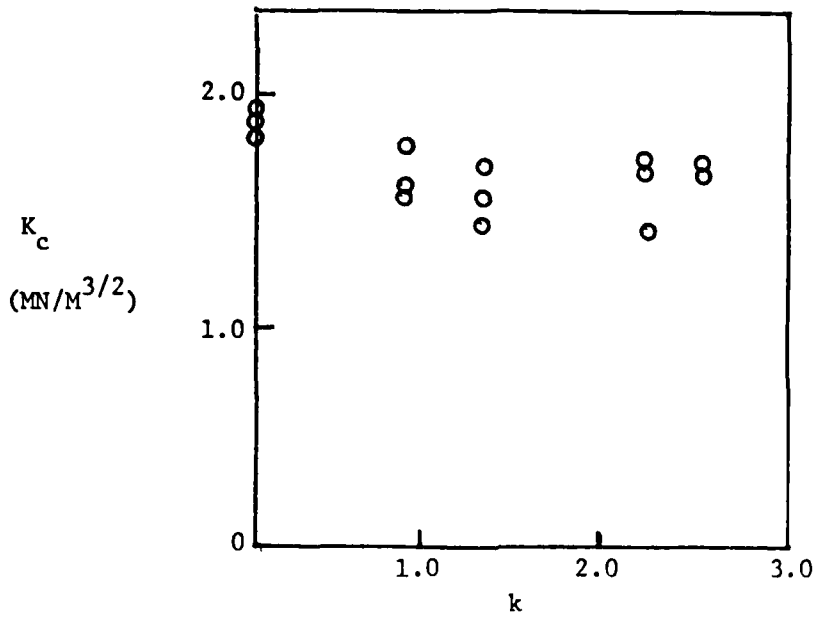

Figure 4: Effect Of Load Biaxiality On K_c In Cross-T Plexiglass Specimens.

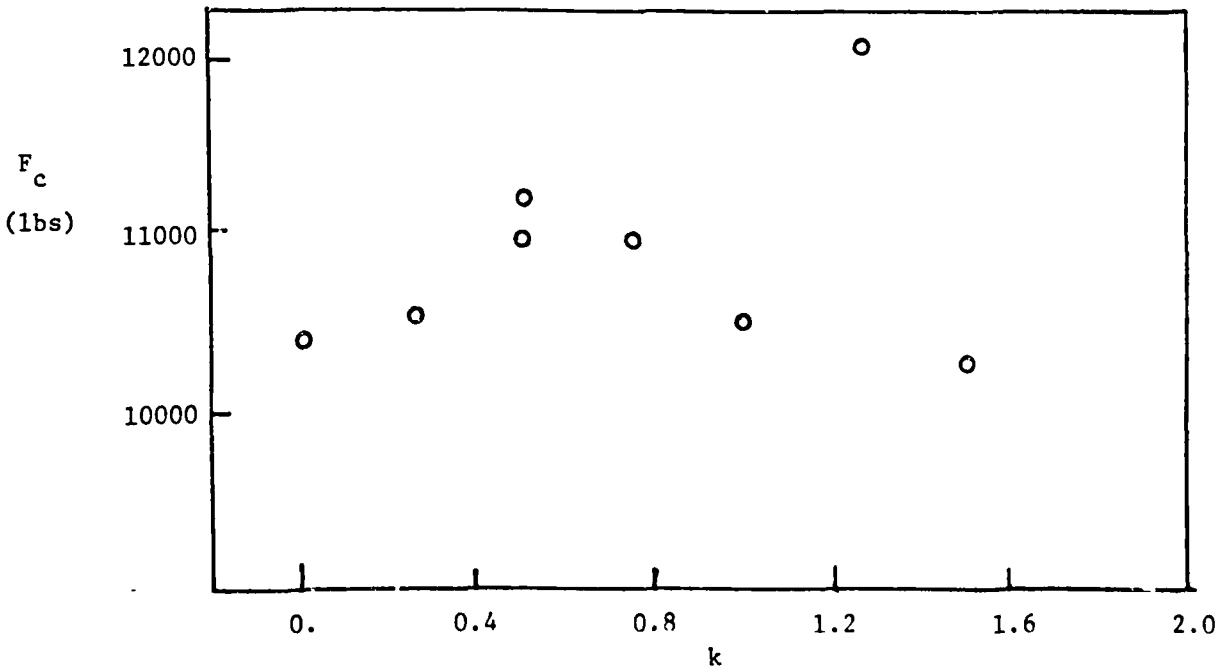

Figure 5: Effect Of Load Biaxiality On Failure Loads In 2024-T3 Sheets.

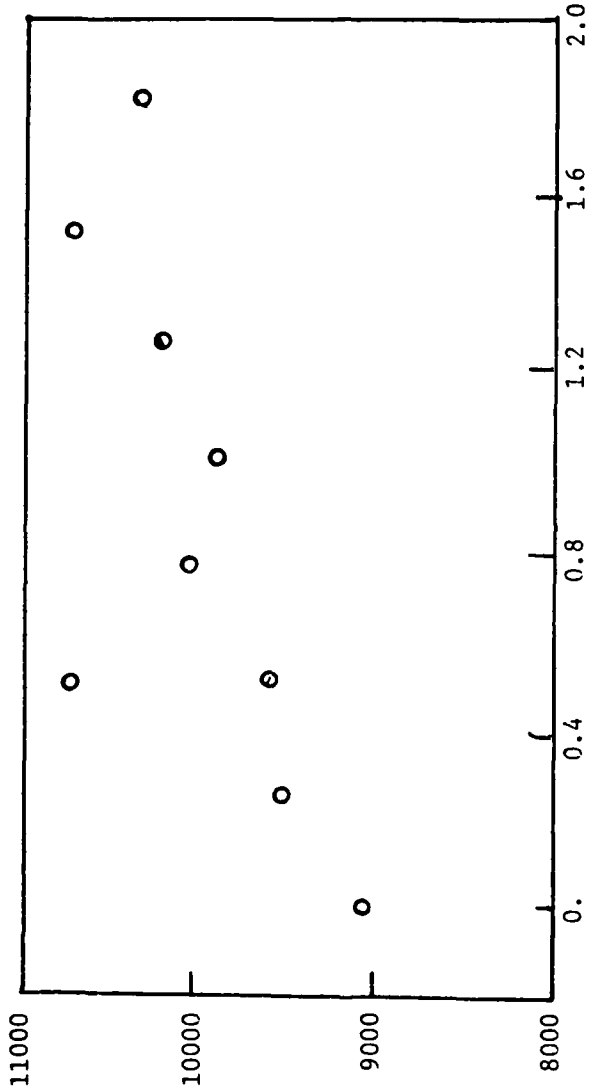

Figure 6: Effect Of Load Biaxiality On Failure Loads In 7075-T6 Sheets.

(Figure 8). The results from [15] on 6061-T6 aluminum, however, show little or no influence. Results reported in [16] also suggest a significant biaxial load effect on fatigue crack propagation rates for both 7075-T6 and 2024-T3 aluminums. These results, however, present too much scatter to conclusively demonstrate more than a qualitative trends.

The fatigue crack growth rate studies discussed above all demonstrate the tendency for increasing biaxial load factor to cause a decrease in crack growth rate. The magnitude of this effect is, however, not adequately demonstrated by the reported results. The scatter in the data, the inconsistencies in the experimental procedures and the lack of reproducibility of the results makes quantitative conclusions impossible. The effect appears to be load level, stress ratio level, material and geometry dependent. Much additional careful and consistent experimentation is needed to adequately characterize the influence of biaxial loading on fatigue crack propagation rates.

Recently, several studies have been undertaken to investigate the influence of load biaxiality on angled crack fracture properties (i.e., mixed-mode effects). In this situation, the biaxiality not only influences the higher order terms in the stress and displacement fields but also the stress intensity factors. Obviously the fracture toughness and the angle of crack propagation will be influenced by the biaxiality (based on stress intensity arguments alone). Evidence exists, however, to indicate that the resultant stress parallel to the crack also influences the angle of propagation. This effect can best be demonstrated by the results of [9, 17, 18]. Recently many combinations of plane and anti-plane load interactions have been studied [9], however, extreme scatter exists and these results have need to be reconfirmed by other investigators.

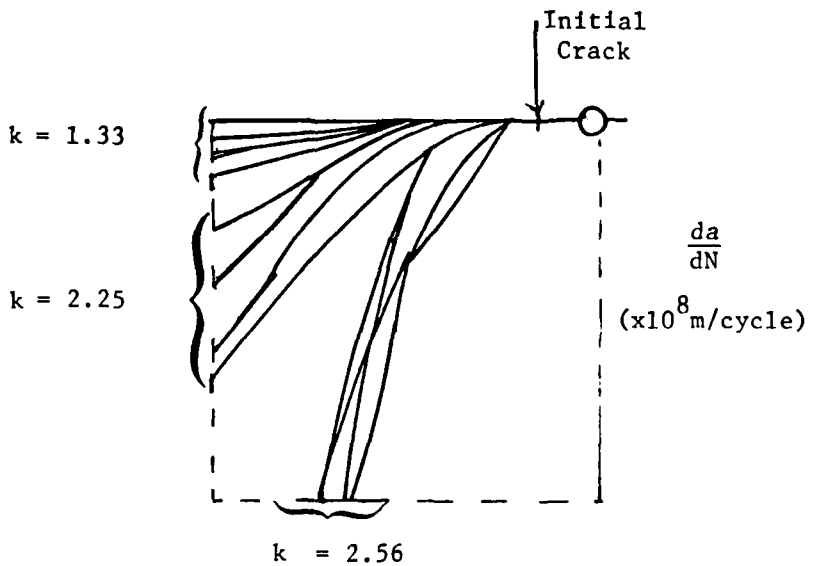

Figure 7: Fracture Paths At Failure For Plexiglass At Several Biaxial Load Levels.

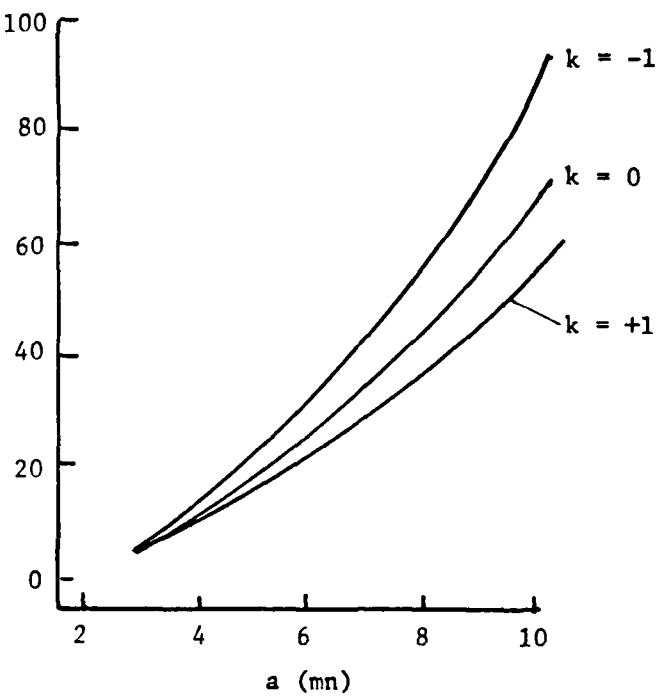

Figure 8: Fatigue Crack Growth Rates In RR58 Alloy At 3 Load Biaxialities.

One difficulty in the experimental determination of biaxial load effects on fracture properties is the significant influence of anisotropy and slight eccentricities on observed phenomenon. Extreme caution must be exercised in these studies. The choice of a proper specimen which eliminates load interaction effects is crucial. Even in the studies which were performed with consistent and careful experimental designs, large scatter is evident in the data. This scatter is often on the order of the effect being measured thus precluding quantitative conclusions. It is beyond the scope of this review to address the matter of experimental scatter and the subsequent interpretation of the results. It is important, however, to be aware of the inability of the current existing data base to quantitatively provide predictive capabilities for material characterization.

ANALYTICAL ASPECTS

The effect of biaxial loading on the stress and displacement fields near a crack tip can yield important information delineating the modes and onset of failure of fracture specimens. Many problems occurring in design applications involve a crack in a biaxial (or even triaxial) external stress environment. This importance has been recognized by many authors and studies concerning the effects of biaxial loading on stress intensity factors, stress distributions and displacement distributions near crack tips have been performed in the past.

Crack problems in the Mathematical Theory of Elasticity involve the solution of "Mixed" Boundary Value Problems. Many techniques have been employed for the solution of these problems. For two-dimensional and axisymmetric problems, the Complex Variable Technique (due mainly to Muskhelishvili [19]), Eigenfunction Expansion Techniques (initiated by Williams [20]), and Transform Techniques leading to either Dual Integral Equations (e.g., the work of Sneddon [21]) or Singular Integral Equations (e.g., the work of Erdogan [22]) are employed. It is beyond the scope of this paper to review these methods. The interested reader is directed to the referenced literature.

Consider the problem of an angled crack in an infinite sheet under in-plane biaxial normal stress applied at infinite as shown in Figure 9. The stress and displacement fields for this configuration can be written as

$$t_{yy} \simeq \frac{K_I}{\sqrt{(2\pi r)}} \cos\frac{\theta}{2}[1 + \sin\frac{\theta}{2} \sin\frac{3\theta}{2}] + \frac{K_{II}}{\sqrt{(2\pi r)}} \sin\frac{\theta}{2} \cos\frac{\theta}{2} \cos\frac{3\theta}{2}$$

$$t_{xx} \simeq \frac{K_I}{\sqrt{(2\pi r)}} \cos\frac{\theta}{2}[1 - \sin\frac{\theta}{2} \sin\frac{3\theta}{2}] - \frac{K_{II}}{\sqrt{(2\pi r)}} \sin\frac{\theta}{2}[2 + \cos\frac{\theta}{2} \cos\frac{3\theta}{2}]$$

$$+ \sigma(1-k) \cos 2\alpha \qquad (1)$$

$$t_{xy} \simeq \frac{K_I}{\sqrt{(2\pi r)}} \sin\frac{\theta}{2} \cos\frac{\theta}{2} \cos\frac{3\theta}{2} + \frac{K_{II}}{\sqrt{(2\pi r)}} \cos\frac{\theta}{2}[1 - \sin\frac{\theta}{2} \sin\frac{3\theta}{2}]$$

$$u_x \simeq \frac{K_I}{\mu} \sqrt{(\frac{r}{2\pi})} \cos\frac{\theta}{2}[\frac{1}{2}(\kappa-1) + \sin^2\frac{\theta}{2}] + \frac{K_{II}}{\mu} \sqrt{(\frac{r}{2\pi})} \sin\frac{\theta}{2}[\frac{1}{2}(\kappa+1)$$

$$+ \cos^2\frac{\theta}{2}]$$

$$+ \frac{(1-k)\sigma}{8\mu}\{r[\cos(\theta+2\alpha) + \kappa \cos(\theta-2\alpha) + 2\sin\theta \sin 2\alpha] + (\kappa+1)\, a \cos 2\alpha\} \qquad (2)$$

$$u_y \simeq \frac{K_I}{\mu} \sqrt{(\frac{r}{2\pi})} \sin\frac{\theta}{2}[\frac{1}{2}(\kappa+1) - \cos^2\frac{\theta}{2}] + \frac{K_{II}}{\mu} \sqrt{(\frac{r}{2\pi})} \cos\frac{\theta}{2}[\frac{1}{2}(1-\kappa) + \sin^2\frac{\theta}{2}]$$

$$+ \frac{(1-k)\sigma}{8\mu}\{r[\sin(2\alpha-\theta) + \kappa \sin(2\alpha+\theta) - 2\sin\theta \cos 2\alpha] + (\kappa+1)\, a \sin 2\alpha\}$$

where

ν is Poisson's Ratio,

u_x is the x component of displacement,

u_y is the y component of displacement,

t_{xx}, t_{yy}, t_{xy}, are the 2-dimensional stress tensor components

and

$\kappa = (3-4\nu)$ Plane strain

$\kappa = (\frac{3-\nu}{1+\nu})$ Plane stress

The stress intensity factors, K_I and K_{II} can be written as

$$K_I = \frac{\sigma}{2}\sqrt{\pi a}[(1+k) - (1-k)\cos 2\alpha]$$
$$K_{II} = \frac{\sigma}{2}\sqrt{\pi a}[(1-k)\sin 2\alpha] \qquad (3)$$

(from Eftis et al. [23]).

These equations include not only the standard singular terms but also a nonsingular term adding a constant to the t_{xx} stress term. This term has been demonstrated to have a significant influence on the maximum tangential stress, maximum shear stress and local strain energy densities (at high biaxiality) for a straight crack problem [24]. This influence will most strongly effect the onset of crack tip plasticity and the subsequent plastic behavior. The plasticity effects will be discussed in a subsequent section dealing with numerical solutions.

From equation (3), it is seen that for the straight crack, $\alpha = 0.$, the stress intensity factors are independent of the biaxial load factor. For elastic problems, the Strain Energy Release Rate (G) and the J-integral are only nominally effected by the biaxial load factor (both in infinite [25] and finite panels [24]). These results imply that, for truly brittle materials, the biaxial load ratio does not alter the fracture load for Mode I problems. Most problems of practical interest, however, involve plasticity and mixed-mode conditions, therefore, biaxial effects may be of importance.

The biaxial load factor is extremely important in the prediction of the angle of crack propagation. Even for Mode I, straight cracks in large biaxial stress fields the angle of crack propagation can deviate from 0 (i.e., self-similar growth) for biaxial load factors larger than 1.3 [24]. Figure 10

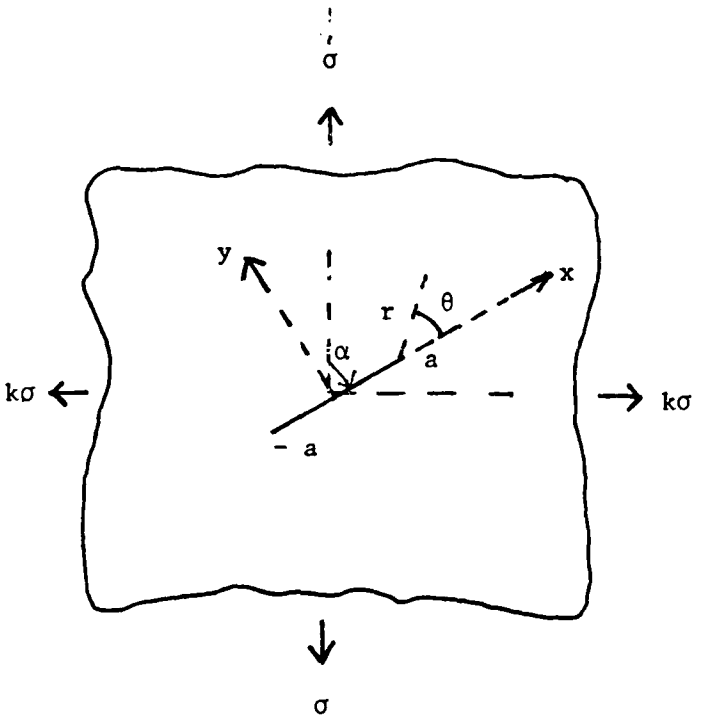

Figure 9: Biaxially Loaded Sheet With Slanted Crack.

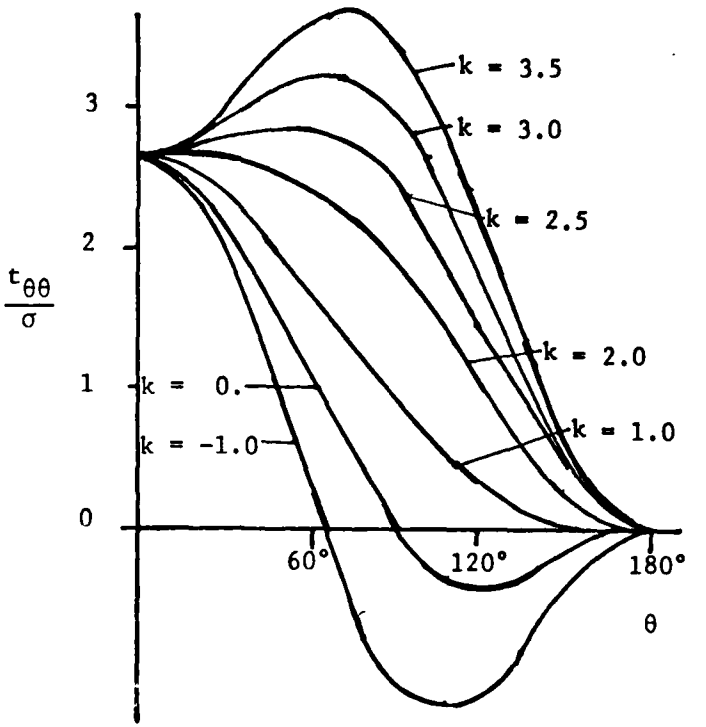

Figure 10: Directions Of Maximum Stress ($t_{\theta\theta}$) For A Flat Crack At Various Biaxial Load Ratios.

shows the variation of the maximum tensile stress (crack opening stress) with orientation for various biaxial load factors with $\alpha = 0$ [7]. Deviation from self-similar growth can be observed (using the maximum opening stress criterion) for large biaxial load factors. Note that the deviation from self-similar growth does not occur for negative biaxial load factors. Similar results can be obtained using the strain energy density criterion [24]. Experimentally deviation from self-similar growth has been observed in PMMA at high biaxial load factors [8].

For mixed mode fracture problems, the angle of propagation and onset crack growth are highly dependent on the biaxial load factor. Since the stress intensity factors are directly effected, each problem must be individually analyzed and general conclusions are difficult to draw. It is important, however, to recognize that the presence of a remote normal stress component parallel to the crack orientation direction can have significant influence on the onset and direction of crack growth [26].

Many solutions have been generated for a wide variety of crack problems involving different geometries and orientations. Consider the problem of a crack in the shape of a circular arc under in-plane biaxial loading as shown in Figure 11. The stress intensity factors for this problem have been generated by Savin [27]:

$$
\begin{aligned}
K_I \quad &\text{(at tip 1)} = \sqrt{R \sin \theta_o}\, \phi_1(\alpha, \theta) \\
K_I \quad &\text{(at tip 2)} = \sqrt{R \sin \theta_o}\, \phi_1(\alpha, -\theta) \\
K_{II} \quad &\text{(at tip 1)} = \sqrt{R \sin \theta_o}\, \phi_2(\alpha, \theta) \\
K_{II} \quad &\text{(at tip 2)} = \sqrt{R \sin \theta_o}\, \phi_2(\alpha, -\theta)
\end{aligned}
\tag{4}
$$

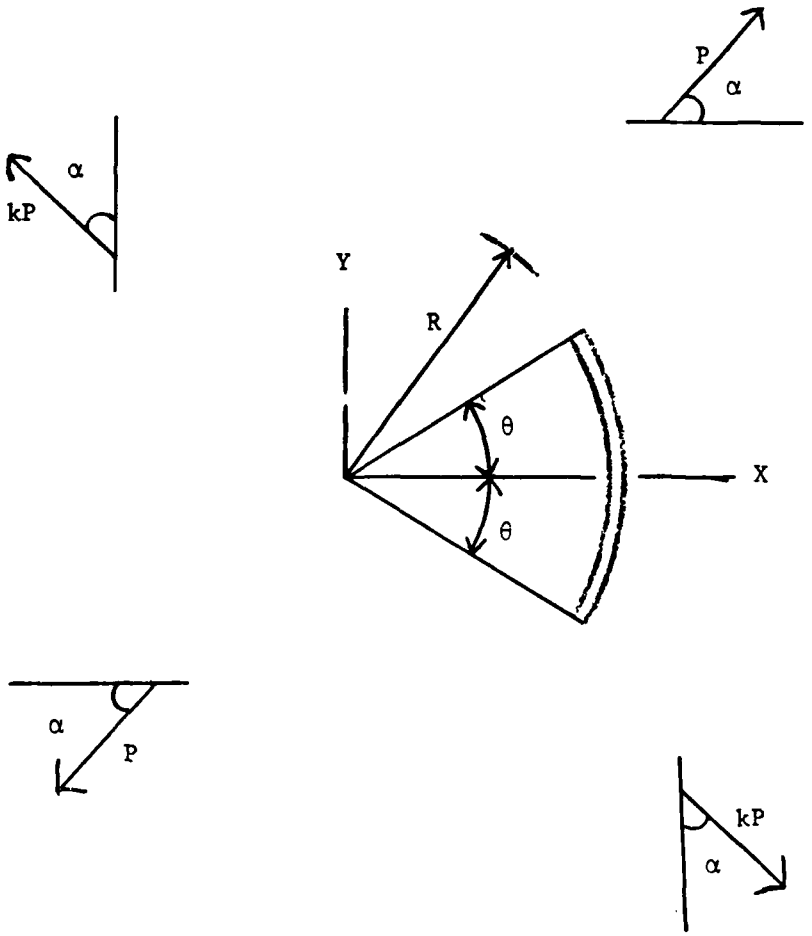

Figure 11: Semi-Circular Crack Subjected To Biaxial Loading At Infinity.

where ϕ_1 and ϕ_2 are given below:

$$\phi_1(\alpha,\theta) = \frac{\sigma}{2}\frac{(1+k) - (1-k)\cos 2\alpha \sin^2\frac{\theta}{2}\cos^2\frac{\theta}{2}}{(1+\sin^2\frac{\theta}{2})}\cos\frac{\theta}{2}$$

$$+ (1-k)\sin 2\alpha \sin\frac{3\theta}{2} + (1-k)\cos(2\alpha - \frac{3\theta}{2}) \quad ,$$

$$\phi_2(\alpha,\theta) = \frac{\sigma}{2}\frac{(1+k) - (1-k)\cos 2\alpha \sin^2\frac{\theta}{2}\cos^2\frac{\theta}{2}}{(1+\sin^2\frac{\theta}{2})}\sin\frac{\theta}{2} \qquad (5)$$

$$- (1-k)\sin 2\alpha \sin^2\frac{\theta}{2}\cos\frac{\theta}{2} - (1-k)\sin(2\alpha - \frac{3\theta}{2})$$

When cracks are subjected to stress nonuniformities due to the presence of geometric irregularities, biaxial loading can alter the resulting stress intensity factors significantly. Consider the problem of two cracks emanating from a circular hole in an infinite medium under biaxial loading as shown in Figure 12. The stress intensity factors at 3 biaxial load levels are shown in Figure 13 as generated by Newman [28]. For short cracks, the influence of the biaxial load factor is significant. The interaction of two cracks in a biaxial stress field has been studied by Badaliance and Gupta [29]. The geometry and loading of that study are shown in Figure 14. The results of a special case are shown in Figure 15a-15d. The results are given at 2 different biaxial load ratios demonstrating the influence of biaxiality. A final 2-dimensional example is the problem of a "kinked" crack in a biaxial stress field as solved by Kitagawa [30]. The geometry and loading for this problem are shown in Figure 16. The resulting stress intensity factors are shown in Figure 17 for various biaxial load levels. The influence for even minimal kinking is seen to be extremely significant.

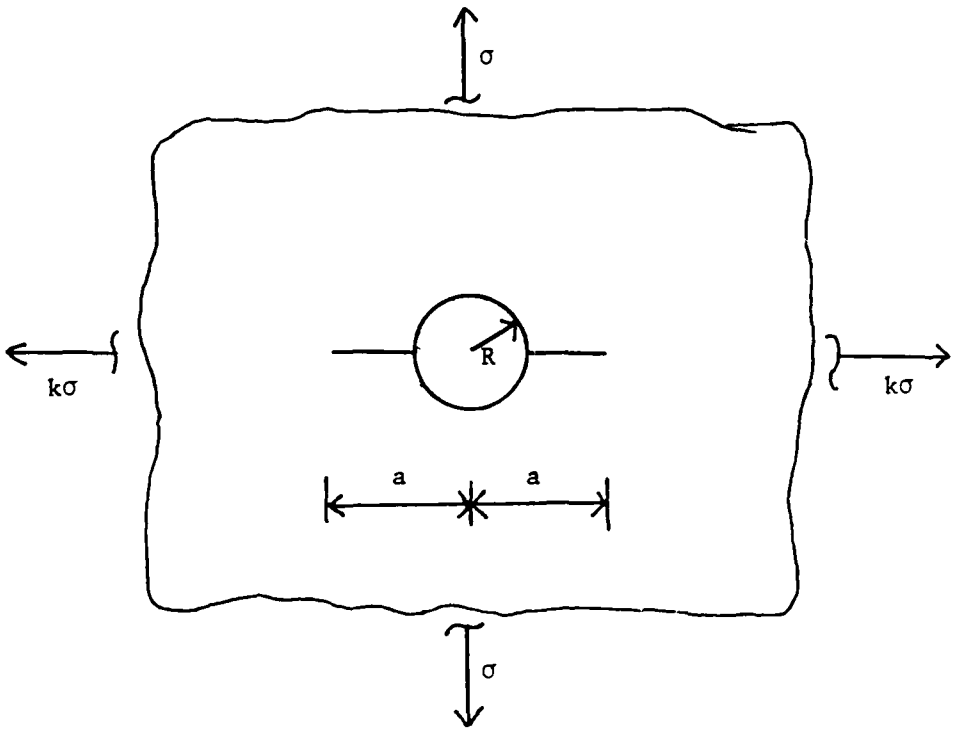

Figure 12: Symmetric Radial Cracks Emanating From A Circular Hole In A Biaxially Loaded Sheet.

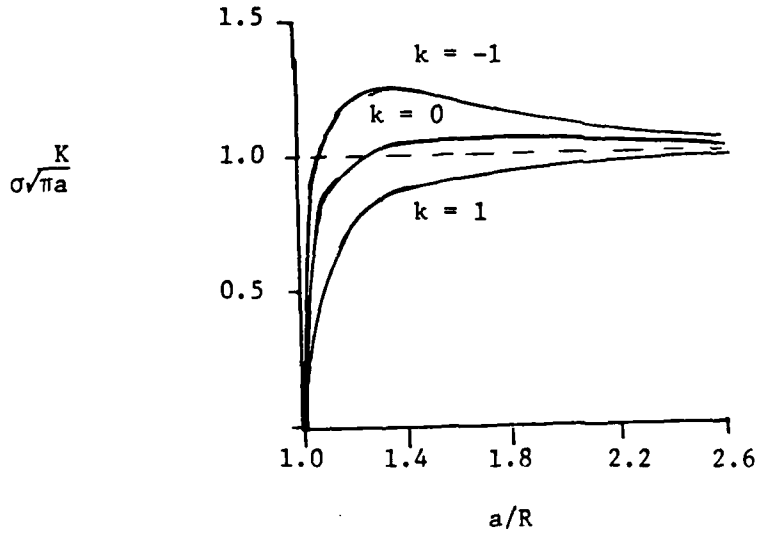

Figure 13: Stress Intensity Factors For Geometry Of Figure 12.

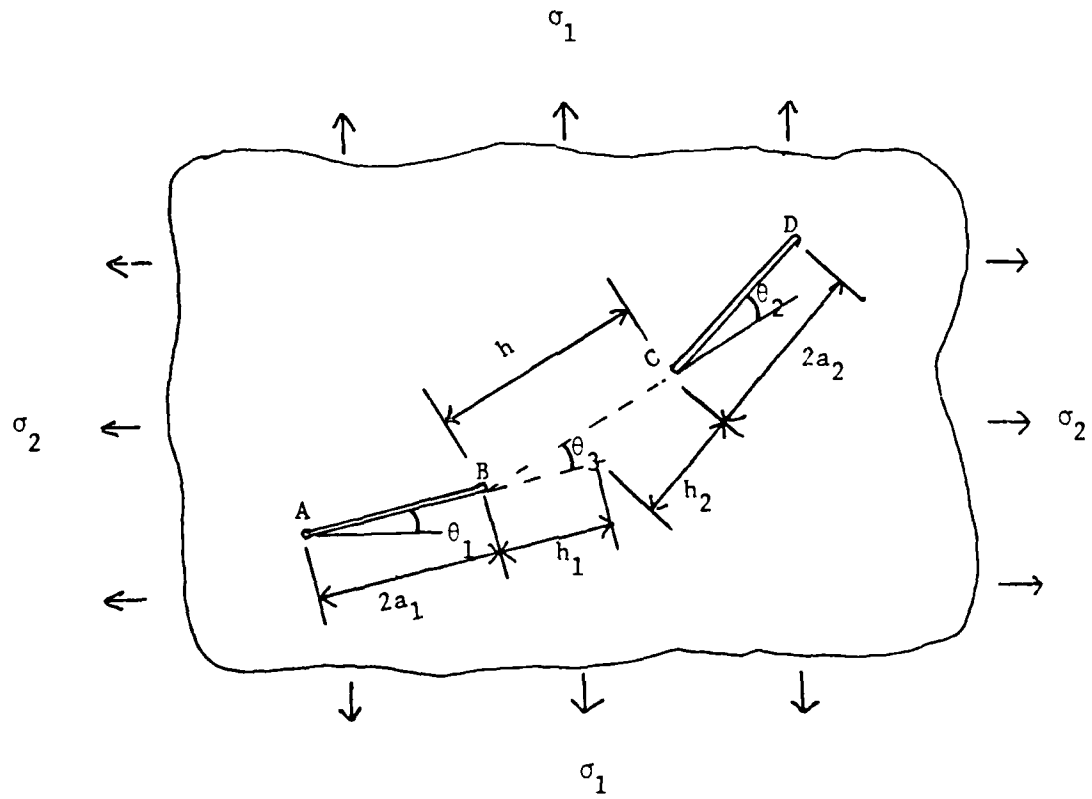

Figure 14: A Pair Of Arbitrary Cracks At Arbitrary Inclinations.

Figure 15 (a,b,c,d): Stress Intensity Factors For The Problem In Figure 14.

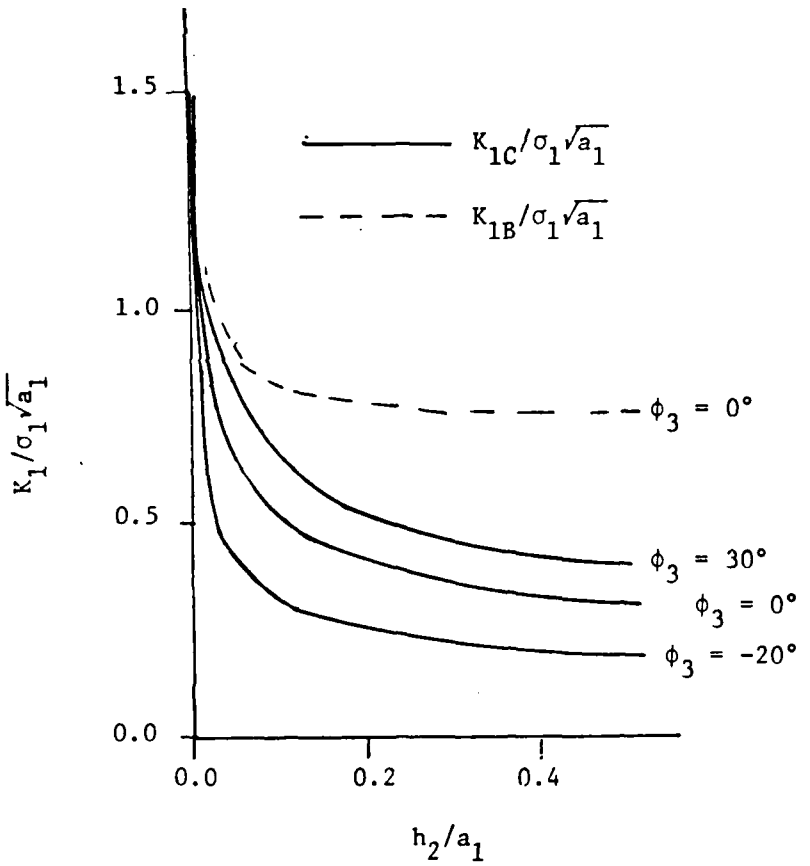

Figure 15a: $\phi_1 = 30°$, $\phi_2 = 0°$

$a_2/a_1 = 0.1$, $h_1 = 0$, $\sigma_2/\sigma_1 = 0.0$

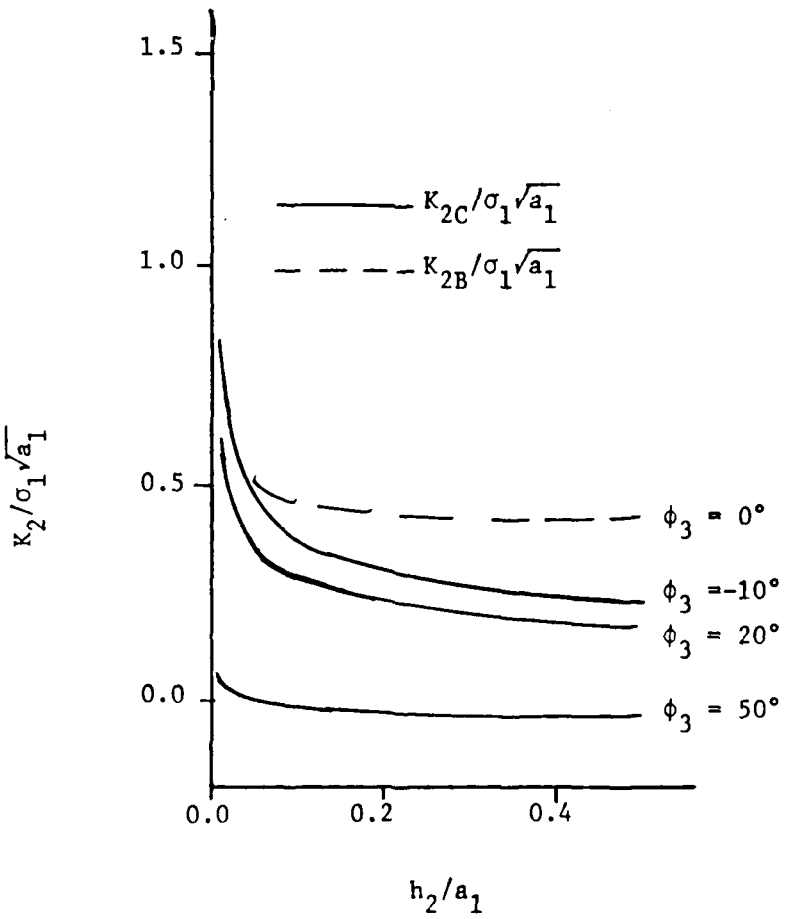

Figure 15b: $\phi_1 = 30°$, $\phi_2 = 0°$

$a_2/a_1 = 0.1$, $h_1 = 0$, $\sigma_2/\sigma_1 = 0.0$

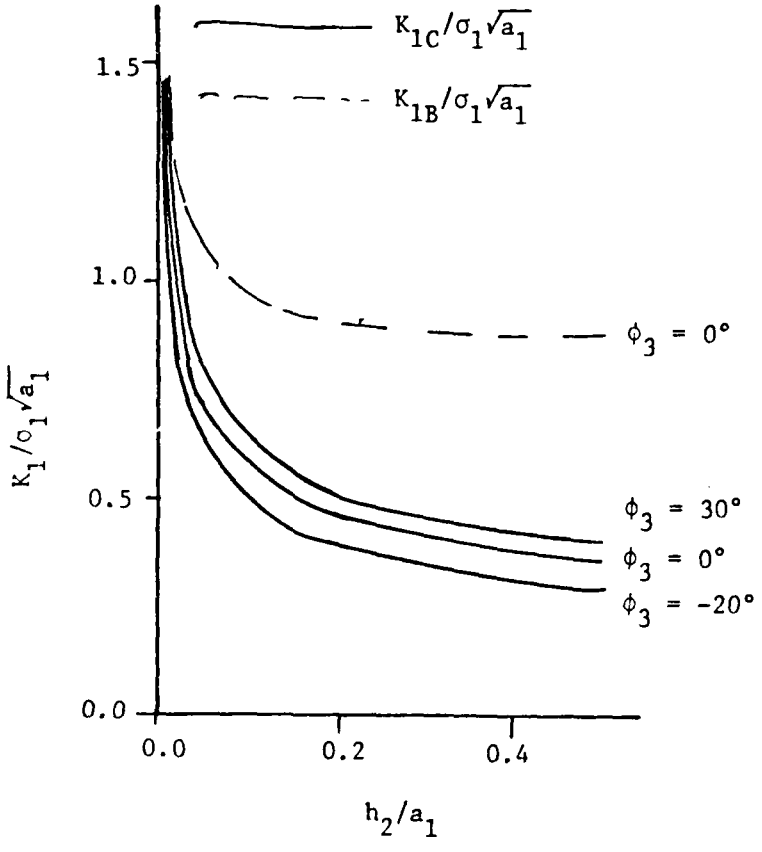

Figure 15c: $\phi_1 = 30°$, $\phi_2 = 0°$

$a_2/a_1 = 0.1$, $h_1 = 0$, $\sigma_2/\sigma_1 = 0.5$

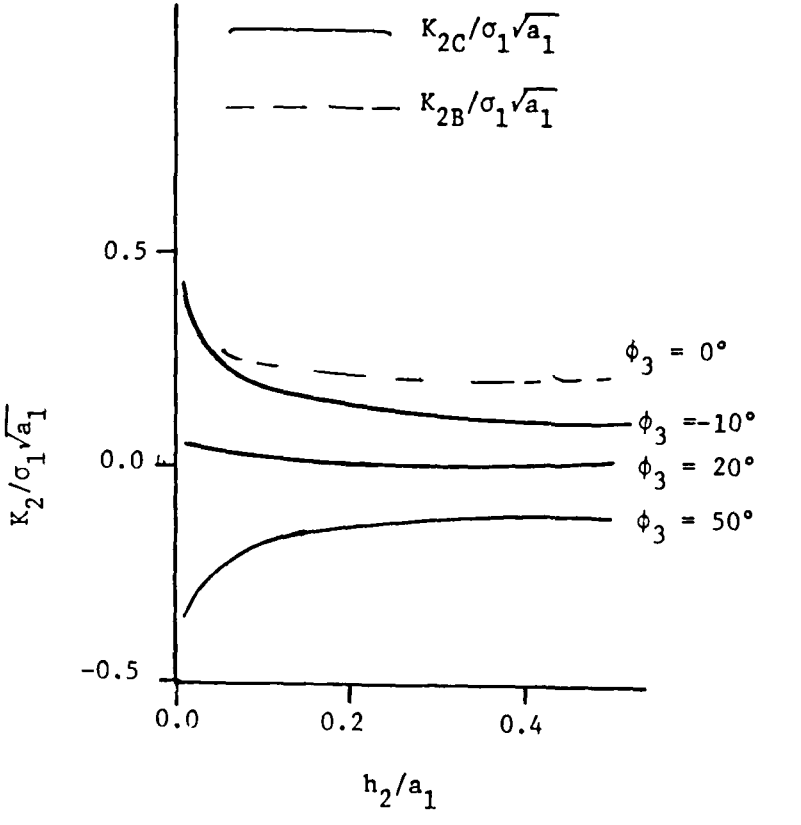

Figure 15d: $\phi_1 = 30°$, $\phi_2 = 0°$

$a_2/a_1 = 0.1$, $h_1 = 0$, $\sigma_2/\sigma_1 = 0.5$

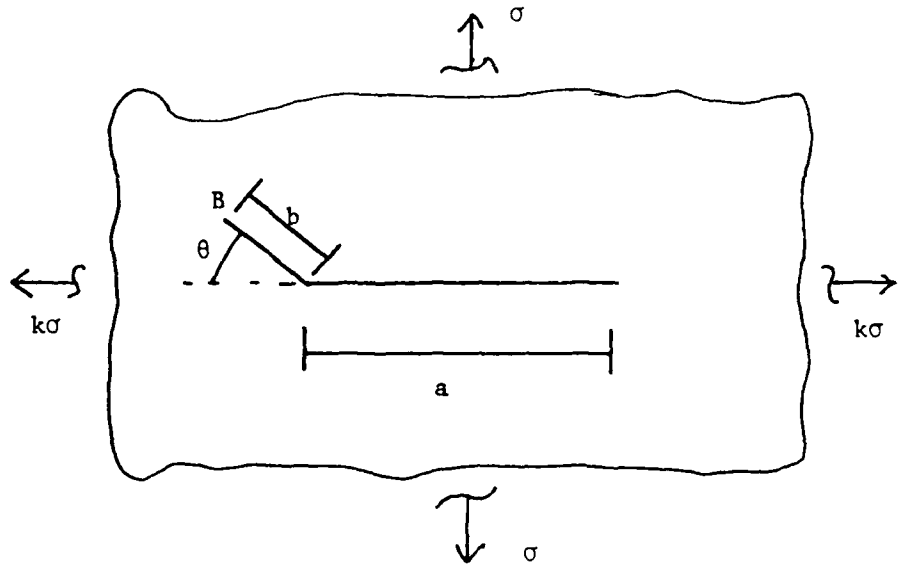

Figure 16: A Kinked Crack In A Biaxial Stress Field.

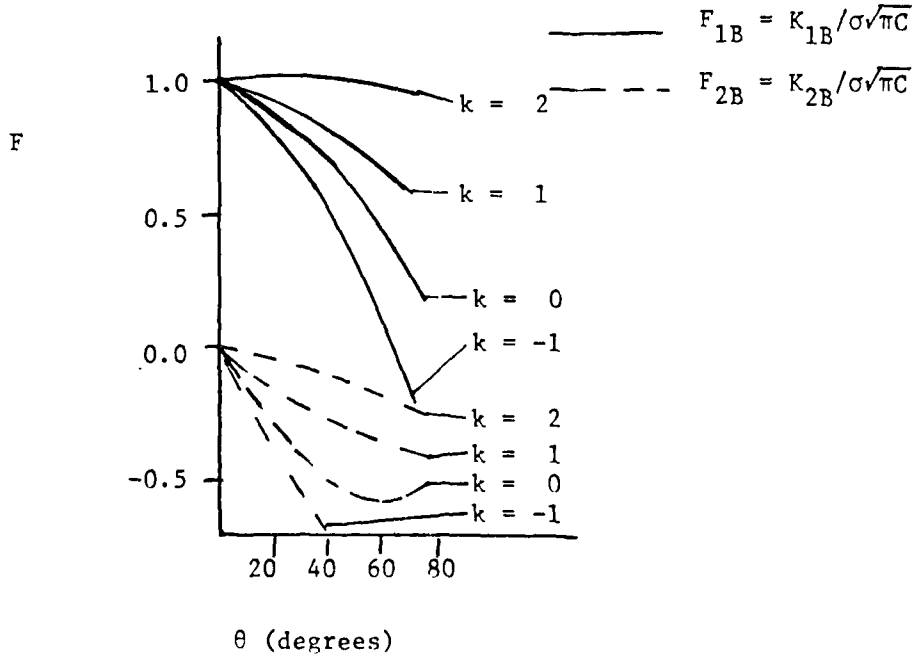

Figure 17: Stress Intensity Factors For The Kinked Crack Problem.

The generation of stress intensity factor solutions for 3-dimensional problems is much more difficult than for two-dimensional problems. An extremely limited class of problems can even be approached analytically and numerical techniques are usually employed. The problem of a circular crack in an infinite 3-dimensional body under biaxial loading has been studied by Sih and Kassir [31]. The problem of a parabolic crack in an infinite 3-dimensional domain has been studied by Kassir [32]. The geometry and loading for this problem are shown in Figure 18. The resulting stress intensity factors can be written as:

$$K_I = \frac{\sigma}{2}\sqrt{\pi}[(1+k) + (1-k)\cos 2\phi](y_o'^2 + 4m^2)^{1/4},$$

$$K_{II} = \frac{\sigma}{\sqrt{2}}\sqrt{\pi}[(1-k)\sin 2\phi]\frac{(mx_o')^{1/2}}{(m^2 + mx_o')^{1/4}}, \qquad (6)$$

$$K_{III} = -(1-\nu)\frac{m}{\sqrt{2}}\sigma(1-k)\sin 2\phi \cdot \frac{1}{(m^2 + mx_o')^{1/2}}.$$

The problem of an embedded elliptical crack under biaxial loading has been studied by Subramonian and Liebowitz [33]. The stress intensity factors for this problem can be written as:

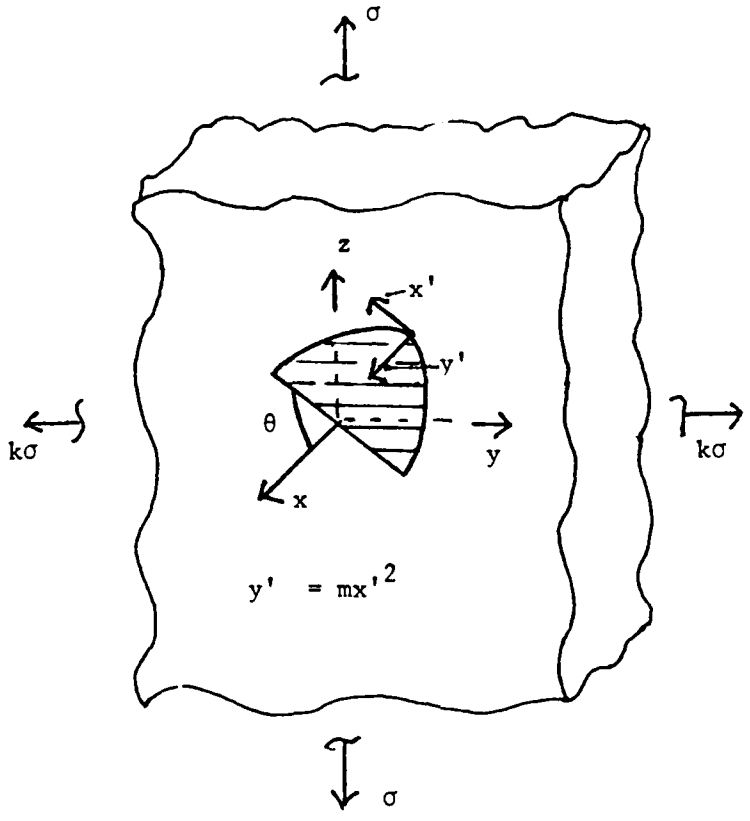

Figure 18: Parabolic Crack In A 3-Dimensional Solid.

$$K_I = \left[\frac{\frac{\sigma}{2}(1+k) + \frac{\sigma}{2}(1-k)\cos 2\phi}{E(k_o)}\right] \cdot \left(\frac{b}{a}\right)^{\frac{1}{2}} (a^2 \sin^2 \phi_o + b^2 \cos^2 \phi_o)^{\frac{1}{4}}$$

$$K_{II} = \frac{-a^2 b^2 k_o^2 \sin \phi_o}{(ab)^{3/2}} \cdot \frac{\frac{\sigma}{2}(1-k)\sin 2\phi (a^2 \sin^2 \phi_o + b^2 \cos^2 \phi_o)^{-\frac{1}{4}}}{(k_o^2 + \nu k_o'^2)E(k_o) - \nu k_o'^2 K(k_o)} \qquad (7)$$

$$K_{III} = \frac{-ab^3 k_o^2 \cos \phi_o (1-\nu)}{(ab)^{3/2}} \cdot \frac{\frac{\sigma}{2}(1-k)\sin 2\phi (a^2 \sin^2 \phi_o + b^2 \cos^2 \phi_o)^{-\frac{1}{4}}}{(k_o^2 + \nu k_o'^2)E(k_o) - \nu k_o'^2 K(k_o)}$$

where $k_o^2 = 1 - b^2/a^2$, $x_o' = a \cos \phi_o$, $y_o' = b \sin \phi_o$ and $k_o'^2 = 1 - k_o^2$, $a > b$; $K(k_o)$ and $E(k_o)$ are complete elliptical integrals of the first and second kind, respectively.

The 3-dimensional solutions presented demonstrate the importance of both crack front curvature and biaxial load factor when considering stress intensity. These solutions also exemplify the difficulty in formulating a 3-dimensional fracture criterion based on energy release rate or critical stress-intensity factors. A fracture criterion which is to be theoretically valid in all domains must be a local criterion predicting the onset critical conditions.

For most loading and geometries in two and three dimensions, numerical techniques must be employed to determine stress intensity factors. Often, for design purposes, it is useful to introduce a finite boundary correction factor into the stress intensity factor solutions presented above. In this manner, many geometries can be handled by tabular or graphical geometric parameters generated previously.

Theoretical and experimental studies performed to date demonstrate that the presence of biaxial loads can be important in the fracture assessment of laboratory specimens and, more critically, design structures. These works also show that biaxial influences are more important in configurations and loadings involving plasticity and complex geometries. These problems must be handled with numerical techniques.

PLASTICITY EFFECTS AND NUMERICAL STUDIES

The fracture analysis of engineering specimens and structures must account for the local crack tip plasticity which exists. The presence of an external biaxial stress field will alter the plastic behavior from that expected without biaxial loads. For small plastic effects, Irwin [34], Dugdale [35] and others have presented simple models which account for plasticity. Unfortunately for most problems of engineering interest these models are inadequate and a full incremental plasticity theory must be employed.

As a first attempt to characterize crack tip plasticity, Hutchinson [36] showed that the near tip stress and strain fields could be written asymptotically in the form

$$t_{ij} = K_\sigma \, r^{-(1/n+1)} \, t_{ij}(\theta)$$
$$\varepsilon_{ij} = K_\varepsilon \, r^{-(n/n+1)} \, \varepsilon_{ij}(\theta) \qquad (8)$$

where K_σ and K_ε are the stress and strain intensity factors, respectively. The assumptions of deformation theory plasticity were employed in the analysis. The functions $t_{ij}(\theta)$ and $\varepsilon_{ij}(\theta)$ are dependent on θ and are given in detail for many problems in [37, 38].

One of the first numerical studies performed to delineate the effects of load biaxiality was carried out by Hilton [39]. He studied the problem of a straight line crack in a two-dimensional infinite panel under uniform biaxial stress applied at infinity. The material was assumed to be nonlinear elastic (i.e., deformation plasticity) and the uniaxial nonlinear behavior was modeled as a power-law hardening type. The results for the stress and strain intensity

factors for various biaxialities and hardening parameters are shown in Figures 19a and 19b. For large values of the strain hardening exponent, these results show an enhanced biaxial response. Compressive loads parallel to the crack also affect the stress (or strain) intensity factors much more than tensile loads.

The effect of biaxial load factors on crack tip plastic deformation has also been studied. Lee and Liebowitz studied the problem of finite thin sheets under uniform biaxial loading under plane stress conditions [39]. A full incremental plasticity theory was used with a power-law hardening model. Their analysis was restricted to small strain theory. The results of that study are presented in Figure 20. Plastic zone area (A_p) is plotted against the biaxial load factor for several load levels. Their results indicate that tensile loads parallel to the crack decrease the plastic zone size (for biaxial load ratios less than 2) whereas compressive loads parallel to the crack increase the plastic zone size. Recent results presented by Moyer and Liebowitz [40] demonstrate similar trends for plane strain specimens. Their analysis employed large deformation theory plasticity and a multilinear uniaxial model.

One parameter which has received much attention for plastic fracture analysis is the crack opening displacement. Adams [41] studied the influence of load biaxiality on the crack opening displacement for many load levels, thin sheets under plane stress conditions were investigated. Using the critical crack opening displacement criteria, he calculated the failure load as a function of the remote loads. His results are shown in Figure 21. Lee and Liebowitz [39] have also studied the effect of applied load biaxiality on the J-integral for various load levels and biaxial ratios. Their results show that for biaxial ratios of practical interest ($|k| < 2$) the J-integral increases

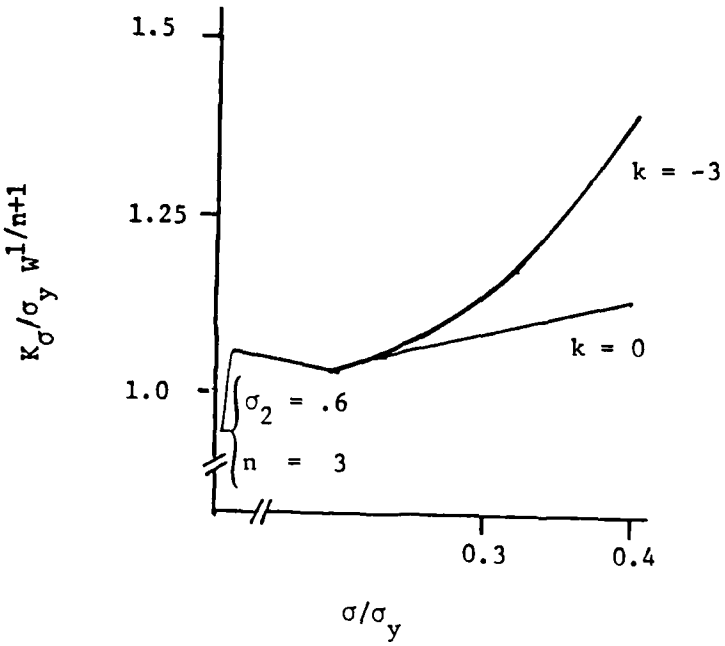

Figure 19a: Variation Of Plastic Stress Intensity Factor With Loading Biaxiality.

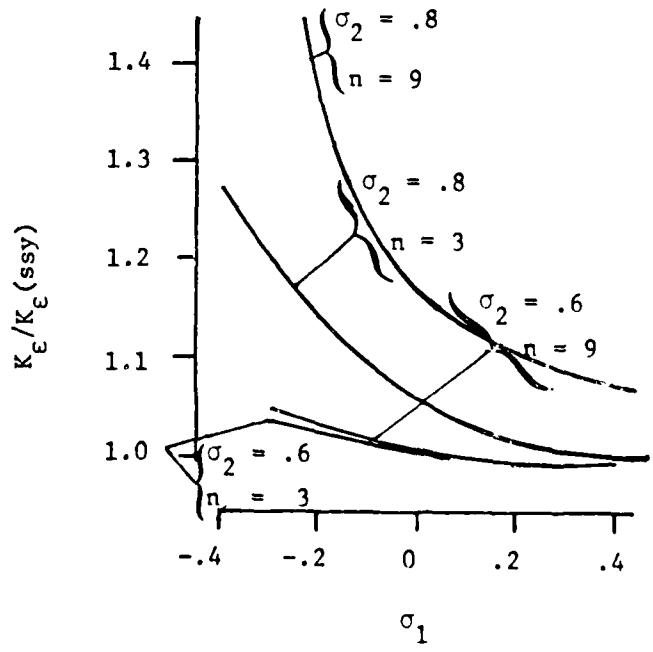

Figure 19b: Variation Of Plastic Strain Intensity Factor With Biaxiality and Hardening.

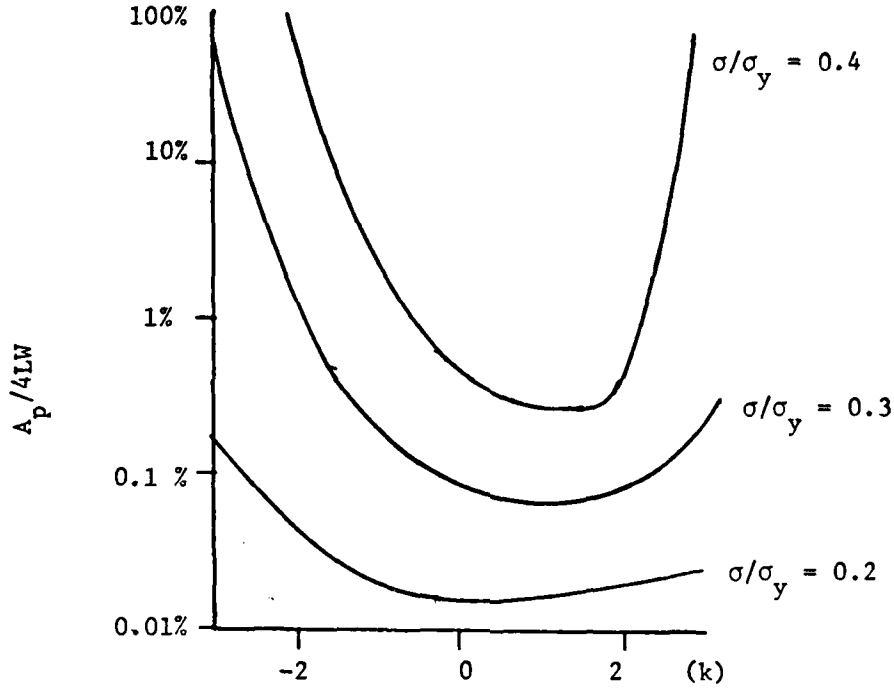

Figure 20: Variation Of Plastic Zone Size With Load Biaxiality.

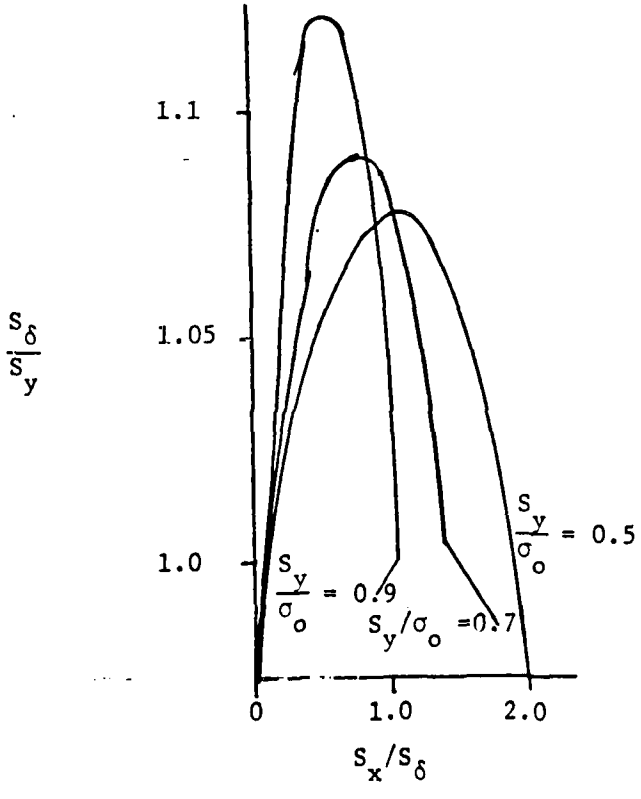

Figure 21: Effect Of Load Biaxiality On Equilibrating Loads By CTOD Methods.

compressive biaxial loads and decreases for tensile biaxial loads. This is consistent with the predicted yield trends as tensile loads parallel to the crack decrease ductility while compressive loads increase ductility.

The subject of slow crack growth is one of fundamental importance for problems involving significant ductility. Most materials in the ductile range exhibit large amounts of crack growth prior to final instability. The effect of applied load biaxiality on crack growth characteristics has attracted a limited amount of research due to the lack of consistent predictive theories to characterize stable growth and due to the inherent difficulties in solving the mathematical problem involved.

Liebowitz et al. [42], developed a computational procedure to study slow crack growth under biaxial load conditions. There results implied that a linear relationship exists between the crack length and the plastic energy dissipated. This result has been assumed by previous workers on the subject of stable crack growth (e.g., Wnuk [43] and Cherapanov [44]). Subsequent studies and tests on various aluminum alloys has shown this relationship to hold true under uniaxial and biaxial loading, however, both the slope and the plastic energy dissipated prior to the onset of growth are material, geometry and load dependent limiting its utility as a fracture criterion.

Lee and Du [45] have further refined the procedure to use either the plastic energy relation or the experimental gauge data as input to the numerical simulation procedure. A typical crack resistance curve starting with plastic energy parameters is shown in Figure 22. Recently Lee et al. [46] have studied the problem of non-self-similar crack growth under biaxial loading conditions. As would be expected, their results show considerable dependence of the predicted fracture path on load biaxiality (both for linear and nonlinear predictions). Their results are presented for a slanted crack

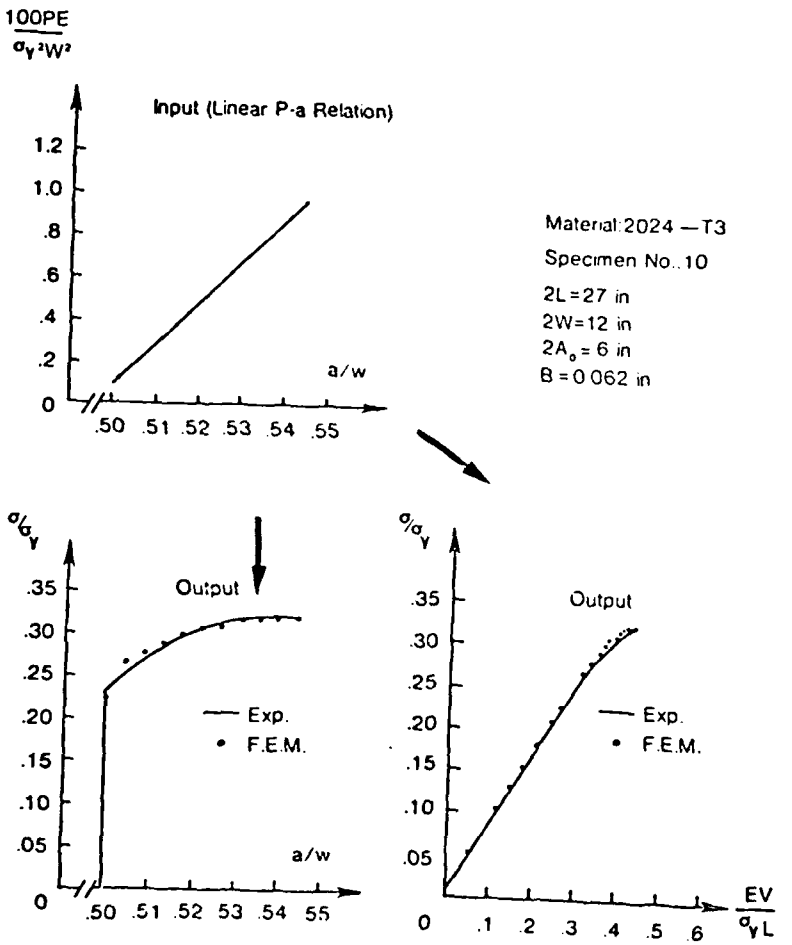

Figure 22: Finite Element and Experimental Results For Slow Crack Growth - Plastic Energy Relation Specified.

in Figures 23a, 23b, and 23c. The solid lines are the actual path predicted from an incremental growth analysis and the dashed lines are the path predicted by a static, pre-growth analysis. It is interesting to note that the actual path deviated from the initially predicted path to a much larger extent at higher biaxial load ratio. Their predictions are based on the assumption of a linear plastic energy-crack growth relation. No experimental studies have been done on mixed-mode plasticity problems involving stable crack growth to date.

Noticeably lacking from the literature are three-dimensional finite element solutions for problems involving slow crack growth or plasticity. The numerical complexities of the problem make it extremely difficult to perform the calculations. Advances in the numerical solution of three-dimensional elastic-plastic crack problems [47] should make biaxial studies feasible in the near future. Due to the fundamentally three-dimensional nature of crack problems involving plastic deformation, much additional work is needed to verify the biaxial effect predicted by two-dimensional analyses. Most of the work performed to date has been under "plane stress" conditions.

Figures 23 (a,b,c): The Initially Predicted And Actual Path Of Crack Growth.

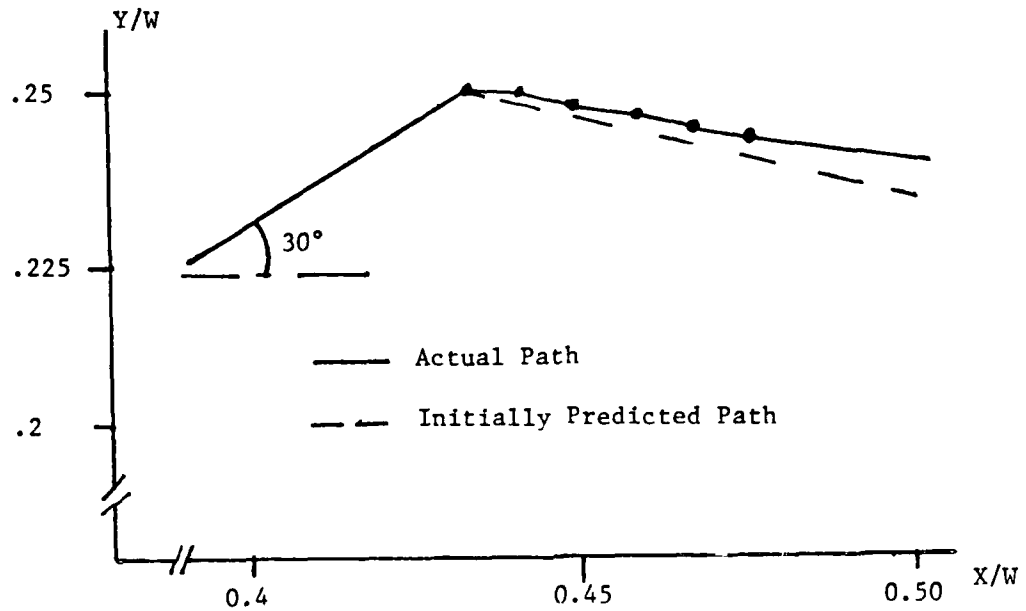

Figure 23a: $\phi = 30°$, $k = 0$.

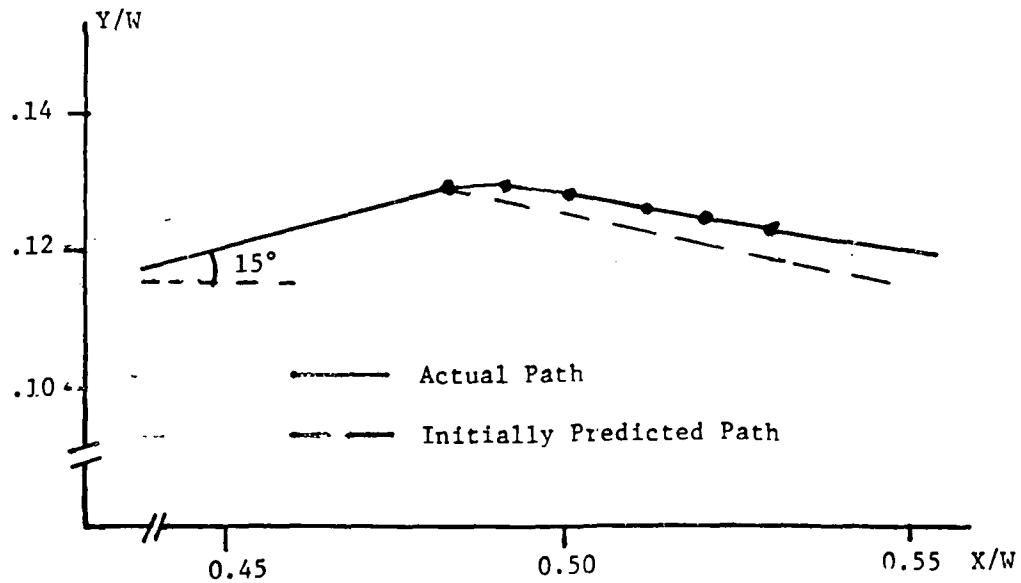

Figure 23b: $\phi = 15°$, $k = 0$.

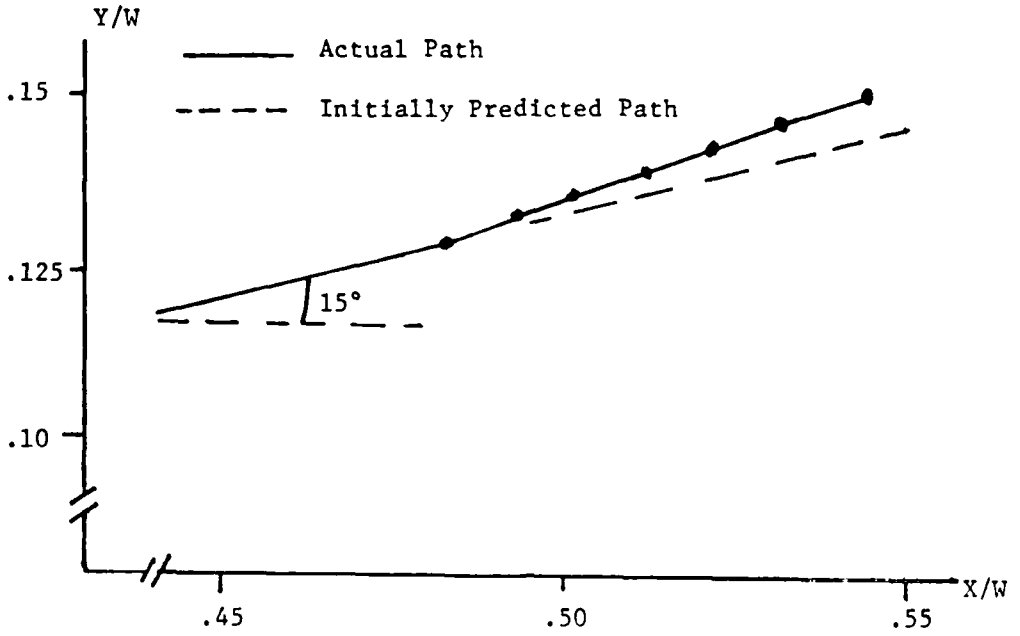

Figure 23c: $\phi = 15°$, $k = 1$.

BIAXIAL EFFECTS IN APPLICATION

Many problems of practical interest to the design of engineering structures involve the solution of problems with cracks in biaxial stress fields. Various problems from the design application of Aircraft, Aerospace and Ship Structures as well as from the Pressure Vessel and Piping industry have been studied theoretically and experimentally. A representative sample from the open literature are summarized below. The results can be obtained from the literature.

Tong and Atluri [48] have investigated the problem of a crack emanating from a lug hole under a biaxial stress field. Using a finite element approach employing hybrid elements, they solved for the stress intensity factors (K_I and K_{II}) as a function of crack orientation. Various aspects of cracks emanating from holes in aircraft structures are discussed by Broek [49]. Many theoretical and numerical approaches have been employed to solve problems involving cracks emanating from loaded holes. Wide variations exist in the reported results and further work is needed. A review of several solution procedures is given in [50].

The problems of stiffened plates and shells with cracks are of fundamental importance to many design applications. Empirical approaches to the problem of stiffened cylindrical shells with cracks is discussed by Kuhn [51] and Anderson and Sullivan [52]. Several semi-empirical and semi-theoretical solutions for the stress intensity factors involved are presented and discussed in [53] by Heath et al. The fatigue properties of stiffened cylinders were investigated by Wang [54] under several biaxial load factors.

Swift [55] has studied the influence of load biaxiality on cracks in stiffened panels and plates. Tensile load parallel to the crack is shown to

panels have been carried out by Ratwani and Wilhelm [56]. J-integral techniques are employed to explain the results obtained experimentally by Swift [57].

The effect of biaxial rivet forces on stiffened sheets with cracks has been studied by Erdogan [58] employing complex stress functions. Several more general loading conditions are considered by Rooke and Cartwright [59]. This problem has been studied experimentally by Broek [60] for both stiffened panels and cylinders. The fundamental solutions generated in [58, 59] are employed to obtain semi-empirical stress intensity factor curves for various loading configurations.

The concept of placing holes in structures to inhibit crack growth and crack instability (so-called stop holes) has gained much attention recently. DeRijk and Motter [61] and VanLeeuwen [62] have conducted independent studies on the effects of stop holes on the fatigue properties of thin sheets. While these studies were performed under uniaxial loading conditions, several possible implications of biaxial effects are discussed through extrapolation of the results. In design applications, the biaxial effects will, out of necessity, need to be accounted for.

The studies cited above all demonstrate the need for considering biaxial loading in application. Though the results of these investigations are highly specialized to the problems being studied (precluding general conclusions as to the nature of biaxial load effects), they emphasize the importance in carefully delineating all important problem parameters (e.g., loading conditions, geometry, etc.) when considering solutions for design purposes.

SUMMARY AND RECOMMENDATIONS FOR FUTURE RESEARCH

The preceding sections have summarized the state of current research into the influence of biaxial load factors on the fracture characteristics of materials and structures. While much work has already been performed, several areas need further investigation.

In the experimental field, further work is needed to delineate the dependence of fracture toughness and fracture load levels on applied load biaxiality. The scatter in the existing data is far to large to make conclusive qualitative assessment possible. Of interest would be careful examination of materials in the higher ranges of ductility where biaxial effects are known to be more severe. Also needed is careful study on the dependence of fatigue properties on both steady and cyclic biaxial loading. Little work has been done on this aspect, especially in the more ductile materials.

Noticeably lacking from the experimental base are slow growth studies under biaxial loads. Numerical predictions have been made by extrapolating results obtained under uniaxial loading. The validity of this approach needs to be assessed experimentally. Also needed are tests on surface crack behavior under biaxial loading.

Analytically, many fundamental solutions have been generated and the predictions of linear elasticity are generally a closed issue in two-dimensions. Further studies should be made, however, to investigate stress intensity factor dependence on load biaxiality in three-dimensional configurations (both for straight and curved through cracks and for surface cracks). These investigations, out of necessity, will need to be performed numerically.

Further studies on stable crack growth are needed to test the various models currently in vogue. It is unknown as to which approaches will hold valid under biaxial conditions. CTOD and Plastic Energy approaches have been used for a limited number of biaxial problems. Many more studies in comparison with experiments must be made to establish the validity of any of the modeling schemes.

Three-dimensional plasticity studies must be undertaken as the basic problems involved in ductile fracture are inherently three-dimensional. Both stationary crack problems and stable growth problems need investigation. With the rapid refinement of the numerical tools available for these analyses, fundamental studies with full three-dimensional models will soon be practical.

ACKNOWLEDGEMENT

This work was sponsored by NASA Grant: #NAG 1-158 and by the Office of Naval Research under Contract Number: N00014-75-C-0946.

REFERENCES

[1] A. A. Griffith, Proceedings Royal Soc. of London, A, Vol. 221, 1921.

[2] G. R. Irwin, Trans. ASME, JAM, Vol. 79, 1957.

[3] H. Liebowitz, J. D. Lee and N. Subramonian, Proceedings Int. Symp. on Fracture Mechanics, Sponsored by Office of Naval Research, Washington, D.C., 1978.

[4] H. Liebowitz, J. D. Lee and J. Eftis, Eng. Frac. Mech., Vol. 10, 1978.

[5] D. L. Jones and J. Eftis, Final Scientific Report, Air Force Office of Scientific Research, Bolling Air Force Base, Washington, D.C., 1980.

[6] J. J. Kibler and R. Roberts, J. Eng. Industry, Trans. ASME, 1970.

[7] P. S. Leevers, J. C. Radon and L. E. Culver, J. Mech. Phys. Solids, Vol. 24, 1976.

[8] J. Eftis and D. L. Jones, Int. J. Fracture, Vol. 20, 1982.

[9] Y. Ueda, K. Ikeda, T. Yao and M. Aoki, Eng. Frac. Mech., Vol. 18, 1983.

[10] P. S. Leevers, J. C. Radon and L. E. Culver, Polymer, Vol. 17, 1976.

[11] A. F. Liu, J. E. Allison, D. F. Dittmer and J. R. Yamane, Report to Air Force Flight Dynamics Laboratory, Wright-Patterson AFB, Dayton, 1978.

[12] G. C. Sih, Mechanics of Fracture, Vol. I (ed. G. C. Sih), Noordhoff, Leyden, 1973.

[13] F. Erdogan and G. C. Sih, Trans. ASME, J. Basic Eng., Vol. 85D, 1963.

[14] C. D. Hopper and K. J. Miller, J. Strain Analysis, Vol. 12, 1977.

[15] K. Ogura, K. Ohji, and Y. Ohkubo, Int. J. Fracture, Vol. 10, 1974.

[16] E. T. Moyer, Jr., H. Liebowitz and P. K. Poulose, Contract Report Summary, Office of Naval Research, #N00014-75-C-0946, February, 1983.

[17] K. Sakai and K. Sakano, J. Soc. Naval Arch., Japan, Vol. 139, 1976.

[18] Y. Ueda, K. Ikeda, T. Yao, M. Aoki, and S. Shibasaki, Trans. JWRI, Vol. 9, 1980.

[19] N. I. Muskhelishvili, Some Basic Problems in the Mathematical Theory of Elasticity, Noordhoff Int. Pub., Leyden, 1977.

[20] M. L. Williams, J. Appl. Mech. (Trans. ASME), Vol. 24, 1957.

[21] I. N. Sneddon, Proceedings Royal Soc. of London, A, Vol. 187, 1946.

[22] F. Erdogan, Mechanics Today (ed. S. Nemat-Nasser), Vol. 4, 1978, Pergamon Press, Oxford.

[23] H. Liebowitz, N. Subramonian and J. D. Lee, Boletin De La Academia De Diencias, Cordoba, Argentina, 1980.

[24] J. Eftis, N. Subramonian and H. Liebowitz, Eng. Frac. Mech., Vol. 9, 1977.

[25] J. Eftis, N. Subramonian and H. Liebowitz, Eng. Frac. Mech., 1977.

[26] H. Liebowitz, J. D. Lee and N. Subramonian, presented at the Poland Conference, 1980.

[27] G. N. Savin, NASA TT F-607, Chapter VIII, 1970.

[28] Newman, J. C. NASA TN D-6376, 1971.

[29] R. Badaliance and G. D. Gupta, Handbook of Stress Intensity Factors (ed. G. C. Sih), 1973, Lehigh University, Bethlehem, PA.

[30] H. Kitagawa, "Passive Analysis of Various Given Cracks and Cracking Processes," Fracture Mechanics and Technology (ed. G. C. Sih and C. L. Chow), Sijthoff and Noordhoff, 1977.

[31] M. K. Kassir and G. C. Sih, Trans. ASME, JAM, Vol. 29, 1962.

[32] M. K. Kassir, Eng. Frac. Mech., Vol. 2, 1971.

[33] N. Subramonian (Unpublished results).

[34] G. R. Irwin, Sagamore Ordnance Materials Conf., Syracuse, NY.

[35] D. S. Dugdale, J. Mech. Phys. Solids, Vol. 8, 1960.

[36] J. W. Hutchinson, J. Mech. Phys. Solids, Vol. 16, 1968.

[37] P. D. Hilton and J. W. Hutchinson, Eng. Frac. Mech., Vol. 3, 1971.

[38] C. F. Shih, Harvard University Report DEAP S-10, 1974.

[39] P. D. Hilton, Int. J. Frac., Vol. 9, 1973.

[40] J. D. Lee and H. Liebowitz, Eng. Frac. Mech., Vol. 9, 1977.

[41] E. T. Moyer, Jr. and H. Liebowitz, to be presented at the Fifth ASCE Engineering Mechanics Specialty Conference, Laramie, WY, August, 1984.

[42] H. Liebowitz, J. D. Lee and N. Subramonian, Nonlinear and Dynamic Fracture Mechanics (ed. N. Perrone and S. N. Atluri), ASME-AMD, New York, 1979.

[43] M. P. Wnuk, Int. J. Frac., Vol. 7, 1971.

[44] G. P. Cherepanov, PMM, Vol. 32, 1968.

[45] J. D. Lee and S. Du, Eng. Frac. Mech., Vol. 16, 1982.

[46] J. D. Lee, S. Du and H. Liebowitz, Eng. Frac. Mech., Vol. 17, 1983.

[47] E. T. Moyer, Jr. and H. Liebowitz, Proceedings ICF Int. Symp. Frac. Mech., Beijing, PRC, 1983.

[48] P. Tong and S. N. Atluri, Proceedings Int. Conf. Frac. Mech., Hong Kong, 1977.

[49] D. Broek, Cracks at Structural Holes, MCIC Report, 1975.

[50] J. Tweed and D. P. Rooke, Int. J. Eng. Sci., Vol. 11, 1973.

[51] P. Kuhn and R. W. Peters, NACA TN-4011, 1957.

[52] A. B. Anderson and T. L. Sullivan, NASA TN-D-3252, 1966.

[53] W. G. Heath, L. F. Nicholls and W. T. Kirkby, AGARD-CP-221, 1969.

[54] T. Swift and D. Y. Wang, AFFDL TR 70-144, 1969.

[55] T. Swift, AGARD AG-176, NATO, 1974.

[56] M. M. Ratwani and D. P. Wilhelm, AFFDL-TR-73-42, 1975.

[57] T. Swift, Prospects of Fracture Mechanics, Noordhoff, Leyden, 1974.

[58] F. Erdogan, Proceedings Fourth U.S. Natl. Cong. Appl. Mech., Vol. 547, 1962.

[59] D. P. Rooke and D. J. Cartwright, Copendium of Stress Intensity Factors, HMSO, London, 1976.

[60] D. Broek, Natl. Aerospace Inst. Report, TR 71033, 1971.

[61] P. DeRijk and A. A. Motter, Natl. Aerospace Inst. Report, TR 70021, 1970.

[62] H. P. VanLeeuwen, Natl. Aerospace Inst. Report, TR 70029, 1971.

LIST OF FIGURES

LIST OF FIGURES (Continued)

END

FILMED

5-85

DTIC